Many Body Effects in Atomic Systems

by

Hao Fu

A dissertation submitted in partial fulfillment
of the requirements for the degree of
Doctor of Philosophy
(Physics)
in The University of Michigan
2007

Doctoral Committee:

Professor Paul R. Berman, Chair
Professor Roberto Merlin
Associate Professor Luming Duan
Assistant Professor David Lubensky
Associate Professor Alberto G. Rojo, Oakland University

To My Parents

ACKNOWLEDGEMENTS

I am most grateful to my thesis advisor, Professor Berman, for his guidance throughout my graduate research. Working in his group has been among my happiest times in Ann Arbor. As a student, I am really lucky to have worked in an atmosphere of such integrity and high intellectual standards that he set for his group. During the last three and a half years, he has always been easily accessible for questions and discussions, from which I have benefited tremendously. I will definitely miss the endless discussions that I had with him on dielectric problems.

I would like to thank Professor Rojo, who taught me a lot about condensation and superconductivity. Without his help, I would not have finished the second part of my thesis. I would also like to thank Professor Duan for his insights on the field of cold atoms. Discussions with him broadened my view on the research of cold atoms.

I wish to thank my fellow students Claudiu Genes, Dylan Manna, Wei Yi, Bing Wang, Jason Kestner, Guin-Dar Lin, Eric Tardiff, Behzad Ebrahimi, Wei Zhang and Yongjian Han for the many interesting and enjoyable discussions I have had with them.

I am forever indebted to my family. Without their unconditional support, it would have been impossible for me to have finished this thesis. In particular, I thank my wife, Xuan, for her constant encouragement and unselfish sacrifice during the years of my study. I dedicate this thesis to my parents, and hope they be delighted by this modest tribute.

TABLE OF CONTENTS

LIST OF FIGURES

Figure

CHAPTER I

Introduction

Many interesting AMO (Atomic, Molecular and Optical) physics phenomena can be understood from a single particle perspective. By studying the details of single particle dynamics, and summing up contributions from all particles, one can generally find a satisfying understanding of the ensemble behavior of such particles. Optical lattices [1], for example, belong to this category.

In atomic systems, however, there are also cases where many body effects can significantly modify the physics of the problem. One has to treat the particle-particle interactions explicitly to correctly describe the physics. Studies of such systems usually lead to interesting connections between AMO and condensed matter physics. Actually, AMO systems, because of their exceptional controllability, are ideal platforms to study many body physics. Over the last decades, interesting many body phenomena, including Bose Einstein condensates [2][3], Mott insulators [4], and fermionic superfluids have been realized [5][6][7]. Study of these systems has proved to be both exciting and revealing. In this thesis, I study two such examples: the modifications of single atom process inside a dielectric [8][9] and the collective behavior of ultra cold Bose [10] and Fermi gases [11].

1.1 Single Atom Decay Inside a Dielectric

Single particle atomic decay, accompanied by recoil of the source atom is among the most basic AMO processes. Most theoretical treatments of this problem are based on a single particle picture. The dynamics of the atom interacting with the vacuum and external fields are treated for individual atoms. With increasing density of the environment in which the decaying atom is found, one has to consider the modification to the decay produced by the environment. This modification of the single particle process inside an atomic gas is important because precision measurement, and quantum computation are based on these single particle processes.

Traditionally, such calculations have been carried out using a macroscopically theory [12][13]. The effects of environment atoms are treated as a dielectric. To find corrections to the single particle processes, various assumptions have been make for the local environment in which the single particle finds itself. Such calculations are less than satisfying because they cannot give a unified way of treating the environmental effects. The corrections are based on the model chosen. In addition, there is not a clear picture on the physical processes that are responsible for particular corrections.

In this thesis, we develop a microscopic theory to calculate the modification of the single particle process inside an atomic gas. The effects of the environment atoms are evaluated perturbatively. Since the theory is quite general, one can apply it to various single particle processes and follow similar procedures to find modifications due to the medium. Moreover, because of the microscopic nature of the theory, one can have clear physical pictures of the underlying mechanisms giving rise to such modifications.

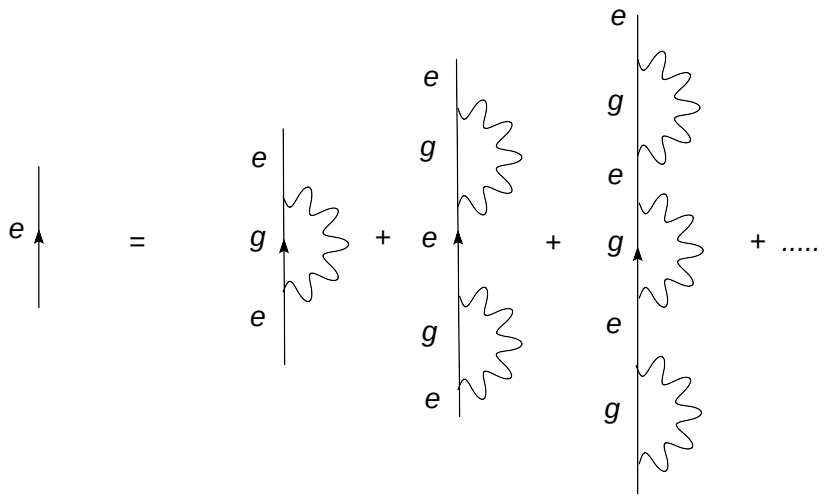

Figure 1.1: Diagrams of an excited atom interacting with the vacuum field

This microscopic theory is applied to two particular single particle processes, namely, spontaneous decay and photon recoil of a source atom inside a dielectric medium.

1.1.1 Spontaneous Decay Inside a Dielectric

The spontaneous decay of an excited atom is determined both by the the properties of the source atom and by the environment. The dependence on the source atom is obvious. Different kinds of atoms generally have different decay rates. The dependence on the environment can be illustrated by putting an atom inside a single mode cavity. In this situation, there is no decay since the atom field dynamics is reversible.

In a microscopic picture, the spontaneous decay in a vacuum can be understood in terms of processes of the type depicted in Fig. (1.1). The excited state of the source atom interacts with the vacuum by radiating and reabsorbing photons [14]. This process introduce a correction to the self energy of the source atom excited state. The real part of the self energy gives a correction to the energy shift, while the finite

imaginary part gives rise to the decay of the source atom excited state. In a medium, the intermediate state, the ground state with one photon is modified. The photon radiated by the source atom can be scattered by the medium atoms. This modifies the photon propagator and thereby modifies the imaginary part of the self energy of the source atom. This observation is the basis of our microscopic calculation [8]. In Chapter 2, we calculation the contribution to the decay from the process of photons scattered by the medium atoms.

Most of the experiments done so far used Eu^{3+} ions as the source radiator [15][16][17][18], as a dopant into Gd_2O_3, Y_2O_3, PbO or B_2O_3 hosts. The resultant noncrystalline structure are immersed into liquids, or supercritical CO_2, where the index of refraction can be varied. After exciting the Eu^{3+} to its excited state, one measures the fluorescence to determine the decay rate as a function of the environmental index of refraction. These experiments have not yet given conclusive results. Moreover, since the ions are doped inside crystals, it decay properties may depend significantly on the properties of the crystal instead of on the liquid or gas used to modify the environmental index of refraction.

1.1.2 Photon Recoil Inside a Dielectric

In spontaneous decay, the photon radiated by the source atom imparts a momentum to the source atom. At room temperature, it is virtually impossible to resolve the effect of photon recoil, which is typically 10 KHz in frequency units. On the other hand, the recoil shift can be observed in laser-cooled gases. In particular, in the extreme case of a Bose-Einstein condensate, the atoms are cooled to an energy $E = \hbar f$ with frequency $f = 100$ Hz [2][3]. In this case, the recoil energy of the source is much larger than the relevant energy scale of the problem and one has to take into account the recoil explicitly.

The photon recoil momentum in vacuum is just the opposite of the photon momentum evaluated at the atomic frequency. In order to calculate the modification of the photon recoil inside a dielectric, we need to consider the process in which the photon radiated by the source atom is scattered by the medium atoms. This scattering modifies the energy and momentum that a photon carries. By momentum conservation, this modifies the recoil momentum imparted to the source atom. This calculation predicts that the source atom recoils according to the canonical photon momentum instead of the vacuum photon momentum. This conclusion is consistent with experimental findings.

Experimentally, the photon momentum inside a medium was measured by immersing mirrors inside a liquid and measuring the photon force on the mirror [19][20]. Recently, with the realization of Bose-Einstein condensate, it is possible to directly measure the photon recoil by turning off the confining trap of the condensate. Actually, since the atom-atom interaction can be turned off almost instantaneously, the time of flight image gives a direct probe of the momentum distribution of the condensate before expansion. It is found that the photon recoil of the source atom is $n\hbar k$ where the n is the index of refraction of the medium and k is the photon wavenumber in vacuum.

1.2 Many body Behavior of Ultra-cold Atomic Gases

These calculations discussed above are essentially single particle calculations. They include many body corrections as perturbations. In atomic systems, there are occasions where the above approach does not suffice to solve the problem. One has to work in the many-body basis from the very beginning.

With the rapid progress in cold atom experiments, several interesting many body

systems have been realized. Studies of such systems can give insight to the study of similar systems in other fields. For example, the study of Bose-Einstein condensates, fermion superfluids and the so-called BEC-BCS crossover, in which the many body ground state continuously change from a BEC type to a BCS type, [5] [6][7][21][22][23][24][25][26] may shed light on the problem of high-temperature superconductivity. The versatility of atomic systems also allows one to realize systems that have not yet been considered theoretically. In the following, we present two such examples.

1.2.1 Tonks Girardeau Gas with a Local Impurity

The so-called Tonks Girardeau gas was proposed several decades ago by Tonks in the classical case and Girardeau for the quantum case [27]. It is a one dimensional Bose gas whose inter-particle interaction it taken to be infinitely positive. As a consequence of the infinite repulsion, the many body wave function has nodes when two particles overlap. In one dimension, this many body wavefunction is similar to the free Fermi many body wavefunction. The only difference is that the bosonic wavefunction is symmetric under permutation while the Fermi wavefunction is anti-symmetric under permutation of the particles. This observation allows one to obtain exact solutions of the many body problem.

This system has been realized recently by two groups [28][29]. In these experiments, particles are confined by optical traps. By increasing the transverse confinement, one can approach an effective one dimensional problem. In order to reach the strongly interacting regime, one needs to increase the ratio of the interaction energy I vs. the kinetic energy K. In a one dimensional homogenous system one can show

that the ratio of the these energies is equal to

$$\gamma = \frac{I}{K} = \frac{mg}{\hbar^2 n}, \tag{1.1}$$

where m is the mass of the particle, g is the interactions strength and n is the one dimensional particle density. To increase γ, one can either increase the effective mass, increase the interaction strength, or decrease the density. In the experiments, the regime with $\gamma \approx 200$ has been achieved.

The impurity problem for the Tonks Girardeau problem is particularly interesting because it is straightforward to realize in experiments. This can be done by introducing impurity atoms or introducing external fields. In addition, it is related to the ion-BEC experiment planned at the University of Michigan. Since the Tonks Girardeau system is exactly solvable, study of this system may provide some theoretical insight into the ion-BEC system.

In chapter 4, we solve the problem of a Tonks Girardeau gas in the presence of a local potential. The single particle density matrix is found as a function of the local potential strength. The effect of the impurity on the condensate fraction and conductance of the Tonks Girardeau gas is discussed.

1.2.2 Atomic Fermi Gas with Spatially Modulated Interaction

Tuning interactions among atoms via Feshbach resonance has been one of the most important techniques discovered in recent atomic experiments [30]. This kind of controllability allows many applications in the study of many body physics. For example, using this technique, a BCS-BEC crossover was realized in atomic systems recently [5][6][7] [21][22][23][24][25][26]. While there are many studies of tuning the interaction in the time domain [7][22][24] [25][31][32][33] there are few studies on tuning interaction in the spatial domain. I try to explore this possibility in a Fermi

gas system.

Experimentally, a degenerate Fermi gas can be prepared by sympathetic cooling or adiabatic switching from a molecular condensate. The typical Fermi frequency is in the kHz range and the particle density is about $10^{12}cm^{-3}$. Since experiments are typically done close to resonance, the scattering length approaches infinity. Consequently, the interaction between Fermi atoms is typically large, where the gap can be of the order of the Fermi energy.

At zero temperature, the attractively interacting Fermi gas becomes a superfluid by forming Cooper pairs. This the basic picture of the BCS theory. In a typical situation, the interaction between particles does not depend on the center of mass coordinate of the interacting particles. With the technique of the Feshbach resonance, it is possible to have atoms interact differently at different positions. Under this kind of interaction, the ground state wavefunction acquire some non-trivial changes.

In the case studied in Chapter 5, we consider a periodically modulated interaction. Using the Bogliubov de Gennes mean field theory, we obtain the ground state and single particle excitation of the system. It is found that the ground state consists of non-zero momentum Cooper pairs. This state is similar to the Fulde-Ferrell-Larkin-Ovchinnikov (FFLO) states [34][35]. The excitation spectrum, on the other hand, has a multiple gap structure.

1.3 Outlines of the Thesis

In Chapter 2 and 3, the work on the modification of the single particle process by the many body environment is presented. Spontaneous decay is studied in Chapter 2 while photon recoil is studied in the Chapter 3. In Chapter 4, the study on the Tonks Girardeau gas with a local potential is presented, and in Chapter 5, the study on

the ultra-cold fermi gas under spatially modulated interaction is presented. Finally, in Chapter 6, a summary of the thesis and a discussion of the directions for future studies are given.

CHAPTER II

Spontaneous Decay of an Atom in a Dielectric

2.1 Introduction

An excited atom decays to its ground state by radiating a photon into vacuum modes. This phenomena was described theoretically by V. Weisskopf and E. Wigner in their 1930 paper [36]. The decay rate can be calculated directly from Fermi's golden rule and is determined by the density of states to which the system can decay and the magnitude of the transition matrix elements. It is obvious that the environment in which the atom finds itself can significantly modify such a process. In particular, the problem of spontaneous emission from an atom imbedded inside a dielectric has attracted considerable interest [37][38][40].

Most theoretical treatments of this problem follow a macroscopic approach[12]. In a macroscopic picture, the modification of the photon density of states can be accounted for directly by assuming an index of refraction for the dielectric. A more subtle modification, however, arises from local field effects. Based on different models of the local environment of the imbedded atom, one obtains different types of local field corrections to the spontaneous decay rate Γ_0 of the impurity atom. For example, if the local environment is modeled as a virtual cavity, the local field can

be calculated as

$$E_{local} = \left(\frac{2+\epsilon}{3}\right) E_{external},$$

which leads to the decay rate of the so-called virtual cavity model,

$$\Gamma_{virtual} = \sqrt{\epsilon}\left(\frac{\epsilon+2}{3}\right)^2 \Gamma_0. \tag{2.1}$$

Another model known as the "real" cavity model, involves the assumption that an empty spherical cavity surrounds the emitter. The local field is

$$E_{local} = \frac{3\epsilon}{2\epsilon+1} E_{external},$$

and this gives a decay rate,

$$\Gamma_{real} = \sqrt{\epsilon}\left(\frac{3\epsilon}{2\epsilon+1}\right)^2 \Gamma_0. \tag{2.2}$$

The quantity ϵ in the above equations is the permittivity of the dielectric. It is connected to the microscopic polarizability α by the Lorentz-Lorenz relation

$$\epsilon = 1 + \frac{N\alpha}{1 - \frac{1}{3}N\alpha},$$

where N is the dielectric number density.

It is of some interest to expand the decay rate in powers of Na. The first order term corresponds to the photon scattered by one of the media atoms, and the second order term corresponds to the photon scattered by two media atoms. Expansions for the decay rates in powers of $N\alpha$ yield

$$\Gamma_{real} = [1 + \frac{7}{6}N\alpha + \frac{19}{72}(N\alpha)^2 + O(N\alpha)^3]\Gamma_0 \tag{2.3}$$

and

$$\Gamma_{virtual} = [1 + \frac{7}{6}N\alpha + \frac{17}{24}(N\alpha)^2 + O(N\alpha)^3]\Gamma_0. \tag{2.4}$$

To first order in $N\alpha$, the real and virtual cavity models give identical results, but they differ in higher order. To determine the validity range of these macroscopic models, calculations using a somewhat more fundamental approach are needed. Several attempts at such microscopic models involve a polariton approach for crystals [39], and a Green's function approach for crystals [41] and disordered dielectrics [42]. In the polariton method, the interaction between the vacuum radiation field and the crystal atoms is solved exactly; the eigenmodes of this system are the polaritons. The source atom then decays by radiating polaritons. This polariton calculation agrees with the virtual cavity result [39]. In the Green's function approach, the modification of the decay rate results from scattering of radiation emitted from the source atom by the dielectric, calculated to all orders in the dielectric density. This calculation reproduces the virtual cavity result with the source atom at an interstitial position and the real cavity result with source atom at a substitutional position in the crystal [41]. For disordered dielectrics, the Green's function method gives the virtual cavity result [42].

All the above calculations are carried out in momentum space. For homogenous media, the use of momentum space can simplify the problem because the momentum of the photon is conserved when scattering from an infinitely large homogenous medium. This simplification allows for a non-perturbative calculation of the local field correction. In calculating the local field correction we are, however, interested in the short distance behavior (local environment). It is therefore more transparent to carry out a calculation in configuration space. Such calculations are generally complicated and the problem can be treated only perturbatively. In our study of the problem, we used an amplitude method in configuration space.

The amplitude method was first used by M. E. Crenshaw and C. M. Bowden [43]

and later extended by P. R. Berman and P. W. Milonni [44] to an isotropic dielectric. The method represents a direct calculation of the modification of the decay rate as a perturbation series in $N\alpha$ [43], [44]. To first order in $N\alpha$, the radiation emitted by the source atom is scattered back to the source atom separately by each dielectric atom; the resultant decay rate agrees with both the virtual and real cavity models to first order in $N\alpha$ [44].

In this chapter, the amplitude method is extended to second order by including scattering events in which the radiation emitted by the source atom is scattered back to the source atom by a combined scattering from two dielectric atoms. It will be seen that the result differs from those of both the real and virtual cavity models; however, when contributions to the decay rate originating from scattering by two dielectric atoms located at the same physical point are included, the calculation reverts to the virtual cavity model. The content of this chapter is based in large part on Ref. [8].

2.2 Model Hamiltonian

The physical system consists of a source atom and a medium of dielectric atoms. The source atom, located at $\mathbf{R} = 0$, has a $J = 0$ ground state and a $J = 1$ excited state, the frequency separation of the ground and excited state denoted by ω_0. The uniformly distributed dielectric atoms have $J = 0$ ground states and $J = 1$ excited states, the frequency separation of the ground and excited state denoted by ω. At $t = 0$, the source atom is excited to the $m = 0$ excited state sublevel, the dielectric atoms are all in their ground states, and there are no photons in the field. The process we consider is radiation emitted by the source atom that is scattered by dielectric atoms back to the source atom. It is assumed that $|\omega - \omega_0| / \Gamma_0 \gg 1$ but that $|\omega - \omega_0| / (\omega + \omega_0) \ll 1$ [rotating wave approximation (RWA)].

We use a multipolar Hamiltonian [45]. The free part is

$$H_0 = \frac{\hbar\omega_0}{2}\sigma_z + \sum_j \sum_{m=-1}^{1} \frac{\hbar\omega}{2}\sigma_z^{(j)}(m) + \hbar\omega_{\mathbf{k}} a^\dagger_{\mathbf{k}\lambda} a_{\mathbf{k}\lambda}, \tag{2.5}$$

where $\sigma_z = (|2\rangle\langle 2| - |1\rangle\langle 1|)$, $|2\rangle$ and $|1\rangle$ are the $m = 0$ excited and $J = 0$ ground state eigenkets of the source atom, respectively, $\sigma_z^{(j)}(m) = \left(|m\rangle^{(j)}\langle m| - |g\rangle^{(j)}\langle g|\right)$ is the population difference operator between excited state $|J = 1, m\rangle$ and ground state $|J = 0, g\rangle$ of dielectric atom j, and $a_{\mathbf{k}\lambda}$ is the annihilation operator for a photon having momentum $\mathbf{k}$ and polarization λ. A summation convention is used, in which any repeated symbol on the right hand side of an equation is summed over, unless it also appears on the left-hand side of the equations.

The interaction part of the Hamiltonian is,

$$V = -\mathbf{d}_0 \cdot \frac{\mathbf{D}(0)}{\epsilon_0} - \mathbf{d}_j \cdot \frac{\mathbf{D}(\mathbf{R}_j)}{\epsilon_0}, \tag{2.6}$$

where $\mathbf{d}_0$ and $\mathbf{d}_j$ are the dipole operators of the source atom located at the origin and a dielectric atom located at position $\mathbf{R}_j$ respectively. The operator $\mathbf{D}$ is the displacement field having positive frequency component

$$\mathbf{D}_+(\mathbf{R}) = i\epsilon_0 \sum_{\mathbf{k},\lambda} \sqrt{\frac{\hbar\omega_{\mathbf{k}}}{2\epsilon_0 V}}\epsilon_{\mathbf{k}}^{(\lambda)} a_{\mathbf{k}\lambda} e^{i\mathbf{k}\cdot\mathbf{R}}, \tag{2.7}$$

where V is the quantization volume and $\epsilon_{\mathbf{k}}^{(\lambda)}$ is an unit polarization vector, with

$$\epsilon_{\mathbf{k}}^{(1)} = \cos\theta_{\mathbf{k}}\cos\phi_{\mathbf{k}}\hat{\mathbf{x}} + \cos\theta_{\mathbf{k}}\sin\phi_{\mathbf{k}}\hat{\mathbf{y}} - \sin\theta_{\mathbf{k}}\hat{\mathbf{z}}, \tag{2.8}$$

$$\epsilon_{\mathbf{k}}^{(2)} = -\sin\phi_{\mathbf{k}}\hat{\mathbf{x}} + \cos\phi_{\mathbf{k}}\hat{\mathbf{y}}. \tag{2.9}$$

In the RWA, one can write

$$V = \sum_{\mathbf{k}} \hbar g_{\mathbf{k}} (\sigma_+ a_{\mathbf{k}} - a_{\mathbf{k}}^\dagger \sigma_-)$$
$$+ \sum_{\mathbf{k},\lambda,m} \hbar \left[g'_{\mathbf{k}\lambda}(m) \sigma_+^{(j)}(m) a_{\mathbf{k}\lambda} e^{i\mathbf{k}\cdot\mathbf{R}} + g'_{\mathbf{k}\lambda}(m)^* a_{\mathbf{k}\lambda}^\dagger \sigma_-^{(j)}(m) e^{-i\mathbf{k}\cdot\mathbf{R}} \right]; \tag{2.10}$$

where

$$g_{\mathbf{k}} = -i\sqrt{\frac{\omega_{\mathbf{k}}}{2\hbar\epsilon_0 V}}\mu(\epsilon_{\mathbf{k}}^{(\lambda)})_0 \tag{2.11}$$

$$g'_{\mathbf{k}\lambda} = -i\sqrt{\frac{\omega_{\mathbf{k}}}{2\hbar\epsilon_0 V}}\mu'(\epsilon_{\mathbf{k}}^{(\lambda)})^*_m, \tag{2.12}$$

$\sigma_\pm$ are raising and lowering operators for the source atom, $\sigma_\pm^{(j)}(m)$ are raising and lowering operators between the excited state $|J=1,m\rangle$ and the ground state $|J=0,g\rangle$ of dielectric atom j, μ is $\sqrt{3}$ times the reduced matrix element of the dipole operator $\mathbf{d}_0$ and μ' is $\sqrt{3}$ times the reduced matrix element between ground and excited state manifolds of the medium atoms. The quantities

$$(\epsilon_{\mathbf{k}}^{(\lambda)})_{\pm 1} = \mp\frac{(\epsilon_{\mathbf{k}}^{(\lambda)})_x \pm i(\epsilon_{\mathbf{k}}^{(\lambda)})_y}{\sqrt{2}}$$
$$(\epsilon_{\mathbf{k}}^{(\lambda)})_0 = (\epsilon_{\mathbf{k}}^{(\lambda)})_z$$

are spherical components of the polarization vectors. The source atom interacts only with the z component of the radiation field.

2.3 Perturbative Calculation in Orders of $N\alpha$

There are three relevant state amplitudes of the system: b_2, the state amplitude for the source atom to be in state $|2\rangle = |J=1,m=0\rangle$ and all dielectric atoms in their ground states, $b_{m_j,}$ the state amplitude for dielectric atom j to be in excited state $|J=1,m\rangle$ all other atoms in their ground states, and $b_{\mathbf{k}}$, the state amplitude

of a photon with momentum $\mathbf{k}$ present and no atomic excitation. In the interaction representation, the equations of motion are

$$i\hbar\dot{b}_2 = V_{2;\mathbf{k}} e^{-i(\omega_\mathbf{k}-\omega_0)t} b_k, \tag{2.13}$$

$$i\hbar\dot{b}_\mathbf{k} = V_{\mathbf{k};2} e^{i(\omega_\mathbf{k}-\omega_0)t} b_2 + V_{\mathbf{k};m_j} e^{i(\omega_\mathbf{k}-\omega)t} b_{m_j}, \tag{2.14}$$

$$i\hbar\dot{b}_{m_j} = V_{m_j;\mathbf{k}} e^{-i(\omega_\mathbf{k}-\omega)t} b_\mathbf{k}. \tag{2.15}$$

Here the $V_{2;\mathbf{k}}$ and $V_{mj;\mathbf{k}}$ are the matrix elements of the interaction part of the Hamiltonian. By formally integrating Eq. (2.14) and substituting it back to Eqs. (2.13,2.15), we obtain the coupled equations for b_2 and b_{m_j}

$$\begin{aligned}\dot{b}_2 = &-\frac{1}{\hbar^2}\int_0^t V_{2;\mathbf{k}}\, V_{\mathbf{k};2} e^{-i(\omega_k-\omega_0)(t-t')} b_2(t')dt' \\ &- \frac{e^{i\Delta t}}{\hbar^2}\int_0^t V_{2;\mathbf{k}}\, V_{\mathbf{k};m_j} e^{-i(\omega_\mathbf{k}-\omega)(t-t')} b_{m_j}(t')dt', \qquad (2.16a)\\ \dot{b}_{m_j} = &-\frac{1}{\hbar^2}\int_0^t V_{m_j;\mathbf{k}}\, V_{\mathbf{k};m'_{j'}} e^{-i(\omega_k-\omega)(t-t')} b_{m'_{j'}}(t')dt' \\ &- \frac{e^{-i\Delta t}}{\hbar^2}\int_0^t V_{m_j;\mathbf{k}}\, V_{\mathbf{k};2} e^{-i(\omega_k-\omega_0)(t-t')} b_2(t')dt', \qquad (2.16b)\end{aligned}$$

where $\Delta = \omega_0 - \omega$. In the Weisskopf-Wigner approximation, one evaluates $V_{2;\mathbf{k}}\, V_{\mathbf{k};2}$ and $V_{m_j;\mathbf{k}}\, V_{\mathbf{k};m_j}$ with k equal to ω_0/c and ω/c, respectively. The integration over k gives a delta function of $t-t'$ and one finds,

$$\begin{aligned}-\frac{1}{\hbar^2}\int_0^t V_{2;\mathbf{k}}\, V_{\mathbf{k};2} e^{-i(\omega_k-\omega_0)(t-t')} b_2(t')dt' &= -\gamma b_2(t) \\ -\frac{1}{\hbar^2}\int_0^t V_{m_j;\mathbf{k}}\, V_{\mathbf{k};m_j} e^{-i(\omega_k-\omega)(t-t')} b_{mj}(t')dt' &= -\gamma' b_m(t),\end{aligned}$$

where

$$\begin{aligned}\gamma &= \left(\frac{1}{4\pi\epsilon_0}\right) 2\mu^2\omega_0^3/3\hbar c^3; \\ \gamma' &= \left(\frac{1}{4\pi\epsilon_0}\right) 2\mu'^2\omega^3/3\hbar c^3,\end{aligned}$$

are half the excited state decay rates of the source and medium atoms, respectively. In Eq. (2.16b), besides the $\gamma' b_m(t)$ term, there are terms that couple b_{m_j} to $b_{m'_{j'}}$, corresponding to scattering of a photon from an atom in position j to an atom in position j'. The summations over $\mathbf{k}$ in the remaining terms can be carried out in a straightforward manner by transforming them to integrals using the prescription $\sum_{\mathbf{k}} \to \left[\mathcal{V}/(2\pi)^3\right] \int d\mathbf{k}$. One finds

$$\dot{b}_2 = -\gamma b_2 - \gamma(\frac{\mu'}{\mu}) e^{i\Delta t} G_{0,m_j}(\mathbf{R}_j, \omega) b_{m_j}(t); \tag{2.17a}$$

$$\dot{b}_{m_j} = -\gamma' b_{m_j} - \gamma(\frac{\mu'}{\mu}) e^{-i\Delta t} G_{m,0}(\mathbf{R}_j, \omega_0) b_2(t) - \gamma' G_{m_j,m'_s}(\mathbf{R}_j - \mathbf{R}_s, \omega) b_{m'_s}(t). \tag{2.17b}$$

We have set $b_2(t-\tau) \approx b_2(t)$ and $b_{m_j}(t-\tau) \approx b_{m_j}(t)$ on the assumption that $\gamma R_0/c, \gamma' R_0/c \ll 1$, where R_0 is the sample size. The quantity $G_{m_j,m'_s}(\mathbf{R}_j - \mathbf{R}_s, \omega)$ is a propagator for scattering from a dielectric atom in sublevel m_j at position $\mathbf{R}_j$ to one in the sublevel m_s at position $\mathbf{R}_s$, given by

$$G_{m_j,m'_s}(\mathbf{R},\omega) = \frac{3}{8\pi} \frac{1}{\pi\omega^3} \int_0^t d\tau \int_{-\infty}^{\infty} d\omega_k \omega_k^3 e^{-i(\omega_k - \omega)\tau} \int d\Omega_{\mathbf{k}} (\epsilon_{\mathbf{k}}^{(\lambda)})^*_{m_j} (\epsilon_{\mathbf{k}}^{(\lambda)})_{m'_s} e^{i\mathbf{k}\cdot\mathbf{R}}, \tag{2.18}$$

while $G_{m,0}(\mathbf{R}_j, \omega)$ is a propagator for scattering from the source atom to a dielectric atom in sublevel m_j at position $\mathbf{R}_j$. In what follows we ignore the difference between ω_0 and ω, consistent with the RWA. The integration over momentum leads to Dirac delta functions of the form $\delta(R - ct)$ and $\delta(R + ct)$. The integration over τ in the range from 0 to t guarantees that only the retarded solution, corresponding to $\delta(R - ct)$, is taken into account. The propagator can be evaluated explicitly. We calculate explicitly $G_{1,1}(\mathbf{R},\omega)$ given in Eq. (2.18). The other $G_{m,m'}(\mathbf{R},\omega)$ are calculated in a similar fashion. To carry out the angular integrations, one expands

$e^{i\mathbf{k}\cdot\mathbf{R}}$ as

$$e^{i\mathbf{k}\cdot\mathbf{R}} = 4\pi \sum_{m=-l}^{l} i^l Y^*_{lm}(\hat{\mathbf{k}}) Y_{lm}(\hat{\mathbf{R}}) j_l(kR), \tag{2.19}$$

uses the fact that $(\epsilon^{(\lambda)}_{\mathbf{k}})^*_1(\epsilon^{(\lambda)}_{\mathbf{k}})_1 = \frac{1}{2}(1+\cos^2\theta) = \frac{\sqrt{4\pi}}{3}[2Y_{00}(\hat{\mathbf{k}}) + \frac{1}{\sqrt{5}}Y_{20}(\hat{\mathbf{k}})]$, and the orthogonality of the spherical harmonics, to obtain

$$G_{1,1}(\mathbf{R},\omega) = \frac{1}{\sqrt{\pi}\omega^3}\int_0^t d\tau \int_{-\infty}^{\infty} d\omega_k \omega_k^3 e^{-i(\omega_k-\omega)\tau}[2Y_{00}(\hat{\mathbf{R}})j_0(kR) - \frac{1}{\sqrt{5}}Y_{20}(\hat{\mathbf{R}})j_2(kR)] \tag{2.20}$$

The spherical Bessel function can written in terms of spherical Hankel functions as $j_l(kR) = \frac{1}{2}[h_l(kR) + h^*_l(kR)]$, transforming Eq. (2.20) into

$$\begin{aligned} G_{1,1}(\mathbf{R},\omega) &= \frac{1}{2\sqrt{\pi}}\int_0^t d\tau \int_{-\infty}^{\infty} d\omega_k e^{-i(\omega_k-\omega)\tau} \\ &\quad \times\{2Y_{00}(\hat{\mathbf{R}})[h_0(kR) + h^*_0(kR)] - \frac{1}{\sqrt{5}}Y_{20}(\hat{\mathbf{R}})[h_2(kR) + h^*_2(kR)]\}. \end{aligned}$$

In the calculation we always make the *Wigner-Weisskopf* approximation. Differences between ω, ω_0 and ω_k are neglected except they appear as exponential factors. In integrating over ω_k, the $h^*_l(kR)$ terms give a contribution proportional to $\delta(R/c+\tau)$ while the $h_l(kR)$ terms give a contribution proportional to $\delta(R/c-\tau)$. We retain only the $\delta(R/c-\tau)$ contributions since they correspond to the retarded solution (outgoing spherical waves). As a consequence, we find

$$G_{1,1}(\mathbf{R},\omega) = \sqrt{4\pi}h_0(k_0R)Y_{0,0}(\hat{\mathbf{R}}) - \frac{1}{2}\sqrt{\frac{4\pi}{5}}h_2(k_0R)Y_{2,0}(\hat{\mathbf{R}}) \tag{2.21}$$

We simply list the explicit expressions for all the propagators in the following.

$$G_{11} = \sqrt{4\pi} h_0(k_0 R) Y_{0,0}(\hat{\mathbf{R}}) - \frac{1}{2}\sqrt{\frac{4\pi}{5}} h_2(k_0 R) Y_{2,0}(\hat{\mathbf{R}}); \tag{2.22a}$$

$$G_{00} = \sqrt{4\pi} h_0(k_0 R) Y_{0,0}(\hat{\mathbf{R}}) + \sqrt{\frac{4\pi}{5}} h_2(k_0 R) Y_{2,0}(\hat{\mathbf{R}}); \tag{2.22b}$$

$$G_{1,-1} = -\frac{3}{2}\sqrt{\frac{8\pi}{15}} h_2(k_0 R) Y_{2,-2}(\hat{\mathbf{R}}); \tag{2.22c}$$

$$G_{-1,1} = -\frac{3}{2}\sqrt{\frac{8\pi}{15}} h_2(k_0 R) Y_{2,2}(\hat{\mathbf{R}}); \tag{2.22d}$$

$$G_{1,0} = -\frac{3}{2}\sqrt{\frac{4\pi}{15}} h_2(k_0 R) Y_{2,-1}(\hat{\mathbf{R}}); \tag{2.22e}$$

$$G_{-1,0} = -\frac{3}{2}\sqrt{\frac{4\pi}{15}} h_2(k_0 R) Y_{2,1}(\hat{\mathbf{R}}), \tag{2.22f}$$

where $Y_{\ell,m}(\hat{\mathbf{R}})$ is a spherical harmonic and $k_0 = \omega_0/c$. The remaining G_{m_j,m'_s}s are obtained using $G_{-1,-1} = G_{11}$, $G_{0,-1} = -G_{1,0}$, and $G_{0,1} = -G_{-1,0}$. The spherical Hankel functions of the first kind, $h_0(k_0R)$ and $h_2(k_0R)$, conform to the appropriate boundary conditions in which only outgoing scattered waves are considered.

In order to solve Eqs. (2.17a,2.17b), we assume that b_2 varies slowly on the time scale $1/\Delta$ (adiabatic approximation). If $b_{m_j} = y_{m_j} e^{-i\Delta t}$, Eqs.(2.17a,2.17b) are transformed into

$$\dot{b}_2 = -\gamma b_2 - \gamma(\frac{\mu'}{\mu}) G_{0,m}(\mathbf{R}_j, \omega_0) y_{m_j}(t) \tag{2.23a}$$

$$(\gamma' - i\Delta) y_{m_j} = -\gamma(\frac{\mu'}{\mu}) G_{m,0}(\mathbf{R}_j, \omega_0) b_2(t) - \gamma' G_{m_j,m'_s}(\mathbf{R}_j - \mathbf{R}_s, \omega_0) y_{m'_s}(t). \tag{2.23b}$$

The formal solution for $\dot{b}_2$ is

$$\dot{b}_2 = -\gamma b_2 + \gamma(\frac{\mu'}{\mu}) G_{0,m_j}(\mathbf{R}_j, \omega_0) \left[\frac{1}{\gamma' - i\Delta + \gamma' \mathbf{G}}\right]_{m_j,m'_s} \gamma(\frac{\mu'}{\mu}) G_{m'_s,0}(\mathbf{R}_s, \omega_0) b_2, \tag{2.24}$$

where $\mathbf{G}$ is an $3N \times 3N$ matrix having matrix elements $G_{m_j,m'_s}(\mathbf{R}_j - \mathbf{R}_s, \omega_0)$. This can be expanded as a power series in $N\alpha$ with $\alpha = -\frac{4\pi\mu'^2}{\hbar\Delta}$. To second order, one

finds

$$\dot{b}_2 = -\gamma b_2 \left[\begin{array}{c} 1 + iN\alpha \frac{k_0^3}{6\pi N} G_{0,m_j}(\mathbf{R}_j, \omega_0) G_{m_j,0}(\mathbf{R}_j, \omega_0) \\ -(N\alpha)^2 (\frac{k_0^3}{6\pi N})^2 G_{0,m_j}(\mathbf{R}_j, \omega_0) G_{m_j,m'_s}(\mathbf{R}_j - \mathbf{R}_s, \omega_0) G_{m'_s,0}(\mathbf{R}_s, \omega_0) \end{array} \right]. \tag{2.25}$$

The term linear in the density was first calculated by P. R. Berman and P. W. Milonni [44]. In this order,

$$\dot{b}_2 = -\gamma b_2 \left[1 + iN\alpha \frac{k_0^3}{6\pi N} G_{0,m_j}(\mathbf{R}_j, \omega_0) G_{m_j,0}(\mathbf{R}_j, \omega_0) \right]. \tag{2.26}$$

Using the prescription that $\sum_j \to N \int d^3R$, one finds

$$\begin{aligned} \dot{b}_2 &= -\gamma b_2 - \gamma i b_2 N\alpha \frac{k_0^3}{6\pi} \int d^3R G_{0,m_j}(\mathbf{R}_j, \omega_0) G_{m_j,0}(\mathbf{R}_j, \omega_0) \\ &= -\gamma b_2 - i\gamma \frac{N\alpha}{3} \left(A_0 + A_1 + A_{-1} \right) b_2, \end{aligned}$$

where the integrals A_m are given by

$$\begin{aligned} A_0 &= 2 \int_0^\infty d\rho \left\{ \frac{-1}{\rho^2} + \frac{1}{5} \left[i \left(\frac{3}{\rho^3} - \frac{1}{\rho} \right) + \frac{3}{\rho^2} \right]^2 \right\} \rho^2 e^{2i\rho}; \\ A_1 &= A_{-1} = 2 \int_0^\infty d\rho \left\{ \frac{3}{20} \left[i \left(\frac{3}{\rho^3} - \frac{1}{\rho} \right) + \frac{3}{\rho^2} \right]^2 \right\} \rho^2 e^{2i\rho}. \end{aligned}$$

with dimensionless variable $\rho = k_0 R$.

The real part of A_m corresponds to a modification of the spontaneous decay rate, while its imaginary part gives rise to a level shift. The imaginary part is divergent due to the singular behavior of $G(r, \omega_0)$ at small distances. This divergent behavior has to be renormalized to give a physical result. Practically, one usually uses a short distance cutoff based on the fact that two atoms experience repulsion when their electron wavefunctions overlap. On the other hand, the real part of A_m, corresponding to the modification of the decay rate, is well-behaved. In the limit when two atoms overlap with each other, a simple calculation leads to a maximum

decay rate of 2γ. For very large R_j, a convergence factor must be added to insure that the integrals are well-behaved at infinity. Actually, in neglecting retardation, we have omitted a step function $\Theta(t - 2R/c)$ in the second term on the right hand side of Eq. (2.17a,2.17b). This step function would provide a natural limit for the R integration, removing the need to add a convergence factor. When a convergence factor of the form $e^{-g\rho}$ is included, the integral can be evaluated analytically. Setting $g = 0$ in the final result, one finds $A_0 = -2$ and $A_1 = -3/4$. It then follows that

$$\dot{b}_2 = -\gamma \left(1 + \frac{7}{6} N\alpha\right) b_2. \tag{2.27}$$

This result agrees with both the real and virtual cavity result.

In order to distinguish real and virtual cavity model, one needs to extend the perturbative calculation to second order,

$$\frac{\delta\gamma^{(2)}}{\gamma} = -(N\alpha)^2 (\frac{k_0^3}{6\pi N})^2 G_{0,m_j}(\mathbf{R}_j, \omega_0) G_{m_j,m_s'}(\mathbf{R}_j - \mathbf{R}_s, \omega_0) G_{m_s',0}(\mathbf{R}_s, \omega_0). \tag{2.28}$$

Using $\sum \to N \int d\mathbf{R}$, one finds

$$\frac{\delta\gamma^{(2)}}{\gamma} = -(N\alpha)^2 (\frac{k_0^3}{6\pi})^2 \int\int d\mathbf{R}_2 d\mathbf{R}_1 G_{0,m_j}(\mathbf{R}_2, \omega_0) G_{m_j,m_s'}(\mathbf{R}, \omega_0) G_{m_s',0}(\mathbf{R}_1, \omega_0). \tag{2.29}$$

The calculation for $\frac{\delta\gamma^{(2)}}{\gamma}$ is tedious, since it involves contributions from different m and m' (nine terms). We show how to calculate one specific contribution, $m_j = 1$, $m_s' = 1$, and then give the final results for the other components. Substituting Eqs.

(2.22a,2.22e) in Eq. (2.29), we find

$$\frac{\delta\gamma^{(2)}(1,1)}{\gamma} = (N\alpha)^2(\frac{k_0^3}{6\pi})^2\frac{6\pi^{\frac{3}{2}}}{5}\int\int d\mathbf{R}_1 d\mathbf{R}_2$$
$$\times h_2(k_0R_2)Y_{2,1}(\hat{\mathbf{R}}_2)h_0(k_0R_{21})Y_{0,0}(\hat{\mathbf{R}}_{21})h_2(k_0R_1)Y_{2,-1}(\hat{\mathbf{R}}_1)$$
$$-(N\alpha)^2(\frac{k_0^3}{6\pi})^2\frac{3\pi^{\frac{3}{2}}}{5\sqrt{5}}\int\int d\mathbf{R}_1 d\mathbf{R}_2$$
$$\times h_2(k_0R_2)Y_{2,1}(\hat{\mathbf{R}}_2)h_2(k_0R_{21})Y_{2,0}(\hat{\mathbf{R}}_{21})h_2(k_0R_1)Y_{2,-1}(\hat{\mathbf{R}}_1). \qquad (2.30)$$

To evaluate this, we expand the Hankel functions as [46]

$$h_l(k_0R_{21})Y_{l,m}(\hat{\mathbf{R}}_{21}) = i^{l_1+l_2-l}(-1)^{l_2+m}\sqrt{4\pi(2l+1)(2l_1+1)(2l_2+1)}$$
$$\times\left[\Theta(R_2-R_1)+(-1)^l\Theta(R_1-R_2)\right]\begin{pmatrix} l_1 & l & l_2 \\ 0 & 0 & 0\end{pmatrix}\begin{pmatrix} l_1 & l & l_2 \\ m_1 & m & m_2\end{pmatrix}$$
$$\times h_{l_1}(k_0R_>)j_{l_2}(k_0R_<)Y_{\ell_1,m_1}(\hat{\mathbf{R}}_>)Y_{\ell_2,m_2}(\hat{\mathbf{R}}_<), \qquad (2.31)$$

where $\begin{pmatrix}\cdots\\ \cdots\end{pmatrix}$ is a $3-j$ symbol, $j_l(x)$ is a spherical Bessel function, and $R_>$ ($R_<$) is the larger (smaller) of R_1 and R_2. When this expansion is used in Eq. (2.30), the angular integration selects only $l = 2, 0$ and $m = 1, -1, 0$ terms, such that

$$\frac{\delta\gamma^{(2)}(1,1)}{\gamma} = -\frac{(N\alpha)^2}{7}\int_0^\infty d\rho_2\rho_2^2\int_0^{\rho_2} d\rho_1\rho_1^2 h_2(\rho_2)h_2(\rho_1)h_2(\rho_2)j_2(\rho_1) \qquad (2.32)$$

with $\rho_1 = k_0R_1$, $\rho_2 = k_0R_2$. To evaluate the above integral, we add a convergence factor $e^{-\epsilon\rho_2}$, and eventually take the limit $\epsilon \to 0$. The imaginary part of the integral diverges as $\rho_2 \to 0$, but the real part is finite and gives the local field correction to the decay rate. The result is

$$\frac{\delta\gamma^{(2)}(1,1)}{\gamma} = \frac{15}{112}(N\alpha)^2.$$

We note that the contributions from other terms may involve factors such as

$$h_0(k_0R_1)h_2(k_0R_{21})h_2(k_0R_2).$$

Direct expansion of $h_2(k_0R_{21})$ gives a divergent result for the decay rate, when the contribution from $R_1 = R_2$ is excluded. Instead, we expand $h_0(k_0R_1)$ in terms of R_{21} and R_2 and integrate over these two variables. This procedure leads to the finite results given in the paper. The fact that we get divergent results when directly expanding $h_2(k_0R_{21})$ in terms of R_1 and R_2 can be traced to the fact that one finds different values for the integrals at $R_1 = R_2$ depending on whether the limit $R_1 = R_2$ is approached from above or below. If the contribution from $R_1 = R_2$ is included, it leads to a divergence that exactly cancels the divergence from the first integral and again leads to the same result given in the text.

The corresponding results for the other terms are

$$\begin{aligned}
\frac{\delta\gamma^{(2)}(-1,-1)}{\gamma} &= \frac{\delta\gamma^{(2)}(1,1)}{\gamma} = \frac{15}{112}(N\alpha)^2, \\
\frac{\delta\gamma^{(2)}(0,0)}{\gamma} &= \frac{25}{63}(N\alpha)^2, \\
\frac{\delta\gamma^{(2)}(0,1)}{\gamma} &= \frac{\delta\gamma^{(2)}(1,0)}{\gamma} = \frac{\delta\gamma^{(2)}(-1,0)}{\gamma} = \frac{\delta\gamma^{(2)}(0,-1)}{\gamma} = \frac{3}{28}(N\alpha)^2, \\
\frac{\delta\gamma^{(2)}(-1,1)}{\gamma} &= \frac{\delta\gamma^{(2)}(1,-1)}{\gamma} = -\frac{3}{56}(N\alpha)^2,
\end{aligned}$$

giving a total second order correction to the decay rate of

$$\frac{\delta\gamma^{(2)}}{\gamma} = 2\frac{\delta\gamma^{(2)}(1,1)}{\gamma} + \frac{\delta\gamma^{(2)}(0,0)}{\gamma} + 4\frac{\delta\gamma^{(2)}(0,1)}{\gamma} + 2\frac{\delta\gamma^{(2)}(-1,1)}{\gamma} = \frac{71}{72}(N\alpha)^2. \quad (2.33)$$

This result differs from both the virtual $\left[\frac{51}{72}(N\alpha)^2\right]$ and real $\left[\frac{19}{72}(N\alpha)^2\right]$ cavity models.

2.4 Comparing with the Green's Function Approach

Our result can be compared with Fleischhauer's [42]. Instead of writing amplitude equations and finding the photon propagator, Fleischhauer used the dyadic Maxwell-Helmholtz equation to solve for the propagator,

$$\left(\frac{1}{c^2}\frac{\partial^2}{\partial t^2} + \bigtriangledown \times \bigtriangledown\right) D^0\left(r_1t_1; r_2t_2\right) = -\frac{i\hbar}{\varepsilon_0}\frac{\omega^2}{c^2}\delta\left(\mathbf{r}_1 - \mathbf{r}_2\right)\delta\left(t_1 - t_2\right)\mathbf{1} \quad (2.34)$$

The solution can be written directly in momentum space,

$$D^0(\mathbf{q},\omega) = \frac{i\hbar}{\epsilon_0}\left[\frac{k^2}{k^2-q^2+i0}\left(\mathbf{1}-\hat{\mathbf{q}}\otimes\hat{\mathbf{q}}\right)+\hat{\mathbf{q}}\otimes\hat{\mathbf{q}}\right].$$

One can transform it to configuration space as

$$D^{(0)}(\mathbf{x},\omega) = -\frac{i\hbar}{\epsilon_0}\frac{\omega^2}{c^2}\frac{e^{ikx}}{4\pi x}\left[P(ikx)\,\mathbf{1}+Q(ikx)\,\hat{\mathbf{x}}\otimes\hat{\mathbf{x}}\right]+\frac{i\hbar}{3\varepsilon_0}\delta(x)\,\mathbf{1},$$

where

$$P(z) = 1-\frac{1}{z}+\frac{1}{z^2};$$
$$Q(z) = -1+\frac{3}{z}-\frac{3}{z^2}.$$

The $\delta(x)$ should be subtracted since it gives a finite contribution to the decay rate when two atoms overlap with each other, and the true photon propagator should be

$$F^{(0)}(\mathbf{x},\omega) = -\frac{i\hbar}{\epsilon_0}\frac{\omega^2}{c^2}\frac{e^{ikx}}{4\pi x}\left[P(ikx)\,\mathbf{1}+Q(ikx)\,\hat{\mathbf{x}}\otimes\hat{\mathbf{x}}\right].$$

Our propagator $G_{m,m'}(\mathbf{R},\omega)$ Eq. (2.18), can be cast into a tensor form,

$$G_{m,m'}(\mathbf{R},\omega) = -\frac{3}{2}i\frac{4\pi}{k}\frac{e^{ikR}}{4\pi R}\left[P(ikR)\,\mathbf{1}+Q(ikR)\,\hat{\mathbf{R}}\otimes\hat{\mathbf{R}}\right].$$

We therefore find that the propagator we used in our study differs from the propagator used in Green's approach only by a prefactor. Both of them describe the field radiated by an oscillating dipole at frequency ω.

At this point, it seems a matter of taste to do the integration (2.29) in momentum or in configuration space. In the Green's function approach, the integral (2.29) is done in momentum space. It yields a virtual cavity result different from our finding [Eq. (2.33)]. The apparent discrepancy can be explained by the way we expand $h_l(k_0R_{21})Y_{l,m}(\hat{\mathbf{R}}_{21})$. The expansion we used is valid for $R_1 > R_2$ or $R_2 > R_1$, but is not defined for $R_1 = R_2$. For a well-behaved integral this will not make any difference

since $R_1 = R_2$ contributes a set of measure zero. In the present case, however, where the dipole-dipole interaction between dielectric atoms diverges when one atom is on top of the other atom, i.e. when $\mathbf{R}_1 = \mathbf{R}_2$, the contribution from $R_1 = R_2$ can be finite.

It is not easy to calculate this contribution in the original form of the integral (2.30). Instead, it proves useful to Fourier transform just *one* of the $G_{m,m'}$ in the integrand. As an example, we consider the integral in the second term of Eq. (2.30)

$$I = \int\int d\mathbf{R}_2 d\mathbf{R}_1 h_2(kR_2) Y_{2,1}(\hat{\mathbf{R}}_2) h_2(kR_{21}) Y_{2,0}(\hat{\mathbf{R}}_{21}) h_2(kR_1) Y_{2,-1}(\hat{\mathbf{R}}_1). \tag{2.35}$$

We Fourier transform $h_2(kR_{21})Y_{2,0}(\hat{\mathbf{R}}_{21})e^{-\epsilon R_{21}}$, using a convergence factor $e^{-\epsilon R_{21}}$ that is physically connected with the boundary condition of outgoing spherical waves. Carrying out the Fourier transform in Eq. (2.35), we find

$$\begin{aligned} I = & -\frac{4\pi i}{k^3} \int\int d\mathbf{R}_2 d\mathbf{R}_1 h_2(kR_2) Y_{2,1}(\hat{\mathbf{R}}_2) h_2(kR_1) Y_{2,-1}(\hat{\mathbf{R}}_1) \\ & \times \int \frac{d\mathbf{p}}{(2\pi)^3} \frac{p^2}{k^2 - p^2 + i\epsilon} Y_{2,0}(\hat{\mathbf{p}}) e^{i\mathbf{p}\cdot(\mathbf{R}_2 - \mathbf{R}_1)}. \end{aligned} \tag{2.36}$$

The angular integrations can be done by expanding $e^{i\mathbf{p}\cdot\mathbf{R}_2}$, $e^{-i\mathbf{p}\cdot\mathbf{R}_1}$ in terms of spherical harmonics and Bessel functions. In this manner one obtains

$$I = \frac{1}{14}\sqrt{\frac{5}{\pi}} \frac{(4\pi)^3 i}{k^3} \int\int dR_2 dR_1 R_2^2 R_1^2 h_2(kR_2) h_2(kR_1) \int \frac{dp}{(2\pi)^3} \frac{p^4}{k^2 - p^2 + i\epsilon}. \tag{2.37}$$

We are interested only in the contribution in the region where $R_1 = R_2$. This contribution can be isolated by integrating R_2 from $R_1 - a$ to $R_1 + a$, and then integrating the resultant expression over p using the method of residues. In the limit that both a and ϵ tend to zero, one obtains the contribution δI from the region $R_1 = R_2$ as

$$Re[\delta I] = Re[\frac{-1}{7}\sqrt{5\pi}\frac{2i}{k^3}\int dR_2 R_2^2 h_2(kR_2) h_2(kR_2)] = \frac{-5\sqrt{5\pi}}{7k^6} \tag{2.38}$$

(the imaginary part of δI diverges). The contribution from the sphere $R_1 = R_2$ is identical to that from $\mathbf{R}_1 = \mathbf{R}_2$ since all other points with $\mathbf{R}_1 \neq \mathbf{R}_2$ on the sphere are regular and contribute zero to the integral. The same calculation can be done for the first integral in the Eq. (2.30). For this term, there is no contribution from the region $R_1 = R_2$ (no delta function like term is found) since $h_0(kR_{21})$ has a lower order divergence at $R_{21} = 0$ than does $h_2(kR_{21})$.

Including contributions of the type (2.38), we find

$$\begin{aligned}
\frac{\delta\gamma^{(2)}(0,0)}{\gamma} &= \frac{1}{3}(N\alpha)^2, \\
\frac{\delta\gamma^{(2)}(1,1)}{\gamma} &= \frac{\delta\gamma^{(2)}(1,-1)}{\gamma} = \frac{7}{48}(N\alpha)^2, \\
\frac{\delta\gamma^{(2)}(0,1)}{\gamma} &= \frac{\delta\gamma^{(2)}(1,0)}{\gamma} = \frac{\delta\gamma^{(2)}(-1,0)}{\gamma} = \frac{\delta\gamma^{(2)}(0,-1)}{\gamma} = \frac{1}{12}(N\alpha)^2, \\
\frac{\delta\gamma^{(2)}(-1,1)}{\gamma} &= \frac{\delta\gamma^{(2)}(1,-1)}{\gamma} = -\frac{1}{8}(N\alpha)^2.
\end{aligned} \tag{2.39}$$

When these are summed, the total

$$\frac{\delta\gamma^{(2)}}{\gamma} = \frac{17}{24}(N\alpha)^2$$

agrees with the virtual cavity result.

2.5 Discussion

The modification of the decay rate of a source atom in a dielectric medium was calculated perturbatively. It was found that the first order calculation in $N\alpha$ agrees with both the real and virtual cavity model. To compare microscopic calculations with the macroscopic model, one has to extend the calculation in higher orders of $N\alpha$. In this chapter the second order contribution to the modified spontaneous emission rate of an impurity atom in a disordered dielectric has been calculated using a microscopic theory.

Depending on the manner in which overlapping atoms are treated, one arrives at different results. If the delta function contributions at $\mathbf{R}_1 = \mathbf{R}_2$ are included, the virtual cavity model is recovered, but if such terms are excluded, neither the real nor the virtual cavity model results are found. It seems to us somewhat of an open question at this point as to whether or not such contributions can be uniquely calculated once Eq. (2.24) is expanded in a power series in the density. The reason for this is that the expansion parameter is *not* small as interatomic distances tend to zero. That the expansion can lead to divergences is already evident if the integrations are carried out using a different set of variables. From physical considerations, however, the decay rate does not diverge, even for interparticle spacings much less than a wavelength. Actually, dielectric atoms within a sphere of radius $\lambda\,(\gamma'/\Delta)^{1/3}$ reradiate collectively; outside this radius, there is destructive interference resulting in some additional finite contribution to the decay rate. In dealing with a homogeneous dielectric, we have performed the ensemble average by integrating over all space assuming a constant density. This averaging process includes configurations where interparticle spacings are sufficiently small to invalidate the expansion (2.25). Nevertheless, the procedure has yielded finite results for the change in the decay parameter. To improve this situation, one has to treat contributions from atoms located at $r < \lambda\,(\gamma'/\Delta)^{1/3}$ and $r > \lambda\,(\gamma'/\Delta)^{1/3}$ separately. For contributions form the close atoms, one need to solve the time evolution of the source atom exactly. This can be done by some numerical simulation. After this contribution is obtained, it can then be combined with the perturbative calculation with a cutoff at small r to give the full result.

In our microscopic model, we have not included the external degree of freedom for the atoms. The atoms were simply modeled as point particles locating at fix

positions. In the real physical systems, the atom-atom interaction significantly modifies the atom locations. In general, one can conjecture that the density-density correlation has the following limits

$$\lim_{|\mathbf{r}_1-\mathbf{r}_2|\to 0} \langle n(\mathbf{r}_1)\, n(\mathbf{r}_2)\rangle = 0,$$

$$\lim_{|\mathbf{r}_1-\mathbf{r}_2|\to \infty} \langle n(\mathbf{r}_1)\, n(\mathbf{r}_2)\rangle = n(\mathbf{r}_1)\, n(\mathbf{r}_2)\,.$$

The correlation for two positions separated by a intermediate distance is the interpolation of these two limits. Our microscopic calculation includes the correct behavior at $|\mathbf{r}_1 - \mathbf{r}_2| = 0$. However, it does not incorporate the correct short distance correlation at $|\mathbf{r}_1 - \mathbf{r}_2| \neq 0$. The correlation simply jumps from one limit, $|\mathbf{r}_1 - \mathbf{r}_2| \to 0$ to the other limit, $|\mathbf{r}_1 - \mathbf{r}_2| \to \infty$. To give a satisfactory description of the local field correction, one has to develop a theory including both the atom internal and external degrees of freedom.

Different experiments support both the real and virtual cavity results [18][17][15]. The source atom in these experiments is usually an impurity ion in a protective molecular cage. No experiments of this nature have been carried out with impurity atomic radiators in a dielectric that consists of a dense atomic vapor. It may be possible to use an alkali metal atom as the source atom and rare gas atoms as the dielectric atoms. With such a system, one could not make the rotating wave approximation used in this paper, but the physics is not changed in any substantive manner. The key feature of the alkali metal - rare gas system is the extremely small quenching cross sections for rare gas collisions to inelastically change the electronic state of the alkali atom [47][48][49]. Any quenching cross sections would appear as a modification of the decay rate that would mask the sought after effect. For rare gas pressures on the order of 100 atmospheres, we estimate that a change in the decay

rate of order of 3% could be observed. To increase the effect it is necessary to find radiator atoms whose first excited state is radiatively coupled to the ground state and dielectric atoms whose lowest excited state is about 0.2eV above the energy of the excited state of the radiator. In this limit, quenching will be negligible, but the detuning Δ is decreased from the alkali-rare gas system by a factor of 50. At the same time, it is necessary to achieve a high pressure for the dielectric atoms. A possible system would be Li radiators with a high density sodium dielectric; the energy mismatch of Li and Na is about 0.25eV, giving a correction factor to the lithium decay rate of $1.3 \times 10^{-21} N$, where N is the sodium dielectric density in units of atoms/cm^3.

CHAPTER III

Photon Recoil of an Atom Inside a Dielectric

In the previous chapter, we presented a microscopic calculation of the spontaneous decay rate of a source atom inside a dielectric medium. When the source atom is cooled to the photon recoil energy, one generally needs to consider the recoil momentum imparted to the source atom as it radiates. This chapter gives an explicit calculation of such a momentum recoil.

3.1 Introduction

The momentum of a photon in a dispersive medium has been considered by many authors, due to its conceptual and practical importance. One of the issues in understanding photon momentum in a medium is how the momentum is conserved when a photon with momentum $\hbar\mathbf{k}$ in the vacuum is scattered from an atom in the medium to a new momentum state $\hbar\mathbf{k}'$ in the vacuum. Should the momentum imparted on the atom be the difference of the momenta in the vacuum $\hbar\mathbf{k}' - \hbar\mathbf{k}$ or the difference of the canonical photon momenta in the medium $n(\hbar\mathbf{k}' - \hbar\mathbf{k})$ [50]? One might argue [51] that, assuming the medium is dilute, the atom is localized in the vacuum space between particles of the medium, therefore the photon, before and after it strikes the atom, travels in the vacuum and its momentum should be conserved in terms

of the vacuum momenta. On the other hand [13], one can also argue that it is the macroscopic field of the incident wave that induces and interacts with polarizations and polarization currents of atoms in the medium and therefore the imparted momentum should be the difference of the canonical photon momenta in the medium. Experimentally, this issue has been studied in two systems. One measures the recoil of a mirror immersed in a liquid when the light is reflected from it [19][20], and more recently [51], a measurement of the recoil frequency of the Bose condensed ^{87}Rb using a two-pulse Ramsey interferometer. Both experiments confirm that atoms recoil according to canonical photon momenta.

Most theoretical studies related to this issue deal mainly with classical fields. Some of the recent work by Loudon [53][52] and Nelson [54] clarified some issues related to momentum in a dielectric from a quantum and microscopic perspective. Milonni and Boyd [50] consider a case where a source atom imbedded in the medium recoils due to its spontaneous decay. They find that the source atom recoils according to $n\hbar\omega_0/c$, where ω_0 is the atomic frequency and c is the speed of light in the vacuum. Their calculation is based on a Heisenberg picture approach and extinction theorem, where the operator expectation value, $\langle P^2 \rangle$ is calculated to be $n^2\hbar^2\omega_0^2/c^2$. Here we present a similar calculation in the Schrödinger picture. The calculation in the Schrödinger picture is particularly revealing because it includes explicitly processes that are responsible for the modification of the momentum imparted by the photon. As we show in the following, the photon traveling in the medium experiences a series of scatterings from media atoms. Different scattering amplitudes interfere to shift the central frequency of the field. Since the source atom is coupled directly to the field, by momentum conservation, the source atom recoils according to the modified central frequency of the radiation. Our calculation is based on a quantum field quantized in

free space, which allows a separate description of the field and the medium, i.e. any wavelength and frequency of the field are calculated unambiguously in the vacuum. The discussion of resolvent method is based on Ref. [14], and the calculation of the photon recoil is based on Ref. [9].

3.2 Resolvent Method

In this chapter, we present an alternative way of doing the microscopic calculation. Instead of writing amplitude equations for different states and then identifying terms corresponding to contributions from different processes [8], we adopt a resolvent approach [14], which allows us to write amplitudes directly from diagrammatic representations of the scattering processes. The evolution operator for a time dependent perturbation satisfies the following equation,

$$i\hbar\frac{d}{dt}U\left(t,t'\right)=\left[H_0+V\right]U\left(t,t'\right)$$

with boundary condition

$$U\left(t,t\right)=1.$$

The quantity H_0 is the time-independent unperturbed Hamiltonian and V is the perturbation. This can be transformed into an integral equation,

$$U\left(t,t'\right)=U_0\left(t,t'\right)+\frac{1}{i\hbar}\int_{t'}^{t}dt_1U_0\left(t,t_1\right)VU\left(t_1,t'\right). \tag{3.1}$$

Here $U_0\left(t,t'\right)$ is the zeroth order time evolution operator,

$$U_0\left(t,t'\right)=\exp\left[-iH_0\left(t-t'\right)/\hbar\right].$$

In order to simplify the integral equation, we make use of the following retarded and advanced propagators,

$$K_+(t,t') = U(t,t')\,\Theta(t-t')$$
$$K_-(t,t') = -U(t,t')\,\Theta(t'-t),$$

where $\Theta(t)$ is the Heaviside step function. With this transformation, Eq. (3.1) can be written as

$$K_+(t,t') = K_{0+}(t,t') + \frac{1}{i\hbar}\int_{-\infty}^{\infty} dt_1 K_{0+}(t,t_1)\,V K_+(t_1,t') \tag{3.2}$$
$$K_-(t,t') = K_{0-}(t,t') + \frac{1}{i\hbar}\int_{-\infty}^{\infty} dt_1 K_{0-}(t,t_1)\,V K_-(t_1,t'). \tag{3.3}$$

Note that the limits of the integration extend from minus infinity to plus infinity. Using the Fourier transforms,

$$G_+(E) = \frac{1}{i\hbar}\int_{-\infty}^{\infty} d\tau e^{iE\tau/\hbar} K_+(\tau)$$
$$G_-(E) = -\frac{1}{i\hbar}\int_{-\infty}^{\infty} d\tau e^{-iE\tau/\hbar} K_-(\tau),$$

one can recast Eqs. (3.2,3.3) into an algebraic equation

$$G(E) = G_0(E) + G_0(E)\,V G(E), \tag{3.4}$$

where

$$G(z) = \frac{1}{z-H}$$

is the so-called resolvent operator. Eq. (3.4) gives a simple way to calculate the full resolvent operators, $G(E)$, from the unperturbed resolvent operators, $G_0(E)$, using a type of gemometric series. It is not hard to relate the resolvent operator to the evolution operator by noting that $U(t,t') = K_+(t,t') - K_-(t,t')$. Such a formula is the basis of the resolvent method, written as

$$U(\tau) = \frac{1}{2\pi i}\int_{-\infty}^{\infty} dE e^{-iE\tau/\hbar}\left[G_-(E) - G_+(E)\right]. \tag{3.5}$$

The procedure to calculate the transition amplitudes is now reduced to finding the matrix elements of the resolvent operator, $G(E)$, given by Eq. (3.4). They can be obtained by inserting complete basis states between interaction operators and resolvent operators. Suppose we are interested in calculating the resolvent operator of an eigenstate of H_0, $|\phi_a\rangle$. We want to include its coupling, given by V, with the rest of eigenstates of H_0, $|\phi_b\rangle$. The resolvent equation can be solved iteratively, given by the following Dyson equation,

$$\begin{aligned} G_{aa}(E) &= G_{0aa}(E) + \sum_b G_{0aa}(E) V_{ab} G_{0bb}(E) V_{ba} G_{0aa}(E) + ... \\ &= \frac{1}{E - H_{0aa} + \Sigma_{aa}(E)}, \end{aligned}$$

where the geometric series has been summed and the self energy is given by

$$\Sigma_{aa} = \sum_b V_{ab} \frac{1}{E - E_b} V_{ba}. \tag{3.6}$$

3.3 Model Hamiltonian and the Recoil Calculation

The calculation is based on a model that we used previously [44][8] in Chapter 2. The source atom, with finite mass M, centered at position $\langle \mathbf{R} \rangle = 0$, has two internal levels, whose frequency separation is denoted by ω_0. The uniformly distributed dielectric atoms have $J = 0$ ground states and $J = 1$ excited states. The frequency separation of the ground and excited states is denoted by ω. We assume the mass of each medium atom to be infinite, which allows us to ignore recoil of the medium atoms. At $t = 0$, the source atom is excited to the $m = 0$ excited state sublevel with center of mass momentum $\langle \mathbf{P} \rangle = 0$, and $\langle \Delta \mathbf{P}^2 \rangle \ll (\hbar k_0)^2$, the dielectric atoms are all in their ground states, and there are no photons in the field. The process we consider is one in which radiation emitted by the source atom is scattered by dielectric atoms. The medium is modeled to be infinitely extended, i.e. radiation is always inside the

medium. The vacuum field amplitudes, the medium atoms' excited state amplitudes, and the source atom center of mass motion are calculated as $t \to \infty$. It is assumed that the medium atoms are far detuned from the source atom, $\omega \gg \omega_0$, and also $\omega_0 \gg \gamma$, where γ is the spontaneous decay rate of the source atom.

The free part of Hamiltonian describing such a system is

$$H_0 = \frac{\hbar\omega_0}{2}\sigma_z + \sum_j \sum_{m=-1}^{1} \frac{\hbar\omega}{2}\sigma_z^{(j)}(m) + \hbar\omega_{\mathbf{k}} a_{\mathbf{k}\lambda}^\dagger a_{\mathbf{k}\lambda} + \frac{\mathbf{P}^2}{2M}, \tag{3.7}$$

where all symbols were defined in Chapter 2. We have also included a term $\mathbf{P}^2/2M$ describing the external motion of the source atom, where $\mathbf{P}$ is the momentum operator for the source atom and M is the mass of the source atom. As before, the summation convention is used. The interaction part that couples the field with the atoms is

$$\begin{aligned} V = {} & \hbar g_{\mathbf{k}} (\mu_0 \cdot \epsilon_{\mathbf{k}}^{(0)} \sigma_+ a_{\mathbf{k}} e^{i\mathbf{k}\cdot\mathbf{R}_0} - \mu_0 \cdot \epsilon_{\mathbf{k}}^{(0)} a_{\mathbf{k}}^\dagger \sigma_- e^{-i\mathbf{k}\cdot\mathbf{R}_0}) \\ & + \sum_j \hbar g'_{\mathbf{k}\lambda} \left[\begin{array}{c} \mu_m \cdot \epsilon_{\mathbf{k}}^{(\lambda)} \sigma_+^{(j)}(m) \left(a_{\mathbf{k}\lambda} e^{i\mathbf{k}\cdot\mathbf{R}_j} - a_{\mathbf{k}\lambda}^\dagger e^{-i\mathbf{k}\cdot\mathbf{R}_j} \right) \\ + \mu_m^* \cdot \epsilon_{\mathbf{k}}^{(\lambda)} \sigma_-^{(j)}(m) \left(a_{\mathbf{k}\lambda}^\dagger e^{-i\mathbf{k}\cdot\mathbf{R}_j} - a_{\mathbf{k}\lambda} e^{i\mathbf{k}\cdot\mathbf{R}_j} \right) \end{array} \right]. \end{aligned} \tag{3.8}$$

All the symbols appearing in the interaction Hamiltonian have been defined in Chapter 2. The source atom interacts only with the z component of the vacuum field. Since the medium atoms are far detuned from the source atom, we include anti-rotating terms in the field-medium atoms' interaction. We have not included such terms for the interaction Hamiltonian between the source atom and the field because we have chosen the initial state to be the source atom excited with no photon in the field.

We want to calculate the recoil energy of the source atom, which includes the contribution from three amplitudes: the source atom in the ground state with one

photon in the field, the source atom in the ground state with one medium atom excited, and the source atom in the ground state with both the field and a medium atom excited. These amplitudes are represented by

$$b_{\mathbf{k}} = \langle 1, \mathbf{q}; g; \mathbf{k}| \, U(\infty) \, |2, 0; g; 0\rangle \tag{3.9}$$

$$b_{m_j} = \langle 1, \mathbf{q}; m_j; 0| \, U(\infty) \, |2, 0; g; 0\rangle \tag{3.10}$$

$$b_{m_j;\mathbf{k},\mathbf{k}'} = \langle 1, \mathbf{q}; m_j; \mathbf{k}, \mathbf{k}'| \, U(\infty) \, |2, 0; g; 0\rangle \, , \tag{3.11}$$

where the state of the system is labelled with source atom internal states, source atom external momenta, medium atoms' internal states, and photon field wave vectors. For example, $\langle 1, \mathbf{q}; g; \mathbf{k}|$ is the state with the source atom in ground state $|1\rangle$ with momentum $\hbar\mathbf{q}$, the medium atoms in ground state $|g\rangle$, and a photon with a wave vector $\mathbf{k}$ present. We use $|m_j\rangle$ to label the state of a medium atom at position $\mathbf{R}_j$ in its $|J = 1, m\rangle$ excited state. The photon polarizations are not written explicitly in the formulas. It should be understood, in the following perturbative calculations, any intermediate states' photon polarizations are summed over in amplitudes, while the final states' photon polarizations are summed over in probabilities.

The system starts at $\tau = 0$. According to Eq. (3.5), the evolution operator can be expressed in terms of the retarded resolvent operator as

$$U(\tau) = -\frac{1}{2\pi i} \int_{-\infty}^{\infty} dE \exp\left(-iE\tau/\hbar\right) G_+(E) \, , \tag{3.12}$$

where the resolvent operator, $G_+(E)$, is defined as

$$G_+(E) = \frac{1}{E + i0 - \hat{H}}.$$

The processes that we want to take into account are shown in Fig. (3.1). Let us focus on the calculation of $b_{\mathbf{k}}$ first,

$$b_{\mathbf{k}} = -\frac{1}{2\pi i} \lim_{\tau\to\infty} \int_{-\infty}^{\infty} dE \exp\left(-iE\tau/\hbar\right) \langle 1, \mathbf{q}; g_m; \mathbf{k}| \, G(E) \, |2, 0; g_m; 0\rangle \, , \tag{3.13}$$

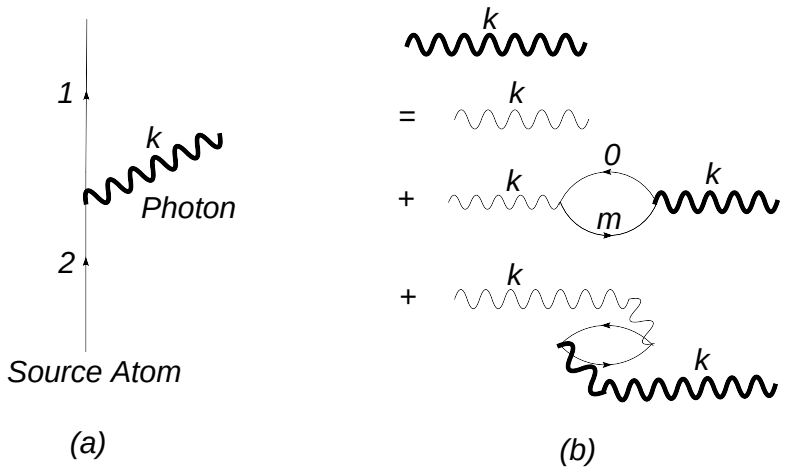

Figure 3.1: (a) The source atom in state $|2\rangle$ spontaneously decays by radiating a normalized photon with wave vector $\mathbf{k}$ and goes to the ground state $|1\rangle$ with external momentum $-\hbar\mathbf{k}$. The thick wavy line corresponds to the normalized photon propagator and straight solid lines correspond to the atom propagator. (b) The photon of wavevector $\mathbf{k}$ being scattered by medium atoms. We include both the rotating and anti-rotating contributions in the intermediate states. A medium atoms can get excited to $J = 1$ sublevel m by absorbing a photon k and return to the ground state by radiating photons. It can also get excited by emitting photons and then deexcited by absorbing other photons from non-rotating wave terms. In this diagram, the time propagation is from left to right. Averaging over the positions of the medium atoms results in conservation of the photon momenta before and after the scattering from medium atoms.

which requires a calculation of the matrix element of the operator. According to Eq. (3.4), the resolvent operator can be expanded to first order in $\hat{V}$ as,

$$\begin{aligned}
&\langle 1, \mathbf{q}; g_m; \mathbf{k}| \, G^{(1)} \, |2, 0; g_m; 0\rangle \\
&= \langle 1, \mathbf{q}; g_m; \mathbf{k}| \, G^{(0)}(E) \, |1, \mathbf{q}; g_m; \mathbf{k}\rangle \, \langle 1, \mathbf{q}; g_m; \mathbf{k}| \, \hat{V} \, |2, 0; g_m; 0\rangle \, \langle 2, 0; g_m; 0| \, G^{(0)}(E) \, |2, 0; g_m; 0\rangle \\
&= \hbar g^*_{\mathbf{k}} \delta_{\mathbf{q},-\mathbf{k}} \left(\mu^*_m \cdot \epsilon_k\right) \frac{1}{E - \hbar\omega_0 + i\hbar n\gamma} \frac{1}{E + i0 - \hbar\omega^r_q - \hbar\omega_k} \mathbf{W}_{m,0}. \qquad (3.14)
\end{aligned}$$

Here $\mathbf{W}_{m,0}$ is the transverse polarization tensor of the photon defined as

$$\begin{aligned}
\mathbf{W}_{m,m'} &= \left(\mu_m \cdot \epsilon^{(\lambda)}_k\right) \left(\mu_{m'} \cdot \epsilon^{(\lambda)}_k\right) \\
&= \left(\epsilon^{(\lambda)}_k \otimes \epsilon^{(\lambda)}_k\right)_{m,m'} = \left(1 - \hat{\mathbf{k}} \otimes \hat{\mathbf{k}}\right)_{m,m'}, \qquad (3.15)
\end{aligned}$$

where two relationships,

$$\mu^*_m \mu_m = \mathbf{1}$$

and

$$\mu^*_0 \cdot \epsilon_k = \left(\epsilon_k \cdot \mu^*_m\right) \mathbf{W}_{m,0}, \qquad (3.16)$$

have been used to derive its transverse property.

In the first order calculation, we neglect the possibility that the photon can be scattered by medium atoms. In Eq. (3.14), the source atom recoil momentum equals the inverse of the photon momentum, $\mathbf{q} = -\mathbf{k}$ (conservation of momentum), resulting from evaluation of the matrix element $\langle \mathbf{p} = \hbar\mathbf{q}| \, e^{i\mathbf{k}\cdot\mathbf{R}} \, |\mathbf{p} = 0\rangle$. We have rearranged the order in the last line of Eq. (3.14) so that the first part,

$$\hbar g^*_{\mathbf{k}} \delta_{\mathbf{q},-\mathbf{k}} \left(\mu^*_m \cdot \epsilon^{(\lambda)}_k\right) \frac{1}{E - \hbar\omega_0 + i\hbar n\gamma}, \qquad (3.17)$$

describes the decay of the source atom in the medium. The imaginary part in the dominator $i\hbar n\gamma$ is added to represent spontaneous decay [14]. The modification of γ in the vacuum to $n\gamma$ in the medium is related to the process that photons scattered

by the medium atoms are reabsorbed by the source atom, as shown in Refs. [44][8]. Here we have neglected the local field correction to the decay rate. The second part of Eq. (3.14),

$$\frac{1}{E+i0-\hbar\omega_q^r-\hbar\omega_k}\mathbf{W}_{m,0}, \tag{3.18}$$

describes the propagation of the photon, where $\omega_q^r=\hbar q^2/2M$ is the recoil frequency associated with the emission of a phone with wavevector $\mathbf{q}$.

In order to carry the calculation of the matrix element of the resolvent operator, $\langle 1,\mathbf{q};g_m;\mathbf{k}|\,G\,|2,0;g_m;0\rangle$, to higher order, it is necessary to consider processes in which the photon is scattered by medium atoms. Including these processes modifies the photon propagator (3.18). For a dilute medium with $N\lambda_0^3\ll 1$, where N is the density of the medium and $\lambda_0=2\pi c/\omega_0$ is the photon wavelength, it is appropriate to make use of the independent scattering approximation, i.e. neglecting the correlation between different scatterings. We need only include contributions from processes shown in Fig. (3.1b), i.e. ladder diagrams, which amount to a self energy insertion [14] to the photon propagator (3.18) in the dominator as

$$\begin{aligned}\sum = &\sum_{j,m,\mathbf{k}'}\langle 1,\mathbf{q};g;\mathbf{k}|\,V\\ &\times\left(\begin{array}{c}|1,\mathbf{q};m_j;\mathbf{k},\mathbf{k}'\rangle\langle 1,\mathbf{q};m_j;\mathbf{k},\mathbf{k}'|\,G^{(0)}(E)\,|1,\mathbf{q};m_j;\mathbf{k},\mathbf{k}'\rangle\langle 1,\mathbf{q};m_j;\mathbf{k},\mathbf{k}'|\\ +|1,\mathbf{q};m_j;0\rangle\langle 1,\mathbf{q};m_j;0|\,G^{(0)}(E)\,|1,\mathbf{q};m_j;0\rangle\langle 1,\mathbf{q};m_j;0|\end{array}\right)\\ &\times V\,|1,\mathbf{q};g;\mathbf{k}'\rangle\,.\end{aligned} \tag{3.19}$$

Using the prescription $\sum_{\mathbf{R}_j}\to N\int d\mathbf{R}$ and $\sum_{\mathbf{k}'}\to\frac{V}{(2\pi)^3}\int d\mathbf{k}'$ we can change sums to integrals. The integration over $\mathbf{R}$ gives $\delta(\mathbf{k}-\mathbf{k}')$ as a result of the translational invariance of the medium. The integration over $\mathbf{k}'$ picks up contributions only at $\mathbf{k}$,

and the self energy can be written as

$$\sum = \hbar^2 NV \left|g_{\mathbf{k}}\right|^2 \mu^2 \left[\frac{1}{E-\hbar\omega_k^r-\hbar\omega}+\frac{1}{E-\hbar\omega_k^r-\hbar\omega-2\hbar\omega_k}\right]. \tag{3.20}$$

Spontaneous decays of the medium atoms are ignored because medium atoms are far detuned from the source atom. The renormalized photon propagator, with the above self energy modification, is

$$\frac{1}{E+i0-\hbar\omega_k^r-\hbar\omega_k-\sum}\mathbf{W} = \frac{1}{E-\hbar\omega_k^r-\left[1-\frac{1}{2}N\alpha\left(E\right)\right]\hbar\omega_k}\mathbf{W}, \tag{3.21}$$

where the polarizability is defined as

$$\alpha\left(E\right) = -\frac{4\pi\mu^2}{\Delta\left(E\right)}, \tag{3.22}$$

and the detuning by

$$\frac{1}{\Delta\left(E\right)} \equiv \frac{1}{E-\hbar\omega_k^r-\hbar\omega}+\frac{1}{E-\hbar\omega_k^r-\hbar\omega-2\hbar\omega_k}. \tag{3.23}$$

The self energy insertion (3.20) brings a correction of order $N\alpha$ to the denominator of the photon propagator, which cannot be obtained from any finite order calculation. Substituting this normalized photon propagator (3.21) back to the first order formula (3.14) and using the fact that $\mathbf{W}^2 = \mathbf{W}$, one finds the relevant matrix element to be

$$\begin{aligned}&\left\langle 1,-\hbar\mathbf{k};g_m;\mathbf{k};0\right|G\left(E+i0\right)\left|2,0;g_m;0\right\rangle \\ &= \hbar g_{\mathbf{k}}^*\left(\mu_0^*\cdot\epsilon_{\mathbf{k}}\right)\frac{1}{E-\hbar\omega_0+in\hbar\gamma}\frac{1}{E-\hbar\omega_k^r-\left(1-\frac{1}{2}N\alpha\right)\hbar\omega_k}.\end{aligned} \tag{3.24}$$

To find the transition amplitude in Eq. (3.9), we need to integrate over E according to Eq. (3.5). The integration includes contributions from two poles, one at $E = \hbar\omega_k^r + \left(1-\frac{1}{2}N\alpha\right)\hbar\omega_k$, and one at $E = \hbar\omega_0 - i\hbar n\gamma$. In the limit $\gamma\tau \gg 1$, only the first pole contributes, since the second one has a finite imaginary part and its

contribution decays as $e^{-n\gamma\tau}$. The amplitude for finding a photon with wavevector $\mathbf{k}$ and source atom with momentum $-\hbar\mathbf{k}$ is then

$$b_{\mathbf{k}} = \lim_{\tau\to\infty} g_{\mathbf{k}}^{*}\left(\mu_0^{*}\cdot\epsilon_{\mathbf{k}}\right)\frac{\exp\left[-i\left(\hbar\omega_k^r+\left(1-\frac{1}{2}N\alpha\right)\omega_k\right)\tau\right]}{\omega_k^r+\left(1-\frac{1}{2}N\alpha\right)\omega_k-\omega_0+in\gamma}, \tag{3.25}$$

and the corresponding probability is,

$$\left|b_{\mathbf{k}}\right|^2 = \left|g_{\mathbf{k}}\right|^2\left|\mu_0\cdot\epsilon_{\mathbf{k}}\right|^2\frac{1}{\left[\omega_k/n-\left(\omega_0-n^2\omega_0^r\right)\right]^2+n^2\gamma^2}, \tag{3.26}$$

with $\omega_0^r = \hbar\omega_0^2/2Mc^2$.

To obtain the resonant frequency from $|b_{\mathbf{k}}|^2$, we need to solve the equation

$$n\frac{\hbar\omega_k^2}{2mc^2}+\omega_k-n\omega_0 = 0.$$

This equation has two solutions, one at

$$\omega_k = n\left(\omega_0-\frac{\hbar\left(nk_0\right)^2}{2m}\right)$$

and the other at

$$\omega_k = -\frac{2mc^2}{n\hbar}.$$

The second is irrelevant and we simply ignore it. We have set $n = 1+\frac{1}{2}N\alpha$ in the limit of small $N\alpha$. We also note that we have not included the local field corrections to the index of refraction. These corrections correspond to higher order corrections in $N\alpha$. The photon frequency centers around $n\left(\omega_0-n^2\hbar\omega_0^r\right)$. The total probability of finding a photon in the field is just the sum over all the $\mathbf{k}'s$

$$\sum_{\mathbf{k}}\left|b_{\mathbf{k}}\right|^2 = \frac{4\pi}{3}\frac{2\mu^2}{\left(2\pi\right)^2\hbar c^3}\int d\omega_k\frac{\omega_k^3}{\left[\omega_k/n-\left(\omega_0-n^2\omega_0^r\right)\right]^2+n^2\gamma^2} = 1. \tag{3.27}$$

In working out the integration, we have used the Wigner-Weisskopf approximation: that is, we extend the integration of ω_k to start from minus infinity, and take into account only the contribution from the pole at $n\left(\omega_0-n^2\omega_0^r+in\gamma\right)$[55][56][57]. We

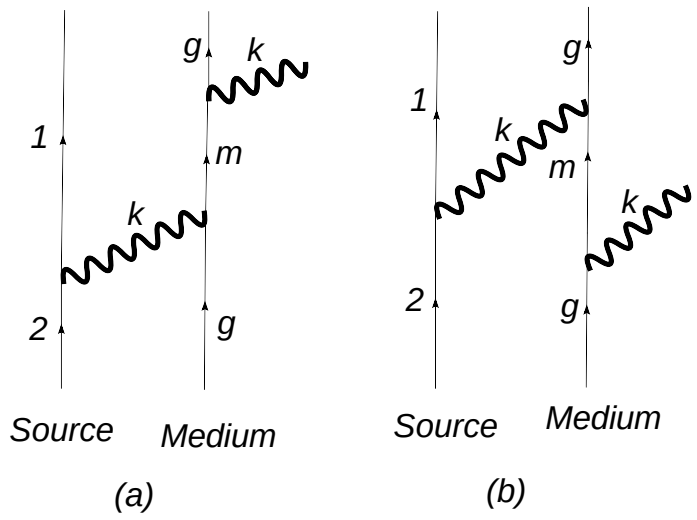

Figure 3.2: Medium atoms are excited by emitting or absorbing normalized photons. Figure (a) corresponds to a rotating situation while figure (b) corresponds to an anti-rotating situation.

note that the integral (3.27) can also be done by closing the contour in the lower half plane. The pole we pick up in this case is $n\left(\omega_0 - n^2\omega_0^r - in\gamma\right)$. This procedure yields the same result. Here the decay rate γ should be evaluated at the photon frequency and it is given by $\gamma = 2\mu^2\omega_k^3/3\hbar c^3$.

Other amplitudes, indicated in Fig. (3.2), can be calculated by the same technique. Let us consider the processes shown in Fig. (3.2). Making use of the normalized photon propagator (3.21), we find the amplitude for a medium atom located at $\mathbf{R}_j$, being excited to a sublevel m, with the source atom recoiled by momentum $-\hbar\mathbf{k}$, to be

$$b_{m_j} = \lim_{\tau\to\infty} |g_{\mathbf{k}}|^2 \mu^2 e^{i\mathbf{k}\cdot\mathbf{R}_j} \frac{\exp\left[-i\left(\hbar\omega_k^r + \left(1 - \frac{1}{2}N\alpha\right)\omega_k\right)\tau\right]}{\omega_k^r + \left(1 - \frac{1}{2}N\alpha\right)\omega_k - \omega_0 + in\gamma} \times \frac{1}{\left(1 - \frac{1}{2}N\alpha\right)\omega_k - \omega}\mathbf{W}_{m,0}. \tag{3.28}$$

It proves more useful to work in momentum space, since one can take advantage of the translational invariance of the problem. We denote the Fourier transforms of b_{m_j} and $b_{m_j;\mathbf{k},\mathbf{k}}$ as $\tilde{b}_m(\mathbf{k})$ and $\tilde{b}_{m;\mathbf{k},\mathbf{k}}(\mathbf{k})$, respectively. Here the only relevant two photon

amplitude is the amplitude where two photons carry the same momentum,

$$\tilde{b}_m(\mathbf{k}) = \lim_{\tau\to\infty} \sqrt{NV}\mu^2 |g_{\mathbf{k}}|^2 \frac{\exp\left[-i\left(\hbar\omega_k^r + \left(1-\frac{1}{2}N\alpha\right)\omega_k\right)\tau\right]}{\omega_k^r + \left(1-\frac{1}{2}N\alpha\right)\omega_k - \omega_0 + in\gamma} \times \frac{1}{\left(1-\frac{1}{2}N\alpha\right)\omega_k - \omega}\mathbf{W}_{m,0}. \tag{3.29}$$

The probability of finding medium atoms excited is

$$\sum_{\mathbf{m},\mathbf{k}} \left|\tilde{b}_m(\mathbf{k})\right|^2 = NV\mu^4 \sum_k \frac{|g_k|^4}{\left[\omega_k/n - (\omega_0 - n^2\omega_0^r)\right]^2 + n^2\gamma^2} \times \left[\frac{1}{\left(1-\frac{1}{2}N\alpha\right)\omega_k - \omega}\right]^2 \mathbf{W}_{0,0}. \tag{3.30}$$

The amplitude corresponding to a medium atom excited with two photons present arises from anti-rotating terms. It can be shown to be

$$\tilde{b}_{m;\mathbf{k},\mathbf{k}}(\mathbf{k}) = \lim_{t\to\infty} \sqrt{NV}\mu^2 |g_{\mathbf{k}}|^2 \frac{\exp\left[-i\left(\hbar\omega_k^r + \left(1-\frac{1}{2}N\alpha\right)\omega_k\right)t\right]}{\omega_k^r + \left(1-\frac{1}{2}N\alpha\right)\omega_k - \omega_0 + in\gamma} \times \frac{1}{\left(1-\frac{1}{2}N\alpha\right)\omega_k - \omega - 2\omega_k}\mathbf{W}_{m,0}, \tag{3.31}$$

and the corresponding probability, summed over different magnetic sublevels is,

$$\sum_{m,\mathbf{k}} \left|\tilde{b}_{m;\mathbf{k},\mathbf{k}}(\mathbf{k})\right|^2 = NV\mu^4 \sum_k \frac{|g_{\mathbf{k}}|^4}{\left[\omega_k/n - (\omega_0 - n^2\omega_0^r)\right]^2 + n^2\gamma^2} \times \left[\frac{1}{\left(1-\frac{1}{2}N\alpha\right)\omega_k - \omega - 2\omega_k}\right]^2 \mathbf{W}_{0,0}. \tag{3.32}$$

The probability $\sum_{m,\mathbf{k}} \left|\tilde{b}_m(\mathbf{k})\right|^2$ and $\sum_{m,\mathbf{k}} \left|\tilde{b}_{m;\mathbf{k},\mathbf{k}}(\mathbf{k})\right|^2$ are of order $N\alpha\omega_k/\omega$, which are negligible when $\omega_k \ll \omega$ and $N\alpha \ll 1$. By now we have calculated all the nonvanishing amplitudes of the system as $\tau \to \infty$. The total probability, the sum of Eqs. (3.27), (3.30), (3.32), is found to equal unity to order $N\alpha$.

The average recoil energy of source atom is calculated solely from the amplitude $b_{\mathbf{k}}$ (3.25) as

$$\left\langle \frac{\hbar^2\mathbf{k}^2}{2M} \right\rangle = \sum_{\mathbf{k}} \frac{\hbar^2\mathbf{k}^2}{2M} |b_{\mathbf{k}}|^2 = n^2\hbar\omega_0^r. \tag{3.33}$$

This result shows that the source atom recoils according to the canonical photon momentum $n\mathbf{k}_0$. This modification of the source atom recoil is directly related to the fact that the photon in the medium is centered at a frequency $n\omega_0 + O\left(\hbar\omega_0^2/Mc^2\right)$ instead of $\omega_0 + O\left(\hbar\omega_0^2/Mc^2\right)$, as is shown in formula (3.25). In the spontaneous decay of the source atom, momentum of the source atom plus the field is conserved. This modification of the central frequency of the photon therefore results in a modification of the source atom recoil. However, this shift in the photon frequency seems surprising, because we expect the frequency to center around the atomic frequency ω_0 from energy conservation considerations. In the following, we give a detailed analysis of the energy conservation to order of the shifted frequency, namely, $n\hbar\omega_0 - \hbar\omega_0 = \frac{1}{2}N\alpha\hbar\omega_0$.

Before we proceed to show energy conservation, it is necessary to note that the source atom excited at $t = 0$ is not in an eigenstate of the system. However, a discussion of energy conservation is meaningful in the sense that the average energy being conserved.

In order to find all the other forms of energy besides the photonic excitation, we should note that as the photon propagates in the medium, medium atoms inside the sphere of $R = ct$ are excited, with a weighting function proportional to $e^{-\gamma(ct-R)}$. Although the excitation probability is of order of magnitude $N\alpha\omega_k/\omega$, its correction to the energy is of order $N\alpha\omega_k$. Including this contribution to the energy, and the interaction energy of the medium atoms with the field, we should be able to recover conservation of energy. In the following we work out explicitly energies associated with different excitations in the system and show that the total average energy is conserved.

The first part of the energy corresponding to the field excitation is

$$\sum_{\mathbf{k}} |b_{\mathbf{k}}|^2 \hbar\omega_k = \left(1 + \frac{1}{2}N\alpha\right)\hbar\omega_0. \tag{3.34}$$

The energy associated with the medium atom excitations is

$$\begin{aligned}
&\sum_{m,\mathbf{k}} \left|\tilde{b}_m(\mathbf{k})\right|^2 \hbar\omega + \sum_{m,\mathbf{k}} \left|\tilde{b}_{m;\mathbf{k},\mathbf{k}}(\mathbf{k})\right|^2 (\hbar\omega + 2\hbar\omega_k) \\
&= -NV\sum_k \hbar^4 |g_k|^4 \mathbf{W}_{00} \frac{1}{(\hbar\omega_k/n - \hbar\omega_0)^2 + \gamma^2} \frac{1}{\Delta'},
\end{aligned} \tag{3.35}$$

where

$$\frac{1}{\Delta'} \equiv -\hbar\omega_m \left\{ \left[\frac{1}{\left(1 - \frac{1}{2}N\alpha\right)\hbar\omega_k - \hbar\omega}\right]^2 + \left[\frac{1}{\left(1 + \frac{1}{2}N\alpha\right)\hbar\omega_k + \hbar\omega}\right]^2 \right\}.$$

Here the difference in the energies of state $\tilde{b}_m(\mathbf{k})$ and $\tilde{b}_{m;\mathbf{k},\mathbf{k}}(\mathbf{k})$ can be ignored, because it amounts to a correction of order $N\alpha\omega_k/\omega$. To leading order in ω_k/ω, we find that

$$\frac{1}{\Delta'} - \frac{1}{\Delta(E)} = -\frac{1}{\hbar\omega}N\alpha\frac{\omega_k}{\omega}, \tag{3.36}$$

which enables us to neglect the difference between $\frac{1}{\Delta'}$ and $\frac{1}{\Delta(E)}$. The detunning $\Delta(E)$ is evaluated at the pole of the photon propagator $E = \left(1 - \frac{1}{2}N\alpha\right)\hbar\omega_k$. Making use of the definition (3.22), one finds that the energy associated with the atomic excitations is

$$\sum_{m,\mathbf{k}} \left|\tilde{b}_m(\mathbf{k})\right|^2 \hbar\omega + \sum_{m,\mathbf{k}} \left|\tilde{b}_{m;\mathbf{k},\mathbf{k}}(\mathbf{k})\right|^2 (\hbar\omega + 2\hbar\omega_k) = \frac{1}{2}N\alpha\hbar\omega_0.$$

The third part of the energy, the interaction energy between excited medium atoms and the field can be calculated as,

$$\begin{aligned}
\langle V\rangle &= \sum_{m,\mathbf{k}} NV\hbar g_{\mathbf{k}} \left(b^*_{\mathbf{k}}\tilde{b}_m(\mathbf{k}) + b^*_{\mathbf{k}}\tilde{b}_{m;\mathbf{k},\mathbf{k}}(\mathbf{k})\right) + h.c. \\
&= \sum_{\mathbf{k}} -N\alpha(\omega_k)\hbar\omega_k \frac{|\hbar g_{\mathbf{k}}|^2}{(\hbar\omega_k/n - \hbar\omega_0 + n^2\hbar\omega_k^r)^2 + n^2\hbar^2\gamma^2} \\
&= -N\alpha(\omega_k)\hbar\omega_k.
\end{aligned} \tag{3.37}$$

Adding all of these contributions, we have

$$\sum_{\mathbf{k}} |b_{\mathbf{k}}|^2 \hbar\omega_k + \left(\sum_{m,\mathbf{k}} \left| \tilde{b}_m (\mathbf{k}) \right|^2 \hbar\omega + \sum_{m,\mathbf{k}} \left| \tilde{b}_{m;\mathbf{k},\mathbf{k}} (\mathbf{k}) \right|^2 \right) \hbar\omega + \langle V \rangle = \hbar\omega_0. \tag{3.38}$$

The frequency shift of the photon in the medium is compensated by the excitation energy of medium atoms and the interaction energy of excited atoms with the field.

3.4 Perturbative Calculations in Configuration Space

Our calculation suggests that the photon radiated by the source atom has average energy $n\hbar\omega_0$ inside a infinitely extended medium. This energy is different from the initial state average energy $\hbar\omega_0$. We have shown in the previous section that the difference of these two energy can be accounted by the excitation of medium atoms and the interaction energy between medium atoms and the field. In the following, we present a perturbative calculation in configuration space. This calculation gives insight into the physical processes responsible for the shift of the photon frequency.

The equation of motion for the relevant amplitudes can be written directly as

$$\begin{aligned} \dot{b}_{\mathbf{k}} (t) = & \frac{1}{i} g_{\mathbf{k}}^* \sum_j (\mu_m^* \cdot \epsilon_{\mathbf{k}}) \exp(-i\mathbf{k} \cdot \mathbf{R}_j) \exp[-i(\omega_j - \omega_k) t] b_{m_j} (t) \\ & + \frac{1}{i} g_{\mathbf{k}}^* (\mu_0^* \cdot \epsilon_{\mathbf{k}}) \exp[-i(\omega_0 - \omega_k) t] b_2 (0, t) \end{aligned} \tag{3.39}$$

$$\dot{b}_{m_j} (t) = \frac{1}{i} \sum_k g_k (\mu_m \cdot \epsilon_{\mathbf{k}}) \exp(i\mathbf{k} \cdot \mathbf{R}_j) \exp[i(\omega_j - \omega_k) t] b_{\mathbf{k}} (t) \tag{3.40}$$

$$\dot{b}_2 (t) = \frac{1}{i} \sum_k g_k (\mu_0 \cdot \epsilon_{\mathbf{k}}) \exp[i(\omega_0 - \omega_k) t] b_{\mathbf{k}} (t), \tag{3.41}$$

where the amplitude $b_{\mathbf{k}}(t)$, $b_{mj}(t)$, $b_2(t)$ are the amplitudes for a state with a photon of type $\mathbf{k}$ and no other excitation, a state with a medium atom located at $\mathbf{R}_j$ excited to internal state m, and a state with the source atom excited respectively. Note that

in zeroth order, the photon can be radiated only by the source atom, and one has,

$$b_{\mathbf{k}}^{(0)}(t) = \frac{1}{i}\left(\int_0^t d\tau\right) g_{\mathbf{k}}^*\left(\mu_0^* \cdot \epsilon_{\mathbf{k}}\right) \exp\left[-i\left(\omega_0 - \omega_k\right)\tau\right] e^{-\gamma\tau}$$
$$= \frac{1}{\omega_k - \omega_0 + i\gamma} g_k^*\left(\mu_0^* \cdot \epsilon_{\mathbf{k}}\right). \tag{3.42}$$

We again assume that we are interested in times that are sufficiently large so that $e^{-\gamma t}$ can be neglected. Our calculation is limited to first order in the scattering. The first order correction to the photon field is the field scattered from one of the medium atoms. To this end, we proceed as the calculation done in Chapter 2. Integrating the $\dot{b}_{\mathbf{k}}$ equation formally over t, and substituting the result into the equations for $b_2(t)$ and $b_{m_j}(t)$, we find the equation for the state amplitude $b_{m_j}(t)$ to be,

$$\dot{b}_{m_j}(t) = -\gamma b_{m_j}(t) - \gamma e^{-i\Delta t} G_{m_j 0}\left(\mathbf{R}_j, \omega_0\right) b_0\left(t - R_j/c\right). \tag{3.43}$$

Note that we have explicitly included the retardation in $b_2(t - R/c)$. The $G_{m_j 0}$ is the propagator defined as in Chapter 2. In first order perturbation, we take $b_2(t) = \exp(-\gamma t)\,\Theta(t)$ in the calculation of b_{m_j}, where $\Theta(t)$ is the Heaviside step function. Under the adiabatic approximation, Eq. (3.43) can be solved as,

$$b_{m_j}(t) = \frac{\gamma}{i\Delta} G_{mj,0}\left(\mathbf{R}_j, \omega_0\right) \exp(-i\Delta t) \exp(-\gamma t) \exp(\gamma R_j/c)\,\Theta\left(t - R_j/c\right), \tag{3.44}$$

which corresponds to the amplitude of one medium atom being excited by the photon radiated by the source atom. The medium atom can scatter radiation and this gives a first order correction to the photon field. Substituting the $b_{m_j}(t)$ amplitude into equation (3.39) and use the prescription, $\sum_{R_j} \to N \int d\mathbf{R}$, we find that

$$\dot{b}_{\mathbf{k}}^{(1)}(t) = \frac{1}{i}\frac{N\gamma}{i\Delta}\left(\int d\mathbf{R}\right) g_{\mathbf{k}}^*\left(\mu_m^* \cdot \epsilon_{\mathbf{k}}\right) \exp\left(-i\mathbf{k}\cdot\mathbf{R}\right) G_{mj,0}\left(\mathbf{R}, \omega_0\right)$$
$$\times \exp\left[-i\left(\omega_0 - \omega_k\right)t - \gamma t\right] \exp(\gamma R/c)\,\Theta\left(t - R/c\right).$$

The integration over the angular part of $\mathbf{R}$ can be done by expanding the $\exp(-i\mathbf{k}\cdot\mathbf{R})$ in terms of spherical harmonics and Bessel functions. In this manner, one obtains

$$b_{\mathbf{k}}^{(1)}(t) = -2\frac{N\pi\gamma}{\Delta} g_{\mathbf{k}} (\mu_0 \cdot \epsilon_{\mathbf{k}}) \int_0^T dt \int_0^{ct} dR R^2 e^{i(\omega_k - \omega_0)t} e^{-\gamma(t-R/c)} \times \left[2h_0(k_0 R) j_0(kR) + j_2(kR) h_2(k_0 R)\right].$$

We first show that the probability of the field is equal to unity to first order in the density. The probability is,

$$P = \sum_{\mathbf{k}} \left| b_{\mathbf{k}}^{(0)}(t) + b_{\mathbf{k}}^{(1)}(t) \right|^2 = \sum_{\mathbf{k}} \left| b_{\mathbf{k}}^{(0)}(t) \right|^2 + 2\,\mathrm{Re} \sum_{\mathbf{k}} b_{\mathbf{k}}^{(0)*}(t)\, b_{\mathbf{k}}^{(1)}(t).$$

The correction comes from the interference of the directly radiated field and the scattered field, and it is given by,

$$2\,\mathrm{Re}\sum_{\mathbf{k}} b_{\mathbf{k}}^{(0)*}(t)\, b_{\mathbf{k}}^{(1)}(t) = -2\frac{N\pi\gamma}{\Delta}\,\mathrm{Re}\sum_k \frac{|g_{\mathbf{k}}|^2 |\mu_0 \cdot \epsilon_k|^2}{(\omega_k - \omega_0) - i\gamma} \int_0^T dt \int_0^{ct} dR R^2 \times e^{i(\omega_k-\omega_0)t} e^{-\gamma(t-R/c)} \left[2h_0(k_0R) j_0(kR) + j_2(kR) h_2(k_0R)\right]. \tag{3.45}$$

The term involving $h_0 j_0$ can be evaluated as,

$$\frac{2V}{(2\pi)^3} \int d^3k \frac{|g_{\mathbf{k}}|^2 |\mu_0 \cdot \epsilon_k|^2}{(\omega_k - \omega_0) - i\gamma} \int_0^T dt \int_0^{ct} dR R^2 e^{i(\omega_k-\omega_0)t} e^{-\gamma(t-R/c)} h_0(k_0R) j_0(kR)$$
$$= \frac{V}{(2\pi)^3} \int d^3k \frac{|g_{\mathbf{k}}|^2 |\mu_0 \cdot \epsilon_k|^2}{(\omega_k - \omega_0) - i\gamma} \int_0^T dt \int_0^{ct} dR e^{i(\omega_k-\omega_0)t} e^{-\gamma(t-R/c)} \frac{e^{i(k_0-k)R} - e^{i(k_0+k)R}}{k_0 k}.$$

We integrate over $\mathbf{k}$ first. The angular part gives $8\pi/3$ and one obtains

$$\frac{1}{(2\pi)^3} \frac{4\pi\mu^2}{3\hbar\epsilon_0 c} \int d\omega_k \frac{\omega_k^2}{\omega_k - \omega_0 - i\gamma} \int_0^T dt \int_0^{ct} dR e^{i(\omega_k-\omega_0)t} e^{-\gamma(t-R/c)} \frac{e^{i(k_0-k)R} - e^{i(k_0+k)R}}{\omega_0}.$$

The phase factors are $\exp\left[i\omega_k\left(t \pm R/c\right)\right]$. The contour should be closed in the upper half plane. We find

$$2\pi\frac{i}{\left(2\pi\right)^3}\frac{4\pi\mu^2}{3\hbar\epsilon_0 c}\omega_0\int_0^T dt\int_0^{ct} dR e^{-\gamma t}e^{-\gamma\left(t-R/c\right)}\left(e^{\gamma R/c}-e^{2ik_0R-\gamma R/c}\right)$$
$$=2\pi\frac{i}{\left(2\pi\right)^3}\frac{4\pi\mu^2}{3\hbar\epsilon_0 c}\omega_0\int_0^T dt\int_0^{ct} dR\left(e^{-2\gamma\left(t-R/c\right)}-e^{2ik_0R}e^{-2\gamma t}\right).$$

The first term is purely imaginary and can be neglected. The second term gives a contribution,

$$-\frac{i\mu^2}{3\hbar\pi\epsilon_0 c}\omega_0\int_0^T dt\int_0^{ct} dR e^{2ik_0R}e^{-2\gamma t}=-\frac{\mu^2}{12\hbar\pi\epsilon_0\gamma}.$$

Therefore, the $h_0 j_0$ term contributes

$$I_1=-\frac{2}{3}\pi\frac{N}{\Delta}\frac{\mu^2}{\hbar}=\frac{1}{6}N\alpha.$$

For the $h_2 j_2$ term, one needs

$$\frac{V}{\left(2\pi\right)^3}\int d^3k\frac{\left|g_k\right|^2\left|\mu_0\cdot\epsilon_k\right|^2}{\left(\omega_k-\omega_0\right)-i\gamma}\int_0^T dt\int_0^{ct} dR R^2 e^{i\left(\omega_k-\omega_0\right)t}e^{-\gamma\left(t-R/c\right)}h_2\left(k_0R\right)j_2\left(kR\right).$$

The integration over $\mathbf{k}$ yields

$$i\frac{\mu^2}{3\hbar\epsilon_0 c^3\pi}\omega_0^3\int_0^{cT} dR R^2 e^{\gamma R/c}h_2\left(k_0R\right)j_2\left(k_0R+i\gamma R/c\right)\int_{r/c}^T dt e^{-2\gamma t}=\frac{5}{6}\frac{\mu^2}{\hbar\gamma},$$

and the contribution to the probability from the second term is

$$I_2=-\frac{5}{3}\frac{N\pi\gamma}{\Delta}\frac{\mu^2}{\hbar\gamma}=\frac{5}{12}N\alpha.$$

Adding up the contributions from I_1 and I_2, we find a correction equal to $\frac{7}{6}N\alpha$. We note that in the first order of perturbation theory, there is a correction to the source atom decay rate. As calculated in the previous chapter, this decay rate is

$$\gamma^{(1)}=\left(1+\frac{7}{6}N\alpha\right)\gamma.$$

This change in the decay rate modifies the photon probability as

$$\sum_{\mathbf{k}} \frac{|g_{\mathbf{k}}|^2 |\mu_0 \cdot \epsilon_k|^2}{(\omega_k - \omega_0)^2 - [\gamma^{(1)}]^2} = \frac{\gamma}{\gamma^{(1)}} = 1 - \frac{7}{6} N\alpha.$$

The contribution from the modification of decay rate exactly cancels the contribution from the interference. This guarantees that the probability of finding a photon in the medium at a sufficiently late time is equal to unity even when the local field correction is considered.

The average energy of the field and the atom can also be calculated in the perturbative approach. Given Eq. (3.44), the energy in the atom is

$$\sum_{m,j} |b_{m_j}|^2 \hbar\omega = \frac{1}{2} N a \frac{\omega_0}{-\Delta}.$$

The interaction energy of the field and the medium atoms is

$$\begin{aligned} V &= \sum_{\mathbf{k},j,m} \hbar g_{\mathbf{k}}^* (m) \sigma_-^{(j)} (m) a_{\mathbf{k}}^\dagger e^{-i\mathbf{k}\cdot\mathbf{R}_j} e^{i(\omega_k - \omega)t} + c.c. \\ &= \sum_{\mathbf{k},j,m} \hbar g_{\mathbf{k}}^* (m) b_{\mathbf{k}}^{*(0)} b_{m_j} e^{-i\mathbf{k}\cdot\mathbf{R}_j} + c.c. \\ &= \sum_{\mathbf{k},j,m} \frac{\hbar g_{\mathbf{k}}^* g_{\mathbf{k}}}{\omega_k - \omega_0 - i\gamma} (\mu_0 \cdot \epsilon_0) (\mu_m \cdot \epsilon_k) \frac{\gamma}{i\Delta} G_{mj,0} (\omega_0) e^{-i\mathbf{k}\cdot\mathbf{R}_j} e^{-i\Delta t - \gamma(t - R_j/c)} + c.c. \end{aligned}$$

After integrating over angle of the vector $\mathbf{R}_j$, one finds

$$\begin{aligned} V = &- \frac{N\gamma\mu^2\pi i}{\hbar\epsilon_0 (2\pi)^3 c^3 \Delta} \int dR R^2 \int d^3\omega_k \omega_k \frac{\sin^2\theta_k}{\omega_k - \omega_0 - i\gamma} \\ &\times e^{i(\omega_k - \omega_0)t} e^{-\gamma(t - R/c)} [2h_0 (k_0 R) j_0 (kR) + h_2 (k_0 R) j_2 (kR)] + c.c. \end{aligned}$$

The integration over the angle of $\mathbf{k}$ gives,

$$\begin{aligned} V = &- i \frac{N\mu^2\gamma}{3\hbar\epsilon_0\pi c^3\Delta} \int dR^2 R \int d\omega_k \omega_k^3 \frac{e^{i(\omega_k - \omega_0)t} e^{-\gamma(t - R/c)}}{\omega_k - \omega_0 - i\gamma} \\ &\times [2h_0 (k_0 R) j_0 (kR) + h_2 (k_0 R) j_2 (kR)] + c.c. \end{aligned}$$

We can complete the contour in the upper half plane to find

$$V = \frac{2N\mu^2\gamma\omega_0^3}{3\hbar\epsilon_0 c^3\Delta} e^{-2\gamma t} \int_0^{ct} dR R^2 e^{\gamma R/c}$$
$$\times \left[2h_0\left(k_0 R\right) j_0\left(k_0 R + i\gamma R/c\right) + h_2\left(k_0 R\right) j_2\left(k_0 R + i\gamma R/c\right)\right] + c.c.$$

The integration follows the same procedure as the calculation in the perturbative calculation of the field probability. One finds that

$$\langle V\rangle = \frac{N\mu^2\omega_0}{\hbar\epsilon_0\Delta} = -N\alpha\omega_0.$$

In calculating the energy of the photon, if we use the Wigner-Weisskopf Approximation (WWA) directly, we get $\hbar\omega_0$. This does not conserve energy since the interaction and medium atom energies do not cancel each other. We instead calculate the correction to the photon energy

$$\sum_{\mathbf{k}} \left|b_{\mathbf{k}}\right|^2 \left(\omega_k - \omega_0\right),$$

under WWA. The correction in zeroth order is zero. Given Eq. (3.45), the correction in energy is

$$2\,\mathrm{Re}\sum_{\mathbf{k}} b_{\mathbf{k}}^{(0)*}\left(t\right) b_{\mathbf{k}}^{(1)}\left(t\right)\left(\omega_k - \omega_0\right) = I_1 + I_2,$$

where

$$I_1 = -4\frac{N\pi\gamma c^3}{\Delta\omega_k\omega_0}\frac{\left|g_{\mathbf{k}}\right|^2\left|\mu_0\cdot\epsilon_k\right|^2}{\left(\omega_k-\omega_0\right)^2+\gamma^2}\left(\omega_k-\omega_0\right)$$
$$\times\left[\frac{\omega_k-\omega_0}{\left(\omega_k-\omega_0\right)^2+\gamma^2}+\frac{1}{\omega_k+\omega_0}+\frac{\omega_k-\omega_0}{2\omega_k\left(\omega_k+\omega_0\right)}\mathrm{Re}\left(e^{2i\omega_k t}-1\right)\right],$$

and

$$I_2 = -2\frac{N\mu^2\pi\gamma c^3}{\Delta\omega_k^2\omega_0}\frac{\left|g_k\right|^2\left|\mu_0\cdot\epsilon_k\right|^2}{\left(\omega_k-\omega_0\right)^2+\gamma^2}\left(\omega_k-\omega_0\right)$$
$$\times\,\mathrm{Re}\left[\frac{e^{2i\omega_k T}}{\left(\omega_k+\omega_0-i\gamma\right)}-\frac{1}{\left(\omega_0-\omega_k-i\gamma\right)}-\frac{f\left(k,k_0,T\right)}{2\omega_0^2}\right].$$

The function f is given by

$$f(k,k_0,t) = 2k^2 + 6(\gamma_E - 3)kk_0 + (11 - 6\gamma_E)k_0^2 + k_0^2\cos(2\omega_k t) + 6(k_0 - k)\left[ci(2\omega_k t) - \log(2) - \log(\omega_k t)\right].$$

We note that there is no pole in the function $f(k,k_0,t)$. Following WWA except for terms of the form $\omega_k - \omega_0$, one gets

$$\int d\omega_k \frac{(\omega_k - \omega_0)\omega_k^2}{\left[(\omega_0 - \omega_k)^2 + \gamma^2\right]^2} \to \int d\omega_k \frac{(\omega_k - \omega_0)\omega_0^2}{\left[(\omega_0 - \omega_k)^2 + \gamma^2\right]^2} = 0,$$

and

$$\int d\omega_k \frac{(\omega_k - \omega_0)^2\omega_k^2}{\left[(\omega_0 - \omega_k)^2 + \gamma^2\right]^2} \to \int d\omega_k \frac{(\omega_k - \omega_0)^2\omega_0^2}{\left[(\omega_0 - \omega_k)^2 + \gamma^2\right]^2} \neq 0.$$

The integration over k gives the correction

$$\sum_k |b_k|^2(\omega_k - \omega_0) = \frac{1}{2}N\alpha\omega_0.$$

This correction conserves the the total energy. We therefore have shown that the perturbative calculation agrees with the non-perturbative results obtained from the resolvent method.

3.5 Discussion

In this chapter we have shown that the source atom recoils according to $n\hbar k_0$, which agrees with the previous theoretical and experimental results [51][19][20][50]. This modification of the photon recoil arises in our calculation as a result of the interference of the different scattering amplitudes. As has been shown in the calculation, while the average frequency of the source atom is at ω_0, only frequencies centered at $n\omega_0$ experience constructive interference. This is very much similar to the case of a source atom radiating in a cavity with the cavity frequency instead of the atomic

frequency. From a quantum point of view, the source atom decays because it radiates and reabsorbs virtual photons. Such a process introduces a finite self energy whose real part gives the level shift and whose imaginary part gives the decay of the atomic excitation [44][8][42]. This process, though not included explicitly in our calculation, is the only way that the source atom "knows about" the environment(vacuum, cavity or dielectric medium) in which is it located. In the cavity, the virtual photon can interfere with those reflected from the cavity walls and constructive interference occurs only at the cavity frequency. In the dielectric medium the virtual photons radiated by the source atom can be scattered by medium atoms and reabsorbed by the source atom during the time $t \preceq 1/\gamma$. Different scattering amplitudes interfere to shift the real radiating frequency to $n\omega_0$. This is a different effect from the level shift, the real part of the source atom self energy, due to the interaction of the source atom with the environment. In our particular example of the source atom located in a dilute medium, the shift due to interacting is of the order $N\alpha\gamma$ while the shift due to interference is of the order $N\alpha\omega_0$.

An alternative explanation can be put forward in terms of eigen-excitations of the system. Actually, if we consider the interaction of the field with the medium atom, the eigenmodes of the system are neither medium atoms being excited nor a photon present, but a superposition of these two type of excitations, a polariton [58]. The source atom decays by radiating polaritons instead of photons. For the energy to be conserved, the polariton energy plus the recoil energy should equal to the initial average energy $\hbar\omega_0$. As we have shown, the photon carries only part of the energy of the eigen excitation. On the other hand, the momentum carried by the medium atoms is negligible, the polariton momentum is just the photon momentum. When we require energy and momentum conservation for the radiating process, the only

possibility is the source atom to recoil according to $n\hbar k_0$.

CHAPTER IV

Tonks Girardeau Gas with a local potential

The study of cold atom gases has been one of the most fruitful research areas in physics in the last decade. Many of its successes can be attributed to its deep connections to a broad range of problems in condensed matter physics, nuclear physics, and atomic physics. Several interesting many body states, including Bose Einstein Condensate (BEC)[2][3], Mott insulators [4], and Fermi superfluids [5][6][7], have been realized experimentally. The cold atom version of these many body states have unique advantages over traditional condensed matter systems. In atomic systems, important parameters of many body systems, such as the external potential, the dimensionality, and the interaction can be tuned using external fields. In the next two chapters, we explore two possibilities in cold atom systems utilizing this extraordinary controllability.

4.1 Introduction

The effect of impurity and disorder on many body systems has been one of the main themes of condensed matter physics [59][60][61]. It plays an important role in our understanding of phenomena such as superconductivity, superfluidity, and Kondo physics. Due to the advantages the cold atom system has, it is tempting to study the effects of impurities in these systems.

This line of research has both been pursued theoretically [66][68][69], and experimentally [70][71][72]. One particular interesting possibility is to introduce ions into a BEC [66], utilizing both the techniques for manipulating atoms and ions. It is predicted that thousands of atoms will be bound by the ion to form a mesoscopic molecule. In such a scenario, the BEC is heavily depleted and a simple perturbative treatment might not be able to describe the system correctly. It would be beneficial to solve this problem in an exactly solvable model and compare it with the perturbatively result.

Recently, an interesting many body system, the Tonks-Girardeau gas, has been realized by two groups [28][29]. Such a system can be analyzed exactly using a boson-fermion mapping technique. We propose to study the impurity effect in such an exactly solvable system. The study serves two purposes: first, it shows, in its simplest form, the interplay between interaction, superfluidity, and impurity. Second, the theoretical predictions can be compared readily with experimental observables.

4.2 Tonks-Girardeau Gas

The Tonks-Girardeau gas was introduced 40 years ago by Girardeau [27]. A Tonks-Girardeau gas is a one-dimensional quantum gas with interaction energy per particle much larger than the kinetic energy per particle. As stated by F. D. M. Haldane [73], "In 1D [...] the symmetry of the wave function cannot be tested by a continuous change of coordinates that exchange particles with close approach (collision). Thus interaction and statistical effects cannot be separated". This peculiar feature of a one dimensional system enables us to map a Tonks-Girardeau gas to a free fermion system, which allows for an exact solution. It turns out later that the more general

one dimensional problem with interparticle interaction taking the following form,

$$V\left(x_{1,}x_2\right) = g\delta\left(x_1 - x_2\right), \tag{4.1}$$

can be solved exactly by Bethe asantz [62]. In our study, we do not discuss this more general case and limit ourselves only to the Tonk-Girardeau case for simplicity.

To facilitate the numerical calculation, we worked on a lattice version of a Tonks Girardeau gas, in which the Hamiltonian is,

$$H = t\sum_i \left(a_i^\dagger a_{i+1} + a_{i+1}^\dagger a_i\right), \tag{4.2}$$

where t is the hopping amplitude between nearest sites. The a_i and $a_i^\dagger$ are annihilation and creation operators for site i. They obey the bosonic commutation relation,

$$[a_i, a_j] = \delta_{ij}. \tag{4.3}$$

The infinite interaction between particles on the same site is included in the following on-site constraints,

$$a_i^2 = \left(a_i^\dagger\right)^2 = 0. \tag{4.4}$$

The on-site constraint is similar to the behavior of Fermi creation and annihilation operators. This similarity suggests the following Wigner-Jordan transformation,

$$a_i = \prod_{\alpha=1}^{i-1} e^{i\pi c_\alpha^\dagger c_\alpha} c_i \tag{4.5}$$

$$a_i^\dagger = c_i^\dagger \prod_{\alpha=1}^{i-1} e^{-i\pi c_\alpha^\dagger c_\alpha}. \tag{4.6}$$

Here the $c_i^\dagger$ and c_i are fermionic operators, which satisfy the anticommunication relation $\left\{c_i, c_j^\dagger\right\} = \delta_{ij}$. Under this transformation, we see that both the boson commutator (4.3) and the on-site constraint (4.4) are satisfied. Substituting this

transformation into the original Hamiltonian (4.2), we have

$$H = t \sum_i \left(c_i^\dagger c_{i+1} + c_{i+1}^\dagger c_i \right). \tag{4.7}$$

Without the on-site constraint, this Hamiltonian is just the Hamiltonian for free fermions. Therefore, the eigenenergies of a Tonks-Girardeau gas equals the those of a free fermion gas. For the many-body ground state, however, one cannot make such conclusions. This is because the fermion wavefunction has to be antisymmetric while the boson wavefunction is symmetric under particle exchanges. Therefore, in order to find the ground state of the Tonks-Girardeau gas, one needs to symmetrize the free fermion wavefunction. The discussion in this chapter is based in large part on Ref. [10].

4.3 Model of the Tonks-Girardeau Gas in an Optical Lattice with an Impurity

The Hamiltonian describing interacting cold bosons can be written in second quantization formula as

$$H = \int d^3x \psi^\dagger(x) \left[-\frac{\nabla^2}{2m} + V(x) + V_{imp}(x) \right] \psi(x) + g \int d^3x \psi^\dagger(x) \psi^\dagger(x) \psi(x) \psi(x), \tag{4.8}$$

where m is the mass of the atom, and $V(x)$ and $V_{imp}(x)$ are the external potentials. Experimentally, such potentials are given by the dipole coupling between atoms and external magnetic or optical fields. $V(x)$ is the external periodic potential produced by the optical lattice, and $V_{imp}(x)$ is a local potential that mimics the effects of a local impurity. The atom-atom interaction takes an s wave contact form. The validity of such an interaction is discussed in the next chapter. At this time, we just take the above form of the interaction and note that g is directly related to the s wave scattering length of atom-atom scattering. The field operators $\psi^\dagger(x)$ and

$\psi(x)$ are the creation and annihilation operators of the boson field. They satisfy the commutation relation,

$$\left[\psi(x), \psi^{\dagger}(x')\right] = \delta(x - x').$$

In an optical lattice, the external potential is periodic. We can expand the field operator in the basis of the Wannier functions,

$$\psi(x) = \sum_{i,n} a_{i,n} W_{i,n}(x)$$
$$\psi^{\dagger}(x) = \sum_{i,n} a_{i,n}^{\dagger} W_{i,n}^{*}(x).$$

Here $a_{i,n}$ and $a_{i,n}^{\dagger}$ are the creation and annihilation operator for a vibrational Wannier state n at site i. They satisfy the Bosonic commutation relation as well. Assuming that the interaction and kinetic energy are much smaller the energy spacing between different Wannier states, one can safely neglect Wannier states with $n > 1$ and expand

$$\psi(x) = \sum_{i} a_i W_i(x)$$
$$\psi^{\dagger}(x) = \sum_{i} a_i^{\dagger} W_i^{*}(x)$$

Substituting the above expansion of the field operator into the Hamiltonian (4.8), we arrive at the following Boss-Hubbard Hamiltonian describing an ultra-cold dilute gas of bosonic atoms in an optical lattice [74],

$$H = t \sum_{i} \left(a_i^{\dagger} a_{i+1} + a_{i+1}^{\dagger} a_i\right) + \frac{1}{2} U \sum_{i} n_i (n_i - 1) + u a_0^{\dagger} a_0 \tag{4.9}$$

The quantity t, which is generally negative, is the hopping amplitude between nearest neighbors

$$t = \int d^3x W(x - x_i) \left[-\frac{\nabla^2}{2m} + V(x)\right] W^{*}(x - x_{i+1}),$$

U characterizes the on-site interaction,

$$U = g \int d^3x \left|W\left(x\right)\right|^4,$$

and u is the local potential strength at site zero

$$u = \int d^3x \left|W\left(x\right)\right|^2 V_{imp}\left(x\right).$$

We are interested in the regime where the interaction energy is much larger than the hopping energy and the impurity energy, i.e. $U \gg t$, $U \gg u$. In this regime, there are no double or higher occupations of the same site. The Hamiltonian can be written as

$$H = t \sum_i \left(a_i^\dagger a_{i+1} + a_{i+1}^\dagger a_i \right) + u a_0^\dagger a_0, \tag{4.10}$$

and the particle interaction can be included by imposing the constraint $a_i^2 = \left(a_i^\dagger\right)^2 = 0$. This is the just the Hamiltonian for a Tonks-Girardeau gas (4.2) with an impurity.

The behavior of the many body system is determined by the ratio of u/t. When $|u/t| < 1$, the kinetic part dominates and the particles distribute uniformly to lower the kinetic energy. On the other hand, when $|u/t| > 1$, the local potential becomes important. In this regime, local charge fluctuations are suppressed and the coherence among particles is degraded. We numerically evaluate the single particle density matrix (SPDM) of the many-body ground state, and compute the effect of a local potential (impurity) on the spectrum of the SPDM, on the "BEC" wave function, and on the superfluidity of the many-body ground state.

In order to solve for the ground state of the system, we can use the same Bose Fermi mapping (4.5,4.6)

$$H = t \sum_i \left(c_i^\dagger c_{i+1} + c_{i+1}^\dagger c_i \right) + u c_0^\dagger c_0 \tag{4.11}$$

The ground state $|G_F\rangle$ of this Hamiltonian corresponds to the well-known Fermi sea, in which fermions fill the single particle levels up to the Fermi surface. The corresponding ground state $|G_B\rangle$ of the boson Hamiltonian(4.10) can be obtained from $|G_F\rangle$ by symmetrizing the corresponding many body fermionic wave function.

4.4 Single Particle Density Matrix

We seek the one particle density matrix [75], which is the expectation value of $a_i^\dagger a_j$ in the ground state,

$$\begin{aligned}\rho_{ij} &= \langle G_B| a_i^\dagger a_j |G_B\rangle \\ &= \langle G_F| c_i^\dagger \prod_{\alpha=1}^{i-1} e^{-i\pi c_\alpha^\dagger c_\alpha} \prod_{\alpha=1}^{j-1} e^{i\pi c_\alpha^\dagger c_\alpha} c_j |G_F\rangle . \end{aligned} \tag{4.12}$$

The diagonal part of the density matrix, ρ_{ii}, gives the density $\langle n_i\rangle = \langle G_B| a_i^\dagger a_i |G_B\rangle$ at site i, while the off diagonal part gives the coherence in the many body ground state for different sites. In the uniform case, the coherence ρ_{ij} depends only on the difference, $|i-j|$. In the presence of a local potential, however, the coherence depends on both i and j separately. In addition to that, ρ_{ij} is much smaller than its uniform counterpart when i and j are on different sides of the local potential.

Diagonalizing the single particle density matrix gives a set of eigenvectors $|n\rangle$, which may or may not be the single particle eigenstates of the noninteracting gas. The corresponding eigenvalues λ_n represent the occupation of state $|n\rangle$. The one state with $\lambda_n \sim N$ (total number of particles) is the "BEC" state [75]. (Note that in 1D, there is no Bose Einstein Condensation in the thermodynamical limit. In the particular case of the Tonks-Girardeau case, the particles that condense into a single state are calculated to be order of $\sqrt{N}$ [63]. However, this state, compared with other states, is the only state that is significantly occupied. With this clarification, we

will call that state the BEC state and the corresponding occupation the condensate fraction).

The evaluation of this density matrix is not simple even when the ground state is known. Here we adopt a technique developed by M. Rigol and A. Muramatsu [65]. We sketch their method as the following. In stead of calculating the single particle density matrix, one can calculate the single particle Green's function

$$G_{ij} = \langle G_B | \, a_i a_j^\dagger \, | G_B \rangle$$

and recover the single particle density matrix by the following identity,

$$\rho_{ij} = G_{ij} + \delta_{ij} \left(1 - 2G_{ii}\right). \tag{4.13}$$

We can directly write the matrix form of the Fermi ground state as

$$|G_F\rangle = \prod_{n=1}^{N_F} \sum_{i=1}^{N} f_{nm} c_m^\dagger \, |0\rangle \,,$$

where N_F is the number of fermions and N is the number of sites. The quantity f_{ni} is the amplitude of site i for the nth single particle eigenstate. The Fermi ground state $|G_F\rangle$ is simply the occupation of lowest single particle states by fermions. We are interested in calculating the state

$$|\phi_j\rangle = c_j^\dagger \prod_{\alpha=1}^{j-1} e^{-i\pi c_\alpha^\dagger c_\alpha} \, |G_F\rangle \,.$$

Note that

$$\prod_{\alpha=1}^{j-1} e^{-i\pi c_\alpha^\dagger c_\alpha} = \prod_{\alpha=1}^{j-1} \left(1 - 2c_\alpha^\dagger c_\alpha\right).$$

Therefore, the effect of $\prod_{\alpha=1}^{j-1} e^{i\pi c_\alpha^\dagger c_\alpha}$ on the Fermi Ground state is to switch the sign of the matrix element f_{nm} for $m < j-1$. To obtain state $|\phi_j\rangle$, we will need to create an additional particle at site j. In the matrix form of f, one simply adds a column to

f with $f_{N+1,j} = 1$ and rest of the column equals to zero. We denote the manipulated matrix as $f'^{(j)}$ in the following.

The single particle Green's function in terms of f' is,

$$G_{ij} = \langle 0| \prod_{n=1}^{N_F+1} \sum_{m=1}^{N} f'^{(i)}_{nm} c_m \prod_{n'=1}^{N_F+1} \sum_{m'=1}^{N} f'^{(j)}_{n'm'} c^\dagger_{m'} |0\rangle = \det \left[\left(f^{(i)} \right)^\dagger f^{(j)} \right].$$

Substituting this result into equation (4.13), we find a numerically simple way to calculate ρ_{ij}. Actually, this method allows us to calculate a system with up to a thousand lattice sites. We focus on the low occupation limit only, which corresponds to a continuum case. In order to check the convergence of our numerical calculations, we fix the number of particles at 9 and calculate the condensate fraction for a lattice of 100 sites and 200 sites. The difference is found to be less than 1%.

For a continuum system of size L, the ground state of a Tonks Gas with N bosons is

$$\Psi_0(x_1, \cdots, x_N) = L^{-N/2} |\det e^{ik_l x_m}|.$$

In terms of the rescaled, dimensionless variables $u_i = x_i/L$, the one particle density matrix is

$$\rho_N(x, x') = L^{-1} \rho_N(u, u').$$

The eigenvalue λ and eigenvector $\varphi(x)$ satisfy the relation,

$$\int_{-L}^{L} \rho_N(x, x') \varphi(x')\, dx' = \lambda \varphi(x).$$

By changing variables, one can write the eigenvalue as

$$\lambda = \left(\int_{-1}^{1} \rho_N(u, u') \varphi(u')\, du' \right) / \varphi(u'),$$

which is independent of the size of the system L. This verifies that 9 particles in 100 lattice sites already converges very well to the continuum case. In the following

calculation, unless otherwise stated, all the calculations are based on a system of 9 particles in a one dimensional lattice of 100 sites, with an impurity located at site zero. Periodic boundary conditions are imposed on this one dimensional chain.

4.5 Condensate Fraction and Condensate Wavefunction

Since all the physics is determined by the ratio u/t, in the following numerical calculations, we fix $t = -1$ and vary u. Fig. (4.1a) shows SPDM spectra for different u's. The peak corresponds to the BEC state and its magnitude is the condensate fraction. The introduction of an impurity lowers the condensate fraction, as shown in Fig. (4.1b). The attractive and repulsive potentials almost equally deplete the condensate fraction for small impurity potential u, with the attractive potential having a slightly larger effect. The physics that gives rise to this behavior, as is shown in the following, is that an attractive local potential has a stronger effect on decreasing the coherence between particles.

Since only the BEC state is significantly occupied, the BEC state determines the most important features of the many-body system. It would be useful to look at the BEC wave function itself (see Fig. (4.2a)). For a repulsive local potential, we find that the BEC density decreases near the impurity. In the case of an attractive potential, for $u > -1$, there is an increase in the probability of the BEC density at the impurity site. For the case of $u < -1$, in contrast to what one might expect, there is a decrease of the BEC density at the impurity site. This feature actually arises from the competition between two effects: the single particle effect, i.e. the potential attracts particles, and the many body effect, i.e. the impurity decreases the coherence among particles. We have also included the particle density plot in Fig.

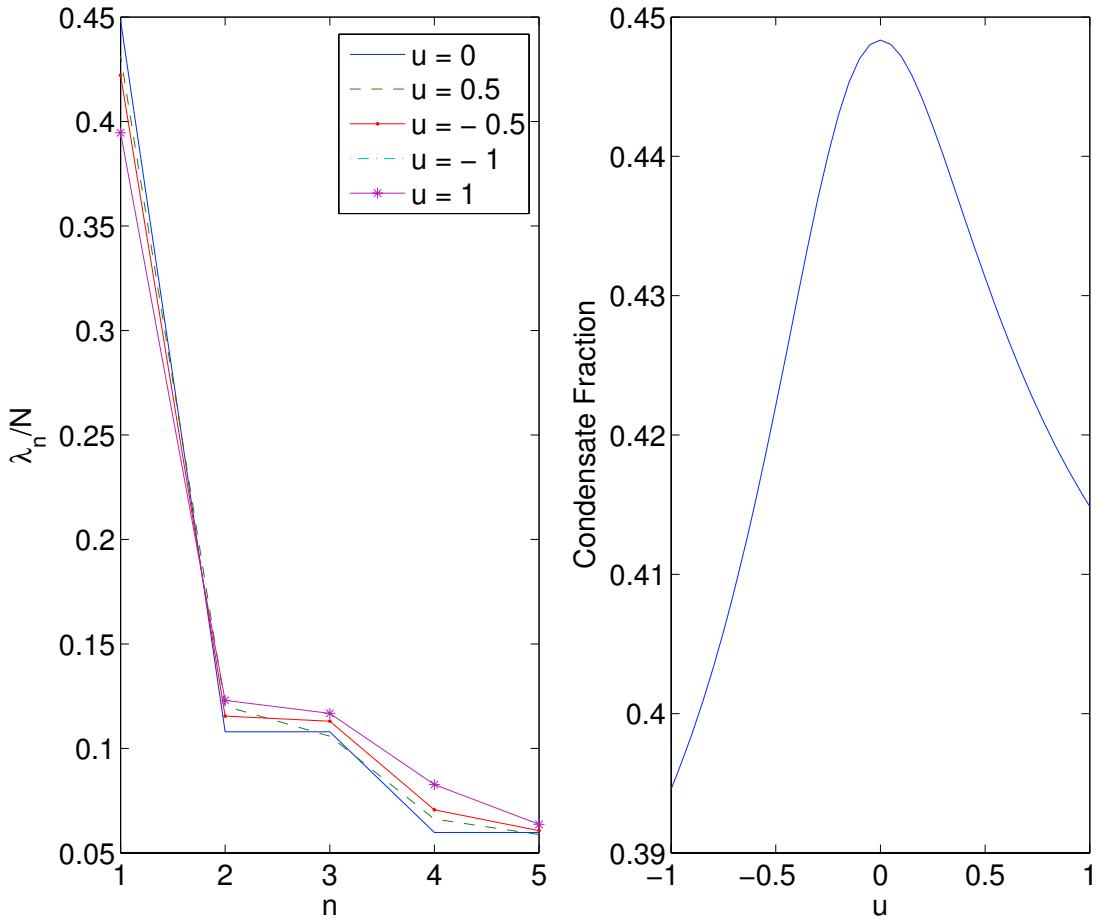

Figure 4.1: (a) SPDM spectra at different local potential strengths u. On the y axis, the SPDM eigenvalues λ_n are normalized to the total number of particles N. The x axis labels different eigenstates $|n\rangle$ of the SPDM. The first state, $|n = 1\rangle$, is overwhelmingly occupied compared with all the others, and is identified as the BEC state. Our numerical calculations show that about 45% of the particles are condensed into this BEC state for $u = 0$. This is of the order $1/\sqrt{N} = 0.3$ [63]. Only the first five largest eigenvalues are shown. (b) Condensate fraction [the occupation of the $|n = 1\rangle$ states in Fig. (4.1a)] as a function of the local potential strength. The attractive potential is seen to have a slightly larger effect in decreasing the condensate fraction.

(4.2b). It shows an increase of particle density for any attractive potential. For the BEC density, we see that, for each attractive potential, there is a peak at the impurity site corresponding to the local bound state. However, due to the lack of coherence between bound and extended states, the bound state is less likely to be found in the BEC state, which results in an overall decrease of the BEC density at site zero compared with the uniform case. This is the main observation of this chapter. To be more specific on how the impurity decreases the coherence among particles, we plot some of the relevant off-diagonal elements of the single particle density matrix (see Fig. (4.3)) In particular, we take the coherence between an arbitrary site and the fifth site next to the local potential site zero as an example. We find that, given the same distance, the coherence between particles on different sides of the impurity is much smaller than that of the particles located on the same side of the impurity. For the same magnitude of the attractive and repulsive potential, we find that the effect of the attractive and repulsive potential are roughly the same, with the attractive one having a stronger effect in decreasing the overall coherence among particles. This actually explains the fact that the attractive potential has a stronger effect on decreasing the condensate fraction. The only place that the attractive potential results in a larger coherence than the repulsive one with the same magnitude is near the impurity site. This is due to the presence of a local bound state, which effectively increase the probability of finding particles at the impurity site.

This single particle bound state is well known [76] in the tight binding Hamiltonian. Its eigenenergy is

$$E = -\sqrt{u^2 + 4t^2},$$

and its wave function localizes in space as $\exp\left[-\alpha\left(E\right)|n|\right]$ with n being the site

number and

$$\alpha\left(E\right) = -\ln\left[\frac{\sqrt{u^2+t^2}-|u|}{2\,|t|}\right], \tag{4.14}$$

corresponds to the inverse of the characteristic length. The nice overlap of the coherence peak and the bound state wave function verifies our argument for the increase of coherence in the vicinity of an impurity. The small peak in the impurity site is purely a single particle effect.

With the picture of the impurity introducing decoherence, it would seem that in higher dimensions, since the impurity has a weaker effect in decreasing coherence among particles, a smaller effect of the impurity should be found. We have verified this point numerically by extending our calculation to two dimensions. The condensate fraction is shown in Fig. (4.4). For dimensions greater than one, there is no simple mapping from bosons to fermions. An exact diagonalization has been done for this case which limits the calculation to a system of five particles in a three by three lattice.

4.6 Superfluidity

It is well known that Bose Einstein condensation is neither necessary nor sufficient for the existence of a superfluid. In a BEC, the long range inter-particle coherence is reflected in the eigenvalue spectrum of the SPDM. In general, the coherence decreases with the increase of inter-particle interaction. Superfluidity, on the other hand is related to the response of the system to an external velocity field. In the Tonks-Girardeau gas, the strong interaction among particles decreases the condensate fraction. However, in the absence of impurity, the system can be mapped exactly to a non-interacting one-dimensional fermionic gas. A velocity field v increases its energy by $\frac{1}{2}Nmv^2$, corresponding to a unity superfluid fraction. This point has been

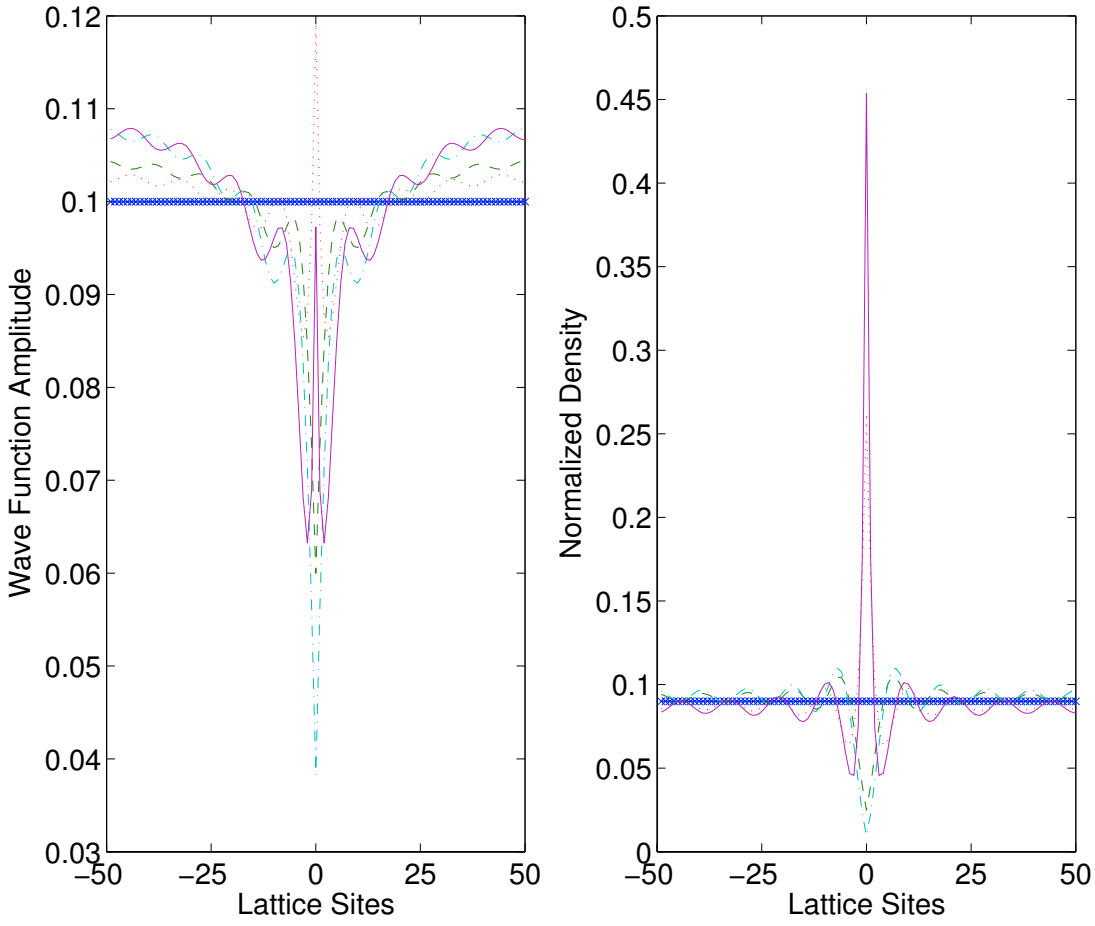

Figure 4.2: (a) The BEC wave functions for different strengths of the local potential are shown. In the special case of u=0, the BEC wave function is constant. Note that the BEC wave function corresponding to $u = -1$ has a lower value at the impurity site compared with the $u = 0$ uniform case. (b) The particle density is shown with respect to lattice sites for different u's. Here we see for attractive u, the particle density at the impurity site is always larger than that of the uniform case.

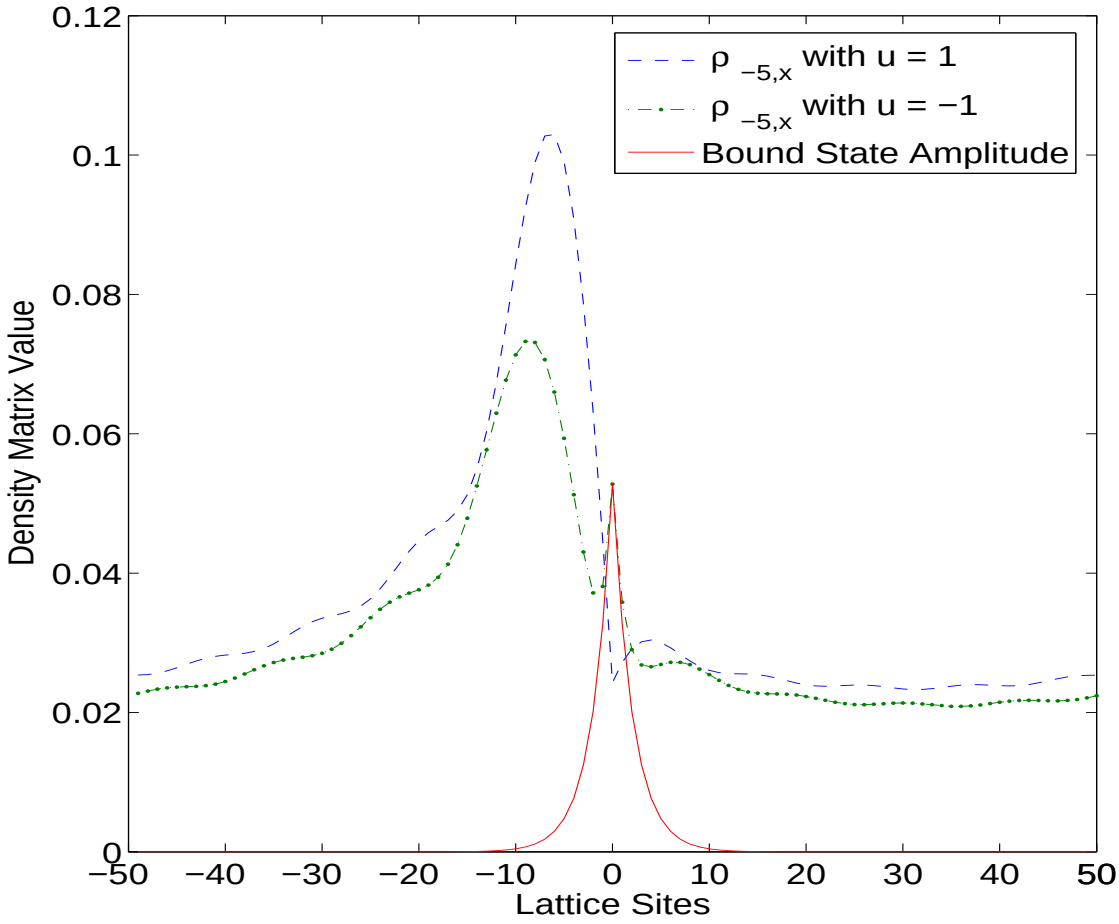

Figure 4.3: The off-diagonal SPDM elements that measure the coherence between lattice site -5 and any arbitrary lattice site is plotted for $u = -1$ and $u = 1$, respectively. The coherence with the negative sites is relatively larger than the coherence with the positive sites. The smaller peak of the coherence for the attractive potential between any sites and the sites 0 can be explained by the increase of the density at impurity site, due to the presence of a bound state. The bound state wavefunction is plotted and it coincides well with the peak of the coherence in the impurity site.

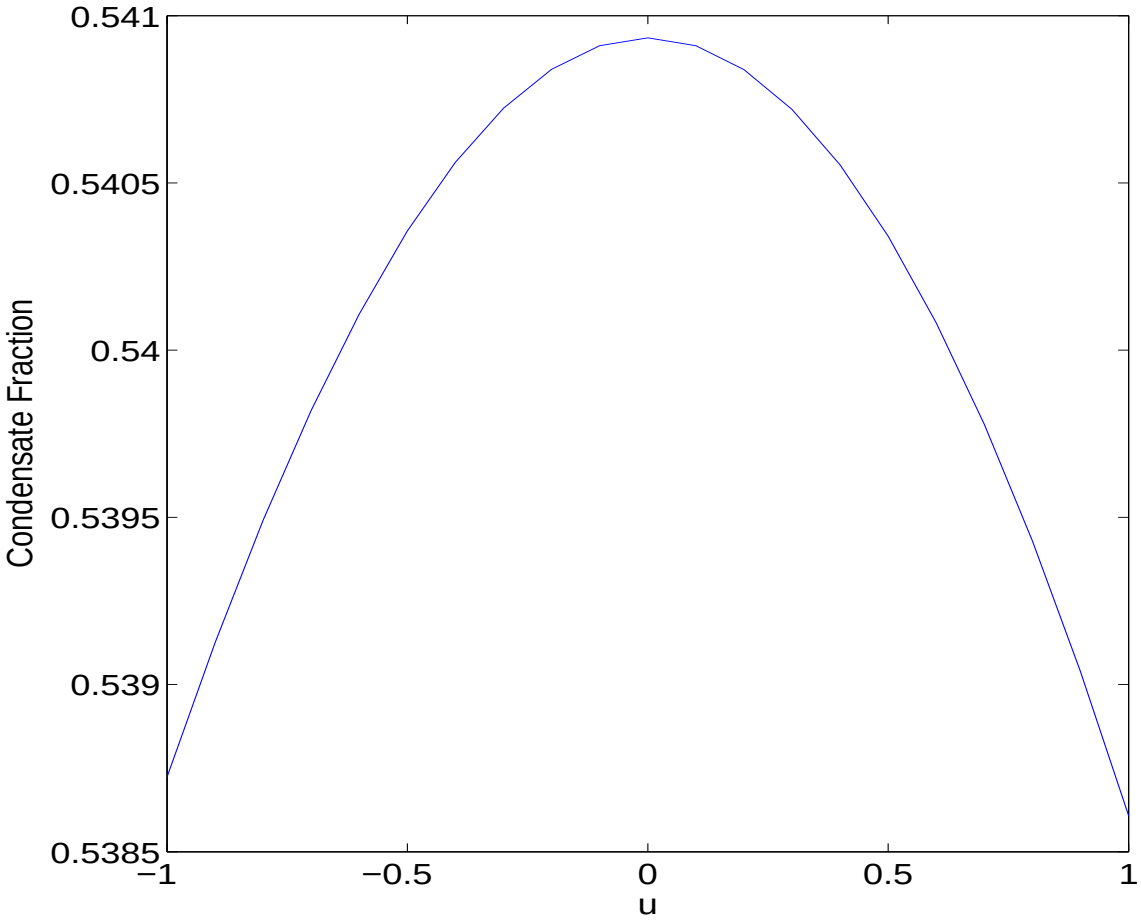

Figure 4.4: This figure shows the condensate fraction in a three by three lattice with an impurity located in the center. The impurity is characterized by a local potential strength u. The total single particle density spectrum is normalized to one. We see that in two dimensions, the condensate fraction is larger than its one dimensional counterpart. Moreover, the relative change of the condensate fraction due to the presence of the local potential is much smaller than in the one dimensional case.

addressed before by Lieb, Sieringer and Yngvason [64]. It is interesting to investigate how the superfluidity is decreased in the presence of an impurity. We emphasize that we use the word superfluidity strictly in the sense of the following phenomenological definition

$$\frac{E(v)}{N} - \frac{E(0)}{N} = \frac{1}{2} f_s m v^2 + O\left(v^4\right),$$

where $E(v)$ is the ground state energy of the many body system in the presence of a perturbative velocity field v, f_s is the superfluid fraction, and m is the mass of the particle. The velocity field is introduced by imposing a twisted boundary condition [64], which amounts to a phase jump $e^{i\varphi}$, $\varphi = \frac{vLm}{h}$, whenever the wave function passes through the boundary. We restrict $\varphi < \pi$ to yield a single valued function. Note that since the definition is based only on the static properties of the many body system, it can tell us only whether the ground state has the property of superfluidity. It cannot predict the stability of the superfluidity.

The results of numerical calculations are shown in Fig (4.5). We see that without impurity, the system exhibits superfluidity with superfluid fraction of unity. The degree of degradation on the superfluid fraction produced by an impurity depends on both the local impurity strength and the size of the system. In a large system, the superfluidity drops sharply with the presence of the local impurity. Note that as far as the spectrum is concerned, the Fermi ground state is equivalent to the boson ground state. This allows an understanding of the superfluidity in a single particle picture. The energy of a single particle in such a system consists of two parts: the kinetic energy, and the part of the energy due to the presence of the local potential. As the lattice size increases, the kinetic energy goes like $\frac{1}{L^2}$, while the mean values of the potential energy due to the local potential goes like $\frac{1}{L}$ for an extended state. Therefore, in the limiting case of large L, the local potential play a more dominant

role than the hopping. For a repulsive potential, the particle has to hop through the barrier. For an attractive potential, since the local bound state is always occupied, for strongly interacting bosons, in order to get through this potential, a potential barrier of order $\frac{1}{L}$ is also present, which gives rise to the sharp drop of superfluidity in the presence of a local potential.

This problem can be understood quantitatively by considering the following single particle model Hamiltonian,

$$H = -\frac{\hbar^2}{2m}\frac{d^2}{dx^2} + g\delta(x), \tag{4.15}$$

with x defined in the regime $[-L, L]$ with the twisted boundary condition. To calculate the eigenenergy with different a boundary condition is elementary since it corresponds to a one dimensional piecewise potential problem. As an example, we consider only two states with energies close to $\frac{\hbar^2\pi^2}{2mL^2}$. This allows us to use a perturbative calculation of $k = \sqrt{2mE}/\hbar$ around $\frac{\pi}{L}$. The solution of equation (4.15) is equivalent to the solution of the following form in the momentum space,

$$k\cos\varphi - k\cos(2kL) - \frac{gm\sin(2kL)}{\hbar^2} = 0.$$

We are looking for solution with $k \sim \frac{\pi}{L}$. This parameter converges slowly and it is found that one has to expand to order $\left(k - \frac{\pi}{L}\right)^4$ to yield a reasonable result. The modification of eigenenergy due to the presence of the velocity field is

$$\left[E(v) - E(0)\right]/2 = \frac{1}{2}mv^2\left(1 - 0.008g^2L^2\right)$$

in the perturbative limit that gL is small. This result shows that the superfluid fraction is

$$f_s = 1 - 0.008g^2L^2.$$

There is no modification to first order in gL, which is consistent with discussions concerning repulsive and attractive potentials.

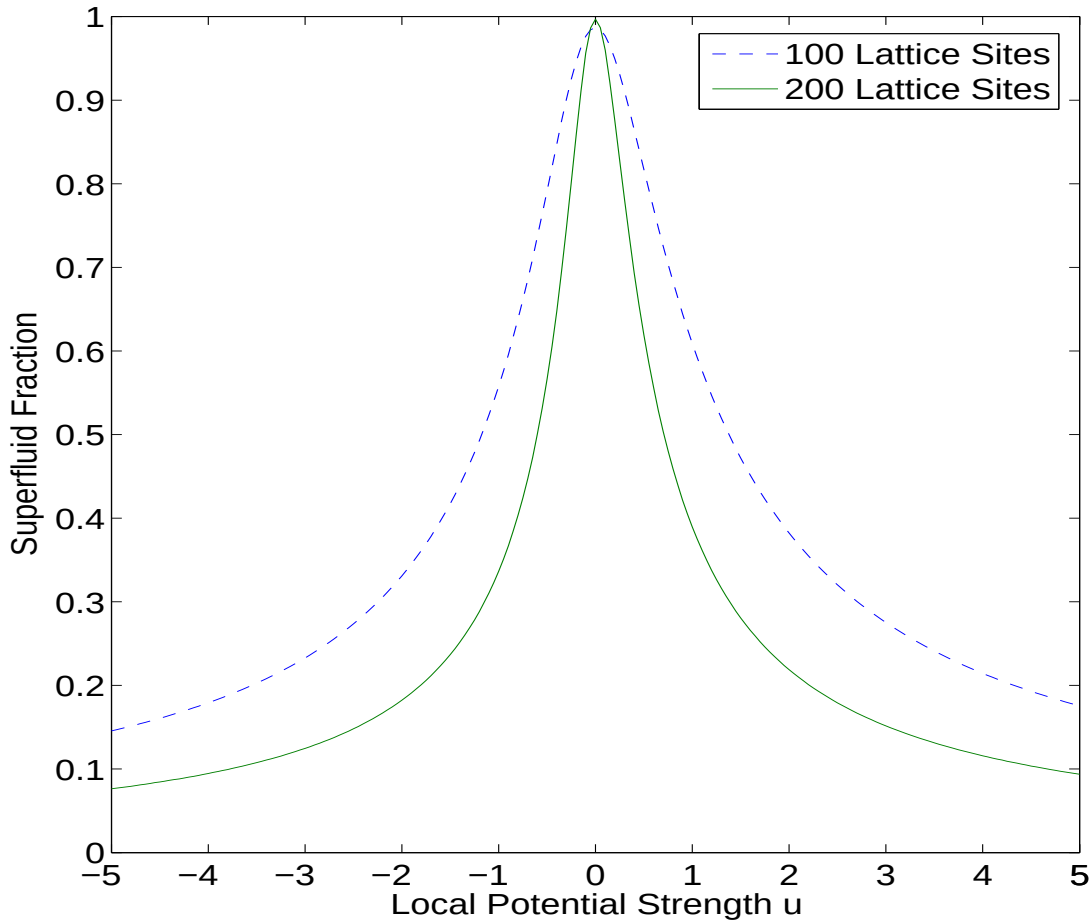

Figure 4.5: Superfluid fraction is plotted as a function of different local potential strength u. The cases of nine particles occupying 100 and 200 lattice sites are shown. The larger the system, the sharper the superfluid peak that is found

4.7 Experimental Observables

The effect of an impurity on the Tonks-Girardeau gas can be studied in an experiment using an optical lattice. The local potential we model here may be realized in an experiment by introducing a focused laser beam, an impurity atom, or an ion at a particular lattice site. If a focused laser beam is chosen to generate the impurity potential, the potential profile is given by $V_{imp}(x) = \frac{|\chi(x)|^2}{\Delta}$, where $\chi(x)$ is the field intensity of the external fields. To make it sufficiently local, the radius of the focus has to be comparable to the lattice spacing. In a optical lattice, the lattice spacing is given by half of the wavelength of the optical lattice laser beam. This means that the impurity laser beam should be focused to the order of a wavelength. When an impurity atom or ion is directly introduced to a Tonks-Girardeau gas, the s wave scattering length can be used to characterized the impurity potential. Similarly, for the impurity potential to be local, the s wave scattering length should be smaller than the wavelength of the optical lattice beam.

To observe the effects of an impurity inside a Tonks-Girardeau gas, one needs to measure experiment observables that are directly related to the single particle density matrix. The real space density distribution will be the same as the free fermion density in the presence of a local potential, which contains information only on the diagonal part of the density matrix. The non-trivial part of the density matrix, the off diagonal coherence, can be detected by measuring the momentum distribution, defined as

$$n(k) = \frac{1}{N} \sum_{m,n=-N/2}^{N/2} \rho_{mn} e^{i(m-n)k}$$

We have ignored the localized Wannier function profile. The direct measurement of the momentum distribution of Tonks-Girardeau gas has been demonstrated recently

[77]. It involves turning off the atom-atom interaction suddenly before the expansion. Experimentally, this sudden approximation requires the time scale of turning off the atom-atom interaction to be much smaller than the inverse of the many body energy scale.

In fig. (4.6) we show the peak value density in momentum space for different impurity strengths. The highest momentum density peak corresponds to the case with no impurity. The attractive potential has a larger effect on the broadening compared with the repulsive one. The superfluidity of the system can be measured by imposing a velocity field on the many-body system. This can be realized in the experiment by changing of the external potential with time. The measurement can be done by looking at the damping motion of the particles.

4.8 Summary

A Tonks-Girardeau gas confined in an optical lattice in the presence of a local potential was studied. In order to evaluate the single particle density matrix of the many-body ground state, the Wigner-Jordan transformation is used. The eigenvector with the largest eigenvalue of the single particle density matrix corresponds to the "BEC" State. We find that the "BEC" state density at the position of the local potential decreases, as expected, in the case of a repulsive potential. For an attractive potential, it decreases or increases depending on the strength of the potential. The superfluidity of this system is investigated both numerically and perturbatively. It is found that the superfluidity is degraded by the impurity, the degradation scales like g^2L^2 in the small gL limit. This effect of impurity on a many-body system can be measured by looking at the momentum distribution and the system response an external velocity field.

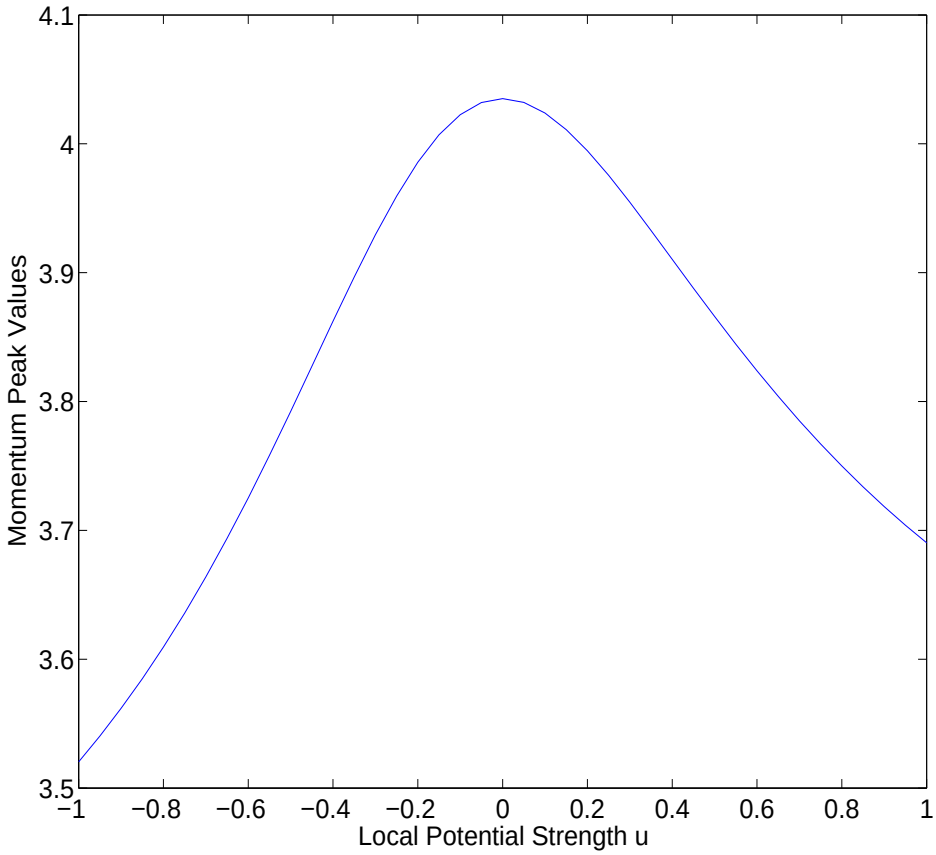

Figure 4.6: The peak value of the density distribution in momentum space. The maximum of zero momentum occupation is reached in the uniform case.

CHAPTER V

A Cold Atomic Fermi Gas with a Spatially Modulated Interaction

Significant progresses has been made in cold atom research in the last twenty years. The exceptional controllability of atom-field interactions has made it possible to realize, in the atomic domain, interactions equivalent to those in condensed matter systems that, to this point, have been studied only theoretically. More importantly, opens up new venues of systems that are not feasible in traditional condensed matter systems. In the previous chapter, we discussed one interesting cold atom system, namely, a Tonks-Girardeau gas with an impurity. In this chapter we study the properties of an ultra-cold atomic Fermi gas with the atom-atom interaction modulated periodically in space.

5.1 Introduction

Most Hamiltonians describing few-body or many-body systems can be divided into two parts: the single particle part, and the two body interaction part. It is usually easier to control the single particle part of a Hamiltonian than the two body part. In particular, one can modify single particle potentials by introducing external fields. However, few experiments have been done trying to manipulate the two body interaction spatially. Consequently, there have been very few theoretical studies of

systems where particles can interact differently in different space points.

For an ultra cold atomic gas, the effective atom-atom interaction is

$$V(\rho) = 4\pi a_s \hbar^2 \delta(\rho)/m,$$

where ρ is the relative coordinate between the two particles, m is the mass of the atom, and a_s is the s-wave scattering length. Near a Feshbach resonance, the scattering length can be described by [79],[31]

$$a_{eff} = a_{bg} - \frac{m}{4\pi\hbar^2 v_0} |g_0|^2,$$

where a_{bg} is the background scattering length, and the second term is the contribution from the nearby Feshbach resonance. The constants g_0 and v_0 are the coupling strength and energy detuning between the scattering channel and the molecular channel, respectively. In magnetic Feshbach resonances [79][31], the detuning v_0 can be controlled by an external magnetic field. In an optical Feshbach resonance [88][89][90][91][93] v_0 can be tuned by varying the laser frequency, and the free bound coupling g_0 can be tuned by varying the laser intensity. A spatially dependent scattering length can be achieved by applying spatially varying external fields. This gives an effective interaction,

$$V(\mathbf{r}, \rho) = 4\pi a_s(\mathbf{r}) \hbar^2 \delta(\rho)/m$$

that depends on both the relative coordinate and the center of mass (COM) coordinate $\mathbf{r}$. This direct substitution of the scattering length locally requires that the scattering length to vary only in a scale much larger than the local scattering length, i. e. $|\bigtriangledown a_s(\mathbf{r})| \ll 1$. In particular, we consider the simplest form of such an interaction,

$$V(\mathbf{r}, \rho) = [g_0 + g\cos(\mathbf{k}_0 \cdot \mathbf{r})]\,\delta(\rho) \tag{5.1}$$

The constant g_0 term, with $g_0 < g < 0$, is added to guarantee that the interaction is always negative. The ground state of the system is therefore a BCS ground state.

In several recent experiments, fermionic atoms were cooled below degenerate temperatures, and superfluid Fermi gases were observed [21][22][23][24][25][7][**?**][5][6][26]. It is interesting to discuss the effect of the modulating interaction on the pairing of the superfluid. The possibility to achieve such a system experimentally is feasible only with recent advances in atomic physics. A relatively obvious phenomenon that arises from such a spatially modulated interaction would be the modulation of the atomic density. Atoms are prone to congregate in locations with maximum attractions. A much more interesting phenomenon resides in the pairing of atoms. In a typical BCS theory, the ground state wave function consists of Cooper pairs with their COM momenta equal to zero. The interaction we propose (5.1) creates coherences between pairs with COM momenta differing by $\mathbf{k}_0$ to lower the free energy of the system. The ground state thus includes Cooper pairs with zero, as well as $\pm\mathbf{k}_0$, $\pm 2\mathbf{k}_0$, COM momenta. However, we find that the probability of occupying higher COM momenta is low due to its kinetic energies and the constant attractive interaction g_0. Our ground state is closely related to the Fulde-Ferrell-Larkin-Ovchinnikov (FFLO) state discussed in the literature [34][35]. In the FFLO state, due to the mismatch of the chemical potential for spin up and spin down particles, particles can pair with non-zero COM momenta to lower the energy. Even though the ground states of these two systems may look similar, the underlying mechanisms are different. In the FFLO case, the spatial symmetry is broken spontaneously while in the system studied in this chapter, the spatial symmetry is broken by external fields.

In this chapter, we consider a fermion gas with the atom-atom interaction varying in space. We first review some basic cold atom physics: the s wave scattering length

description of the cold atom interaction, the Feshbach resonance, and the BEC-BCS crossover scenario of a Fermi gas near a Feshbach resonance. In our study of the spatial modulation effect, we use the mean field Bogliubov de Gennes approach. The ground state and excited state properties of the Fermi gas is investigated. A detection scheme is presented at end of the chapter. The discussions of s wave scattering lengths and Feshbach resonances are base on Stoof's work [92], and the discussion of the spatially modulated fermi gas is based on Ref. [11].

5.2 Describing Cold Atom Interactions with s Wave Scattering Lengths

At low temperature, the atom-atom scattering is dominated by the s wave channel. This observation can be used to simplify the description of the ultra cold atom-atom interaction. In this section, we first calculate the energy shift of the two body system due to atom-atom interactions. We show that this shift can be described by a T matrix [92]. This T matrix is then related to the s wave scattering length to find the effective atom-atom interaction at low temperatures.

We consider a system of two non-identical atoms with equal mass m interacting in free space with the Hamiltonian

$$H = \frac{p_1^2}{2m} + \frac{p_2^2}{2m} + V\left(r_1 - r_2\right).$$

We define V_q as the Fourier transform of the true atom-atom interaction $V\left(\mathbf{r}_1 - \mathbf{r}_2\right)$. Without this interaction, eigenstates of the system are plane waves. In the following calculation, we work in the center-of-mass frame and label only the relative coordinate. Including the interaction, we can calculate the energy shift of state $|k\rangle$ in

perturbation theory as

$$\Delta E_k = \langle \mathbf{k} | V | \mathbf{k} \rangle + \left\langle \mathbf{k} \middle| V G_+^0 \left(\frac{\hbar^2 k^2}{m} \right) V \middle| \mathbf{k} \right\rangle + \left\langle \mathbf{k} \middle| V G_+^0 \left(\frac{\hbar^2 k^2}{m} \right) V G_+^0 \left(\frac{\hbar^2 k^2}{m} \right) V \middle| \mathbf{k} \right\rangle + ..., \tag{5.2}$$

where

$$G_+^0 (E) = \frac{1}{E - H_0 + i0}$$

is the zeroth order resolvent operator we have discussed in the third chapter. We can write the Lippman-Schwinger equation explicitly in momentum space as

$$T (\mathbf{k}', \mathbf{k}; E) = V (\mathbf{k}' - \mathbf{k}) + \int \frac{d k''}{(2\pi)^3} V (\mathbf{k}' - \mathbf{k}'') \frac{1}{\hbar^2 \mathbf{k}^2 / m - \hbar^2 \mathbf{k}''^2 / m + i0} T (\mathbf{k}, \mathbf{k}'; E) . \tag{5.3}$$

According to Eq. (5.2), the energy shift can be written in terms of the T matrix as

$$\Delta E_k = \langle \mathbf{k} | T | \mathbf{k} \rangle = T (\mathbf{k}, \mathbf{k}; E) .$$

This formula shows that by replacing the bare interaction V with the T matrix, the exact energy shift can be calculated as a first order perturbation. The formula works for two non-identical atoms. For identical terms, an additional T matrix $T (-\mathbf{k}, \mathbf{k}; E)$ should be included.

We have thus related the energy shift to the T matrix. This T matrix can be determined from scattering properties. At low temperature, the scattering is dominated by the s wave. The scattering properties are solely determined by the energy. In the following, we use the following simplified notation for the S and T matrices,

$$S (k) = S \left(\mathbf{k}', \mathbf{k}; \frac{\hbar^2 k^2}{m} \right) ; \tag{5.4}$$

$$T (k) = T \left(\mathbf{k}', \mathbf{k}; \frac{\hbar^2 k^2}{m} \right) . \tag{5.5}$$

The S matrix describing low energy scattering is,

$$S(k) = (1 - 2ika_s),$$

where the a_s is the s wave scattering length. Recall that the T matrix is related to the S matrix by

$$T(k) = \frac{2\pi i\hbar^2}{mk}\left[S(k) - 1\right], \tag{5.6}$$

such that,

$$T(k) = \frac{4\pi\hbar^2}{m}a_s.$$

We note that the T matrix is independent of energy for low temperature scattering. If we Fourier transform to configuration space, we recover the effective interaction used widely in the literature [95],

$$V(r) = \frac{4\pi\hbar^2}{m}a_s\delta(\mathbf{r}) \tag{5.7}$$

We note that this effective interaction is ill-defined for large momenta. The renormalization of the interaction is discussed in the next section in the case of a Feshbach resonance.

5.3 Feshbach Resonance

Feshbach resonance occurs when two colliding atoms have an energy equal to that of a quasi-bound molecule. The energy scheme is plotted in Fig. (5.1)

Near the resonance, the scattering properties of the two atoms can be determined solely by the molecular resonance. This provides a mechanism to tune atom-atom interaction in experiments. Feshbach resonances were first demonstrated in a sodium Bose Einstein condensate [30]. For BEC systems, the usefulness of the resonance is fairly limited because of the increase of the three-body loss near the resonance. For

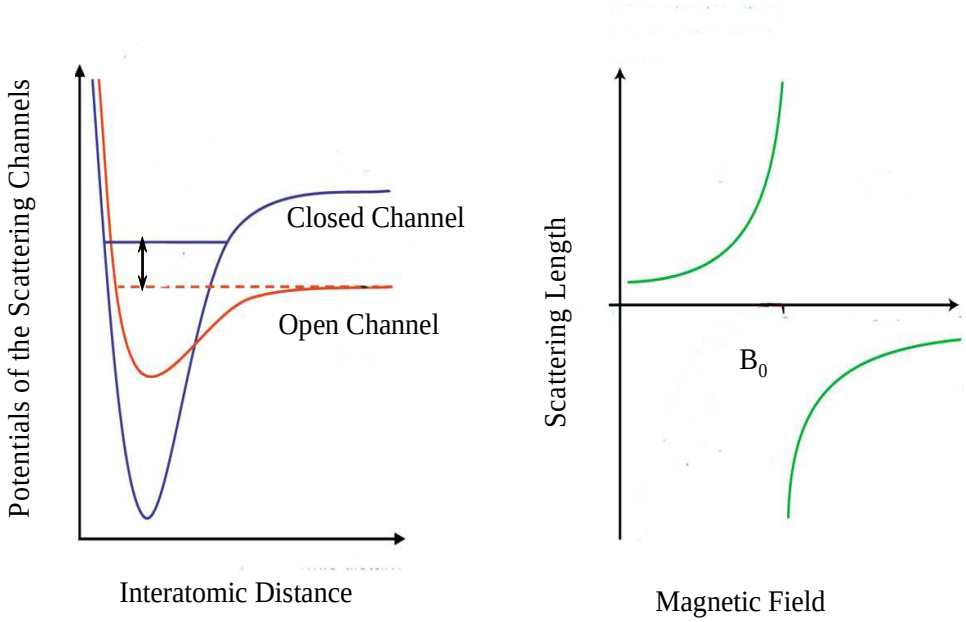

Figure 5.1: Energy schemes and scattering lengths across a Feshbach resonance.

Fermi systems, however, three body loss is inhibited by the Pauli exclusion principle. It was indeed demonstrated in later experiments on fermions that the loss rate of the Feshbach molecule is negligible.

Near a Feshbach resonance, the scattering process can be described by three parameters, the coupling between the open and the closed channels, the energy difference between the open and the closed channels and the background scattering length. Following Kokkelmans [80], we use the following contact forms,

$$V^P(\mathbf{r}) = V^P \delta(\mathbf{r});$$

$$V_c(\mathbf{r}) = V_c \delta(\mathbf{r}).$$

Here $V^P(\mathbf{r})$ is the open channel interaction and $V_c(\mathbf{r})$ is the free bound coupling. Since we are interested only in the low energy physics, the nature of the short range interaction is not important. We have chosen the potential as a delta function to simplify calculations. This choice is only a matter of convenience. For example,

one can choose the potential to be a square well potential, as long as the effective range of the potential is much smaller than the characteristic length of the problem. This point has been numerically verified by Kokkelmans [80], where the scattering properties of different modeling potentials are compared with the true potential. The problem is to relate the parameters V^P, g and dress molecular energy v to the physical observables.

The T matrix can be calculated as

$$\begin{aligned} T\left(\mathbf{k},\mathbf{k}';\hbar^2k^2/m\right) &= V^p\left(\mathbf{k}'-\mathbf{k}\right)+\frac{\left|V_c\right|^2}{\hbar^2\mathbf{k}^2/m-v+i0} \\ &+\int\frac{d^3k''}{\left(2\pi\right)^3}V^p\left(\mathbf{k}'-\mathbf{k}''\right)\frac{1}{\hbar^2\mathbf{k}^2/m-\hbar^2\mathbf{k}''^2/m+i0}T\left(\mathbf{k}'',\mathbf{k}\right) \\ &+\frac{\left|V_c\right|^2}{\hbar^2\mathbf{k}^2/m-v+i0}\int\frac{d^3k''}{\left(2\pi\right)^3}\frac{1}{\hbar^2\mathbf{k}^2/m-\hbar^2\mathbf{k}''^2/m+i0}T\left(\mathbf{k}'',\mathbf{k}\right). \end{aligned}$$

At low temperature, the scattering is dominated by the s wave contribution. Therefore, the T matrix does not have angular dependence. In addition, for elastic scattering, the magnitude of the momentum should be conserved. We use the simplified notation for the T matrix defined in Eq. (5.5). The above Lippman-Schwinger equation can be simplified as

$$\begin{aligned} T\left(k\right) &= V^p\left[1+\int\frac{d\mathbf{k}''}{\left(2\pi\right)^3}\frac{1}{\hbar^2\mathbf{k}^2/m-\hbar^2\mathbf{k}''^2/m+i0}T\left(k\right)\right] \\ &+\frac{\left|V_c\right|^2}{\hbar^2\mathbf{k}^2/m-v+i0}\left[1+\int\frac{d\mathbf{k}''}{\left(2\pi\right)^3}\frac{1}{\hbar^2\mathbf{k}^2/m-\hbar^2\mathbf{k}''^2/m+i0}T\left(k\right)\right]. \end{aligned}$$

The integral over $\mathbf{k}''$ is divergent, which is directly related to the delta function form we have assumed for the atom-atom interaction. We can quantify this divergence by introducing a high momentum cut off at K. The T matrix, in terms of the cut off

momentum, is

$$T(k) = V^P - \frac{V^P m}{2\pi^2\hbar^2} T(k) \left[k - \tanh^{-1}\frac{k}{K} + \frac{i\pi}{2}k \right] + \frac{|V_c|^2}{\hbar^2 k^2/m - v} \left\{ 1 - \frac{1}{2\pi^2}\frac{m}{\hbar^2} T(k) \left[k - \tanh^{-1}\frac{k}{K} + \frac{i\pi}{2}k \right] \right\}.$$

Solving for $T(k)$, we get

$$T(k) = \frac{V^P + \frac{|V_c|^2}{\hbar^2 k^2/m - v}}{1 + \left(K - \tanh^{-1}\frac{k}{K} + \frac{i\pi}{2}k\right)\frac{m}{2\pi^2\hbar^2}\left(V^P + \frac{|V_c|^2}{\hbar^2 k^2/m - v}\right)}.$$

The corresponding $S(k)$ matrix can be calculated using Eq. (5.6) as

$$S(k) = -i2k\frac{m}{4\pi\hbar^2}\frac{-vV^P + |V_c|^2}{-v + \alpha\left[-vV^P + |V_c|^2\right]} + 1. \tag{5.8}$$

We have neglected terms of order k/K. Here the parameter α is defined as,

$$\alpha = \frac{mK}{2\pi^2\hbar^2}.$$

On the other hand, for Feshbach resonances, the S matrix can be written out in terms of physical observables. Expanding the exponential to first order in k in the low momentum limit, we find

$$\begin{aligned} S(k) &= (1 - 2ika_{bg}) \left[1 - \frac{2ik|V_{c0}|^2}{-\frac{4\pi\hbar^2}{m}(v_0 - \hbar^2k^2/m) + ik|g_0|^2} \right] \\ &= 1 - 2ik\left(a_{bg} - \frac{m|V_{c0}|^2}{4\pi\hbar^2 v_0} \right). \end{aligned} \tag{5.9}$$

Note that the U, V_{c0}, v_0 are the parameters that are used in the S matrix to characterized scattering near the resonances. These are experimentally measurable quantities. They give the location of the resonance, its width and its strength. From this we can deduce that

$$a = a_{bg} - \frac{m|Vc_0|^2}{4\pi\hbar^2 v_0}, \tag{5.10}$$

is the modified scattering length due to the closed channel. By equating the two S matrices (5.8,5.9) we can find that the background interaction far from the resonance is

$$U = \frac{4\pi\hbar^2 a_{bg}}{m} = \frac{|V_{c0}|^2}{v_0} + \frac{-vV^P + |V_c|^2}{-v + \alpha\left[-vV^P + |V_c|^2\right]}, \tag{5.11}$$

defined in terms of the contact potential parameters. To find a renormalization condition, we need to find an appropriate relation between the contact potential parameters V^P, g, v and $U, g_{0,} v_0$, to reproduce relation (5.10). This can be done by defining

$$\Gamma = \frac{1}{1 - \alpha U}; \tag{5.12}$$

$$V^P = \Gamma U; \tag{5.13}$$

$$V_c = \Gamma V_{c0}; \tag{5.14}$$

$$v = v_0 + \alpha\Gamma V_{c0}^2. \tag{5.15}$$

This relation relates the physical observables U, V_{c0}, and v_0 with the parameters V^P, V_c, and v that one uses in theories.

One can then directly write the many body Hamiltonian with the delta function parameters as

$$K = \int d^3x \begin{bmatrix} \sum_\alpha \psi_\sigma^\dagger(x)\left(-\frac{1}{2m}\bigtriangledown^2 - \mu\right)\psi_\sigma(x) + \phi^\dagger(x)\left(-\frac{1}{m}\bigtriangledown^2 - \mu\right)\phi(x) \\ +V^P\psi_\uparrow^\dagger(x)\,\psi_\downarrow^\dagger(x)\,\psi_\downarrow(x)\,\psi_\uparrow(x) \\ +V_c\phi^\dagger(x)\,\psi_\downarrow(x)\,\psi_\uparrow(x) + V_c\phi(x)\,\psi_\downarrow^\dagger(x)\,\psi_\uparrow^\dagger(x) \end{bmatrix}, \tag{5.16}$$

where $\psi_\sigma(x)$ is the field operator for the open channel atoms with spin σ, $\phi(x)$ is the molecular field operator, and μ is the chemical potential. In K and Li experiments, one finds broad Feshbach resonances: that is, the width of the resonance is much larger than all other relevant energy scales. Therefore, the population of the

molecular state is negligible near the resonance. One can eliminate the molecular population and reach the following single channel model,

$$K = \int d\mathbf{r} \sum_a \psi_\alpha^\dagger(\mathbf{r}) \left(-\frac{1}{2m} \bigtriangledown^2 - \mu \right) \psi_\alpha(\mathbf{r}) + \frac{1}{2} \int d\mathbf{r} \sum_{\alpha,\beta} g \psi_\alpha^\dagger(\mathbf{r}) \psi_\beta^\dagger(\mathbf{r}) \psi_\beta(\mathbf{r}) \psi_a(\mathbf{r}), \tag{5.17}$$

where the effective single channel interaction is

$$\begin{aligned} g &= V^P - \frac{V_c^2}{v} \\ &= \frac{U - \frac{V_{c0}^2}{v_0}}{1 - \alpha \left(U - \frac{V_{c0}^2}{v_0} \right)} \\ &= \frac{\tilde{U}}{1 - \alpha \tilde{U}}, \end{aligned}$$

with the $\tilde{U}$ being the bare effective interaction between atoms,

$$\tilde{U} = U - \frac{V_{c0}^2}{v_0}.$$

5.4 Mean Field Bogliubov-de Gennes Approach

In the previous section, we assumed that the system is uniform. In particular, we assumed that the interaction g is a constant in the whole space. This restriction is not necessary. As long as the modulation of the interaction is slow compare to the chemical potential of the many body system, the effective interaction can acquire a spatial dependence,

$$K = \int d\mathbf{r} \sum_a \psi_\alpha^\dagger(\mathbf{r}) \left(-\frac{1}{2m} \bigtriangledown^2 - \mu \right) \psi_\alpha(\mathbf{r}) + \frac{1}{2} \int d\mathbf{r} \sum_{\alpha,\beta} g(\mathbf{r}) \psi_\alpha^\dagger(\mathbf{r}) \psi_\beta^\dagger(\mathbf{r}) \psi_\beta(\mathbf{r}) \psi_a(\mathbf{r}). \tag{5.18}$$

The dependence of $g(r)$ on position is shown explicitly.

To solve the above problem, we write Eq. (5.18) in the following effective single particle mean field form,

$$\begin{aligned} K_{eff} = & \int d^3x \sum_a \psi_\alpha^\dagger(x) H_e \psi_\alpha(x) \\ & + \frac{1}{2} \int d^3x \sum_{\alpha\beta} \Delta_{\alpha\beta}(x) \psi_\alpha^\dagger(x) \psi_\beta^\dagger(x) + \Delta_{\alpha\beta}^*(x) \psi_\beta(x) \psi_a(x) \\ & - \frac{1}{2} \int d^3x \sum_{\alpha\beta} V_{a\beta}(x) \psi_\beta^\dagger(x) \psi_a(x) + \frac{1}{2} \int d^3x \sum_{\alpha\beta} U_{\alpha\alpha}(x) \psi_\beta^\dagger(x) \psi_\beta(x), \end{aligned} \tag{5.19}$$

where we have taken the mean field as

$$\begin{aligned} \Delta_{\alpha\beta}(x) &= -g(x) \langle \psi_\beta(x) \psi_a(x) \rangle \\ V_{a\beta}(x) &= g(x) \left\langle \psi_\alpha^\dagger(x) \psi_\beta(x) \right\rangle \\ U_{\alpha\alpha}(x) &= g(x) \left\langle \psi_\alpha^\dagger(x) \psi_\alpha(x) \right\rangle, \end{aligned} \tag{5.20}$$

and $H_e = H_0 - \mu$ is the single particle part of the potential. For s wave scattering $g_{a\beta} = g$ for $\alpha \neq \beta$ and $g_{a\beta} = 0$ for $\alpha = \beta$. In our system, we assume equal spin populations, therefore, $U_{\downarrow\downarrow}(x) = U_{\uparrow\uparrow}(x)$. We can simplify Eq. (5.19)

$$\begin{aligned} K_{eff} = & \int d^3x \begin{bmatrix} \sum_a \psi_\alpha^\dagger(x) H_e \psi_\alpha(x) \\ + \Delta(x) \psi_\uparrow^\dagger(x) \psi_\downarrow^\dagger(x) + \Delta^*(x) \psi_\downarrow(x) \psi_\uparrow(x) \end{bmatrix} \\ & + \int d^3x \left[U(x) \psi_\uparrow^\dagger(x) \psi_\uparrow(x) + U(x) \psi_\downarrow^\dagger(x) \psi_\downarrow(x) \right]. \end{aligned} \tag{5.21}$$

This single particle Hamiltonian can be diagonalized by the following transformation

$$\begin{aligned} \psi_\uparrow(x) &= \sum_n u_n(x) \gamma_{n\uparrow} - v_n^*(x) \gamma_{n\downarrow}^\dagger \\ \psi_\downarrow(x) &= \sum_n u_n(x) \gamma_{n\downarrow} + v_n^*(x) \gamma_{n\uparrow}^\dagger. \end{aligned} \tag{5.22}$$

Here $\gamma_{n\sigma}$ and $\gamma^{\dagger}_{n\sigma}$ are the Fermi creation and annihilation operator, satisfying anti-commutation relations. They correspond to eigenstates of the effective single particle potential (5.21)

$$H = E_g + \sum_{n\alpha} \varepsilon_n \gamma^{\dagger}_{n\alpha} \gamma_{n\alpha}.$$

We define the ground state as that for which

$$\gamma_{n\alpha} |0\rangle = 0$$

. Using commutation relations one can show that

$$\begin{aligned} [\psi_{\uparrow}(x), K_{eff}] &= H_e \psi_{\uparrow}(x) + \Delta(x) \psi^{\dagger}_{\downarrow}(x) + U(x) \psi_{\uparrow}(x) \\ [\psi_{\downarrow}(x), K_{eff}] &= H_e \psi_{\downarrow}(x) - \Delta(x) \psi^{\dagger}_{\uparrow}(x) + U(x) \psi_{\downarrow}(x), \end{aligned} \tag{5.23}$$

which, together with (5.22) yield the Bogoliubov de Gennes (BdG) equation [104]

$$\begin{aligned} E_n u_n &= H_e u_n + \Delta(x) v_n + U(x) u_n \\ E_n v_n &= -H^*_e v_n + \Delta^*(x) u_n - U(x) v_n. \end{aligned} \tag{5.24}$$

We can write the above equations and Eq. (5.20) in momentum space as

$$(\varepsilon_k - \mu) u_{\mathbf{k}} + U_{\mathbf{k}'} u_{\mathbf{k}-\mathbf{k}'} + \Delta_{\mathbf{k}'} v_{\mathbf{k}-\mathbf{k}'} = E u_{\mathbf{k}}; \tag{5.25}$$

$$-(\varepsilon_k - \mu) v_{\mathbf{k}} - U_{\mathbf{k}'} v_{\mathbf{k}-\mathbf{k}'} + \Delta^*_{\mathbf{k}'} u_{\mathbf{k}+\mathbf{k}'} = E v_{\mathbf{k}}; \tag{5.26}$$

$$-\frac{1}{V} v^{(n)}_{\mathbf{k}'} v^{(n)}_{\mathbf{k}+\mathbf{k}'-\mathbf{k}''} \tilde{g}_{\mathbf{k}''} = U_{\mathbf{k}}; \tag{5.27}$$

$$\frac{1}{V} v^{(n)}_{\mathbf{k}'} u^{(n)}_{\mathbf{k}+\mathbf{k}'-\mathbf{k}''} \tilde{g}_{\mathbf{k}''} = \Delta_{\mathbf{k}}; \tag{5.28}$$

$$\frac{2}{V} v^{(n)}_{\mathbf{k}} v^{(n)}_{\mathbf{k}} = \bar{n}. \tag{5.29}$$

A summation convention is used for any momentum that appears twice on the left hand sides of these equations. The spin index can be neglected due to the symmetry between spin up and down.

Recall that we want to study the following form of modulation,

$$g(\mathbf{r}) = [g_0 + g\cos(\mathbf{k}_0 \cdot \mathbf{r})].$$

In the following, we take $\mathbf{k}_0$ along the z direction. With this choice, $\Delta(\mathbf{r}), U(\mathbf{r})$ are functions of z only. In momentum space, we can solve the single particle problem in a set of subspaces corresponding to constant k_x and k_y. The Fourier transforms of $u(\mathbf{r}), v(\mathbf{r}), g(\mathbf{r}), \Delta(\mathbf{r})$, and $U(\mathbf{r})$ are defined as $u_{\mathbf{k}}, v_{\mathbf{k}}, g_{\mathbf{k}}, \Delta_{\mathbf{k}}$, and $U_{\mathbf{k}}$, respectively. We can take $u(\mathbf{r}), v(\mathbf{r})$ and $\Delta_{\mathbf{k}}$ to be real without loss of generality. Since we are dealing with a problem invariant under reflection $\mathbf{r} \to -\mathbf{r}$, we can also take $a_{\mathbf{k}}, b_{\mathbf{k}}, \Delta_{\mathbf{k}}$ and $U_{\mathbf{k}}$ to be real. The quantity $\varepsilon_{\mathbf{k}} = \hbar^2 k^2/2m$ is the kinetic energy of a particle with wave vector $\mathbf{k}$, and V is the quantization volume. We note that near a Feshbach resonance the chemical potential, μ, need to be self-consistently determined using the an average density of the Fermi gas $\bar{n}$ in Eq. (5.29).

5.5 Ground State Properties and the Excitation Spectrum

We can solve the BdG equations self-consistently using numerical iteration. The self-consistent gap is found to have only three components in momentum space, namely, $k_z = 0, \pm k_0$. Due to the form of the interaction we choose (5.1), the zero momentum component of the gap, Δ_0, is always larger than the $\pm k_0$ components of the gap, $\Delta_{\pm k_0}$. The pairing of the many body ground state ,$|0\rangle$, is directly related to the expectation value, $\langle 0| a_{\mathbf{k}\uparrow} a_{\mathbf{q}-\mathbf{k}\downarrow} |0\rangle$. Since the modulation of the interaction is along the z direction, the non zero COM pairing occurs only in the z direction. The system is homogeneous along the x and y directions. In these directions, pairing occurs with opposite momenta. Without loss of generality, we can limit ourselves to the study the Cooper pairs formed by the atoms with $k_x = k_y = 0$. It can be shown

that

$$\langle 0|\, a_{k_z\uparrow} a_{q-k_z\downarrow}\, |0\rangle = \sum_n u_{k_z}^{(n)} v_{k_z-q}^{(n)}. \tag{5.30}$$

The numerical result is presented in figure(5.2a).

We find that only states with the COM momenta $\mathbf{q} = 0, \pm\mathbf{k}_0$ are occupied. The probability of finding Cooper pairs with higher integral multiples of $\mathbf{k}_0$ is negligible. Given the magnitude of the coupling between different COM components, descried by the g term in the interaction (5.1), it is surprising that atom pairs do not occupy states with COM momenta corresponding to higher harmonics of k_0. Actually this result can be explained by the nonlinear property of the BdG equations. Atom pairs tend to occupy as few COM states as possible because the interaction energy is proportional to the square of $\langle 0|\, a_{k_z\uparrow} a_{q-k_z\downarrow}\, |0\rangle$. By occupying only these three COM states, the pairing energy is maximized in magnitude. One can see clearly from Fig. (5.2a) that the pairing occurs mostly for atoms near the Fermi surface. We note that generally the pairing amplitude $\langle 0|\, a_{k_z\uparrow} a_{k_0-k_z\downarrow}\, |0\rangle$ does not equal the pairing amplitude $\langle 0|\, a_{k_z\uparrow} a_{-k_0-k_z\downarrow}\, |0\rangle$. This is because, for $k_z \neq 0$, either $k_0 - k_z$ or $-k_0 - k_z$ is closer to the Fermi surface. We emphasize that pairs occupy several COM states coherently. A direct consequence of this is that one particular atom, say an atom with momentum $\mathbf{k}$ and spin up, can form pairs simultaneously with several spin down atoms with momenta $-\mathbf{k}$, $\mathbf{k}_0 - \mathbf{k}$,and $-\mathbf{k}_0 - \mathbf{k}$, respectively. Right at the Fermi surface, pairings with opposite momenta dominate, and therefore the amplitudes $\langle 0|\, a_{\mathbf{k}_F\uparrow} a_{\mathbf{k}_0-\mathbf{k}_F\downarrow}\, |0\rangle$ and $\langle 0|\, a_{\mathbf{k}_F\uparrow} a_{-\mathbf{k}_0-\mathbf{k}_F\downarrow}\, |0\rangle$ are small. Slightly away from the Fermi surface, the pairing with zero COM is not as strong and one starts to see pairings with nonzero COM. This feature of the ground state is closely related to the single particle excitation spectrum discussed below.

The eigenenergies that we found by solving Eqs. (5.25)(5.26) are the single particle

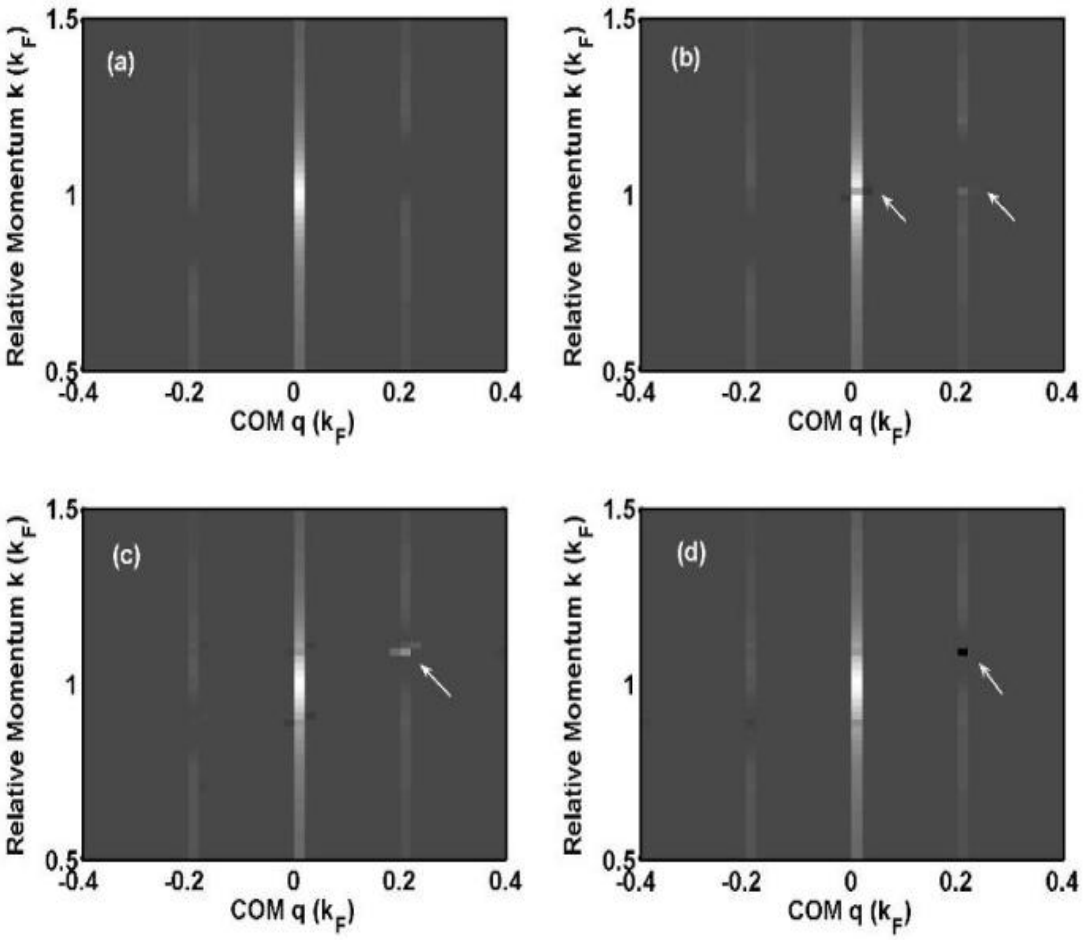

Figure 5.2: Pairing amplitudes $a_{k_z\uparrow}a_{q-k_z\downarrow}$ as a function of q and k_z. Plot (a) corresponds to the ground state, (b) to the first excited state, (c) to the excited state right before the second gap (the 20th excited state in Fig. (5.3)), and (d) to the excited state right after the second gap (the 21st excited state in Fig. (5.3)). Only momenta close to the fermi surface are shown. The arrows are used as guides to the eyes. It points to the k_z and $q's$ where significant changes in the pairing amplitudes, $a_{k_z\uparrow}a_{q-k_z\downarrow}$, take place. We have used a units with fermi momentum and fermi energy to be one. The numerical values for the parameters are: $g_0 = 20$, $g = 15$, and $k_0 = 0.2$. The self-consistent gaps and chemical potential are found to be, $\Delta_0 = 0.13$, $\Delta_{\pm k_0} = .06$ and $\mu = 0.85$.

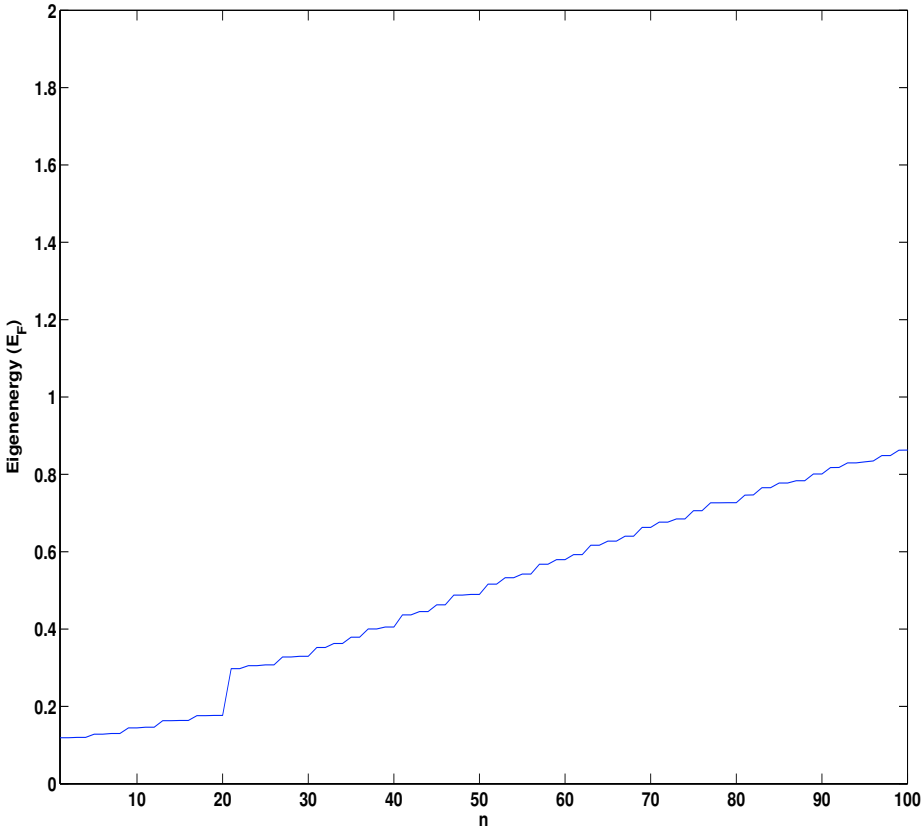

Figure 5.3: Plot of the single particle excitation energy. Here we only look at the quasi-particles with $k_x = k_y = 0$. The n labels the eigenstates. The second gap locates between the state $n = 20$ and $n = 21$. The other "mini gaps", for example, gaps between the state $n = 22$ and the state $n = 23$, comes from the finite grid of our numerical calculation. We have used same numerical values for relevant parameters as Fig. (5.2).

excitation energies of the many body state. The excitation gap, $\Delta(\mathbf{r})$, is positive everywhere in real space with its minimum being $\Delta_0 - \Delta_{k_0}$. This minimum is the lower bound of the excitation gap. Above the gap, the excitation spectrum is continuous. However, for quasi-particles with a particular value of k_x and k_y, say, $k_x = k_y = 0$, additional gaps emerge due to the periodic modulation of the interaction along z direction [see Fig(5.3)].

The modulation therefore induces band gap structures in the quasi-particle ex-

citations. According to the standard BCS theory, excitation gaps emerge because extra energies are needed to break Cooper pairs. In the following, we develop a semi-quantitative understanding of the excitation spectrum plotted in Fig. (5.3) in a pair breaking picture. The pairing amplitudes in an excited state $|n\rangle$ are,

$$\langle n\left|a_{k\uparrow}a_{q-k\downarrow}\right|n\rangle = \langle 0\left|a_{k\uparrow}a_{q-k\downarrow}\right|0\rangle - u_k^{(n)}v_{k-q}^{(n)}.$$

The pairing amplitudes for several excited states are shown in Fig. (5.2b, 5.2c, 5.2d). For low energy excitations, the pair breaking occurs near the Fermi surface. In other words, the pairs $a_{k_z\uparrow}a_{q-k_z\downarrow}$ with k_z close to $\pm k_F$ are most easily broken. In the numerical calculation, we actually find that the pair breaking happens as a superposition of breaking the pair $a_{k_z\uparrow}a_{q-k_z\downarrow}$ and breaking the pair $a_{-k_z\uparrow}a_{q+k_z\downarrow}$. The energy related to this superposition is small. In the following we focus only on one side of the Fermi surface. For the lowest excited state $|1\rangle$, the change in the pairing amplitudes occurs right at the Fermi surface. The amplitude $\langle 1|\, a_{\mathbf{k}_F\uparrow}a_{-\mathbf{k}_F\downarrow}\,|1\rangle$ is found to be close to zero. This is a very significant change compared with the large ground state pairing amplitude, $\langle 0|\, a_{\mathbf{k}_F\uparrow}a_{-\mathbf{k}_F\downarrow}\,|0\rangle$. On the other hand, as we mentioned in the discussion of the ground state properties, the pairing amplitude $\langle 0|\, a_{\mathbf{k}_F\uparrow}a_{\mathbf{k}_0-\mathbf{k}_F\downarrow}\,|0\rangle$ and $\langle 0|\, a_{\mathbf{k}_F\uparrow}a_{-\mathbf{k}_0-\mathbf{k}_F\downarrow}\,|0\rangle$ are close to zero because of the dominant pairing amplitude $\langle 0|\, a_{\mathbf{k}_F\uparrow}a_{-\mathbf{k}_F\downarrow}\,|0\rangle$. In the lowest excited state, now that the $a_{\mathbf{k}_F\uparrow}a_{-\mathbf{k}_F\downarrow}$ pair is broken, the particle $a^\dagger_{\mathbf{k}_F\uparrow}$ is free to pair with particles $a^\dagger_{\pm\mathbf{k}_0-\mathbf{k}_F\downarrow}$ and this decrease the energy by a amount $\Delta_{k_0.}$ If we neglect the contribution from the kinetic energy and the Hartree term in the Hamiltonian, the first gap can be estimated from the above pair breaking picture to be

$$\sum_k \left[2\Delta_0 u_k^{(n)}v_k^{(n)} + 2\Delta_{k_0}u_{\pm k_0+k}v_k\right] \approx 0.09.$$

This is close to the value 0.10 obtained from solving the BdG equations. The exci-

tation energy increases continuously as the excitation gets further and further away from the Fermi surface. The states with energies right below and above the second gap, the state $n = 20$ and the state $n = 21$ in Fig. (5.3), have sudden changes of their signs for the pairing amplitudes $a_{k\uparrow}a_{\pm k_0-k\downarrow}$ for several $k's$. These $k's$ are indicated in Figs. (5.2c, 5.2d) by arrows. We estimate the energy cost for this sign change to be 0.09, which is close to the observed value of 0.11. Therefore, the phase flips of the pairs with nonzero COM momenta give rise to the second gap. Similar observations can be made for gaps at higher energies. However, as the kinetic energy increases, the gap structure gets more and more obscure. Actually, with parameters used in the calculation, only two gaps are observed. We would like to emphasis that, after summation over the contribution from different k_x and k_y, the additional gap we discussed above, is not a true second gap in the excitation spectrum. However, it nevertheless induces a sharp change of the density of states. Such effects, arising from the rich structures of the pair wavefunction, can be observed in experiments.

5.6 Experimental Observables

Experimentally, the spatial modulation of the atom-atom scattering length can be achieved via magnetic or optical Feshbach resonances. However, it is not easy to generate spatial variations of the magnetic field on a scale smaller than the sample size. Optical Feshbach resonances are more promising to realize the desired system. By coupling the incident channel of two atom scattering to the molecular state closed channel [88][89][90], one can induce the desired spatial modulation using an optical lattice. In an optical lattice the intensity and polarization of the laser field vary periodically in space to introduce a spatial variation of atom-molecule coupling, which leads to the desired spatially modulation of the scattering length. The laser

fields need to be tuned far away from the resonance of a single atom to minimize the effect of the field on the single particle part of the Hamiltonian. This technique has recently been demonstrated in experiments using alkali atoms [91][93] and alkaline earth atoms [94]. In the alkali atom experiments, large loss rates are observed. This difficulty may be circumvented by using stronger laser fields and detuning further away from the molecular levels. On the other hand, it was also found recently [94] that alkaline earth atom systems give much smaller loss rates. Nevertheless, we use the alkali atom experimental data in our numerical calculations, since they are the only Fermi gas experiments available. In particular, we use data from the recent experiments [24][25][7][5][6][26] for ^6Li. We have taken the unit of energy as the Fermi energy $E_F = (3\pi^2\bar{n})^{1/3} \sim 3\mu k$ and the unit of wave vector as k_F. The background scattering length is $a_{bg} \sim -0.5$ in these units. The wavevector $\mathbf{k}_0$, characterizing the variation of the interaction (5.1), needs to be taken smaller than the Fermi momentum. If we introduce the modulation via laser fields, the modulation is of the order of wavelengths, say $k_0 \sim .2$. Note that this choice automatically satisfies the condition $k_0 \ll 2\pi/a$, necessary for the validity of Eq. (5.1). The coupling strength is about $g_0 \sim -20$. This gives an interaction energy $\bar{n}g_0 \sim -2$. As has been stated earlier, the coupling between different COM g is smaller in magnitude than g_0.

The observation of this novel pairing in the ground state involves measurements of the COM momenta of pairs. This can be done by pair-wise projecting Cooper pairs into molecules by a fast sweep from BCS side of the resonance to the BEC side. In such a process, the many body Cooper pairs are transformed into bound molecules. After this procedure, the molecules of the condensate coherently occupy momentum states $\mathbf{q} = 0$, $\mathbf{q} = \pm\mathbf{k}_0$, which can be measured by a time of flight image of the molecules. Such measurements have already been performed in several

BEC-BCS cross over experiments [5][6][26]. Another way of observing the pairing correlation, recently demonstrated experimentally [97][98], is to measure the shot noise correlations.

For the excited states properties, one needs to measure the radio frequency (RF) spectrum. RF spectra have been proposed [99][100][101][102][103] and recently used to measure the Fermi gas pairing gap [78]. In experiments, two of the hyperfine levels of the atoms, $|1\rangle, |2\rangle$ are identified as the spin up and spin down states. A probing RF field couples one of the hyperfine levels, say $|2\rangle$, to a third hyperfine level $|3\rangle$. The coupling can be written as

$$\Omega e^{i\omega t} \int d^3x \psi_3^\dagger(x) \psi_2(x) + h.c..$$

The coupling strength is denoted by Ω which can be adjusted by the laser power and laser detuning. The $\psi_3(x)$ and $\psi_2(x)$ are the Fermi field operators for atoms in hyperfine states $|3\rangle$ and $|2\rangle$, respectively. In momentum space, this can be written as

$$\frac{\Omega e^{i\omega t}}{V} \sum_k a_{k;3}^\dagger a_{k,2} + h.c..$$

The excitation from a superfluid level $|2\rangle$ to normal state level $|3\rangle$ requires first breaking the Cooper pair formed by $|1\rangle$ and $|2\rangle$, and then exciting according to the mean field shifted energy levels. As observed in the experiment of Li [78] the mean field effects can be suppressed; therefore, the main feature of the RF spectra arises from the pairing. The transition rate can be evaluated directly from our BdG solution of the quasiparticle excitations by Fermi's golden rule as

$$R(\omega) = \frac{2\pi}{\hbar} \frac{\Omega^2}{V} \sum_{n,k} \left| v_{-k_z}^{(n)}(k_x, k_y) \right|^2 \delta \left[E_n(k_x, k_y) + \hbar\omega_{23} - \mu + \frac{\hbar^2 k^2}{2m} - \hbar\omega \right]. \quad (5.31)$$

Here $\hbar\omega_{23}$ is the energy difference between the hyperfine state $|2\rangle$ and $|3\rangle$.

Such calculation turns out to be numerically challenging. They require a very fine grid in momentum space. However, in the case that $k_0 \ll k_F$, we can adopt a Local Density Approximation (LDA) approach. Such an approximation utilizes the fact that most of the contribution to the radio frequency signal comes from quasiparticles with momentum $k \sim k_F$. Given the condition that $k_0 \ll k_F$, one can neglect the gradient of the modulation of the interaction. In LDA the RF spectrum is calculated locally and the final result is a summation of local contributions [99][100][101][102][103],

$$R(\omega) = \int d^3 r R_{loc}(r, \omega),$$

where the $R_{loc}(r, \omega)$ is the local contribution according to Eq. (5.31) with its parameters determined locally. For the particular parameters we studied in this paper, $k = k_F/5$. Such parameters do not necessarily validate the LDA approximation. We nevertheless carry out the LDA calculation and compare the result with the direct BdG calculation.

For LDA, at each local point we define a local gap and chemical potential, $\Delta(r), \mu(r)$. The energy conservation condition is

$$f = \sqrt{[\varepsilon_k - \mu(r)]^2 + \Delta(r)^2} + \varepsilon_k - \hbar\omega - \mu(r) = 0,$$

and the ε_k can be found to be

$$\varepsilon_k = \frac{\hbar^2\omega^2 - \Delta^2(r)}{2\hbar\omega} + \mu(r).$$

One can calculate the threshold frequency by requiring $\varepsilon_k > 0$,

$$\hbar^2\omega^2 + 2\mu(r)\hbar\omega - \Delta^2(r) > 0;$$

leading to

$$\hbar\omega_{th} = \sqrt{\Delta^2(r) + \mu^2(r)} - \mu(r)$$

Note that in the uniform case, one can find an analytical formula for the wavefunction of the Cooper pair with

$$v_k^2 = \frac{E_k - (\varepsilon_k - \mu)}{2E_k}$$

and

$$E_k = \sqrt{\left(\frac{\hbar^2\omega^2 - \Delta^2(r)}{2\hbar\omega}\right)^2 + \Delta^2(r)} = \frac{\Delta^2(r) + \hbar^2\omega^2}{2\hbar\omega}.$$

Therefore, according to Eq. (5.31) the local signal is

$$R_{loc}(r,\omega) = \frac{2\pi}{\hbar}\frac{\Omega^2}{V}D(\varepsilon_k)\frac{\Delta^2(r)}{\Delta^2(r) + \hbar^2\omega^2}\Theta\left(\frac{\hbar^2\omega^2 - \Delta(r)^2}{2\hbar\omega} + \mu(r)\right)\left|\frac{1}{\partial f/\partial\varepsilon_k}\right|,$$

with

$$\partial f/\partial\varepsilon_k = 1 + \left(\frac{\partial\sqrt{[\varepsilon_k - \mu(r)]^2 + \Delta(r)^2}}{\partial\varepsilon_k}\right)_{\varepsilon_k} = \frac{2\omega^2}{\Delta^2(r) + \omega^2}.$$

The final result for $R_{loc}(r,\omega)$ can be found as

$$R_{loc}(r,\omega) = \frac{\pi}{\hbar}\frac{\Omega^2}{V}D(\varepsilon_k)\frac{\Delta^2(r)}{\omega^2}\Theta\left(\frac{\hbar^2\omega^2 - \Delta(r)^2}{2\hbar\omega} + \mu(r)\right).$$

Note that $\Delta(r)$ and $\mu(r)$ are extracted from numerical BDG solutions.

$$\Delta(r) = \Delta_0 + \Delta_{k_0}\cos(k_0 z);$$

$$\mu(r) = \mu - U(r) = \mu - U_0 - U_{k_0}\cos(k_0 z).$$

Here ω is the detuning of the laser frequency from the frequency difference in $|2\rangle$ and $|3\rangle$, and Ω is the coupling between them. $D(\varepsilon_k)$ is the free particle density of states and it is proportional to $\sqrt{\varepsilon_k}$. The chemical potential of state $|3\rangle$ is taken to be zero and the RF spectrum is shown in figure (5.4).

For the direct BdG evaluation, we make use of the fact that there are only three components for Δ and U in momentum space, namely, the zero and the $\pm k_0$ components. This observation suggests that in BdG equations (5.25) (5.26) u_k and v_k

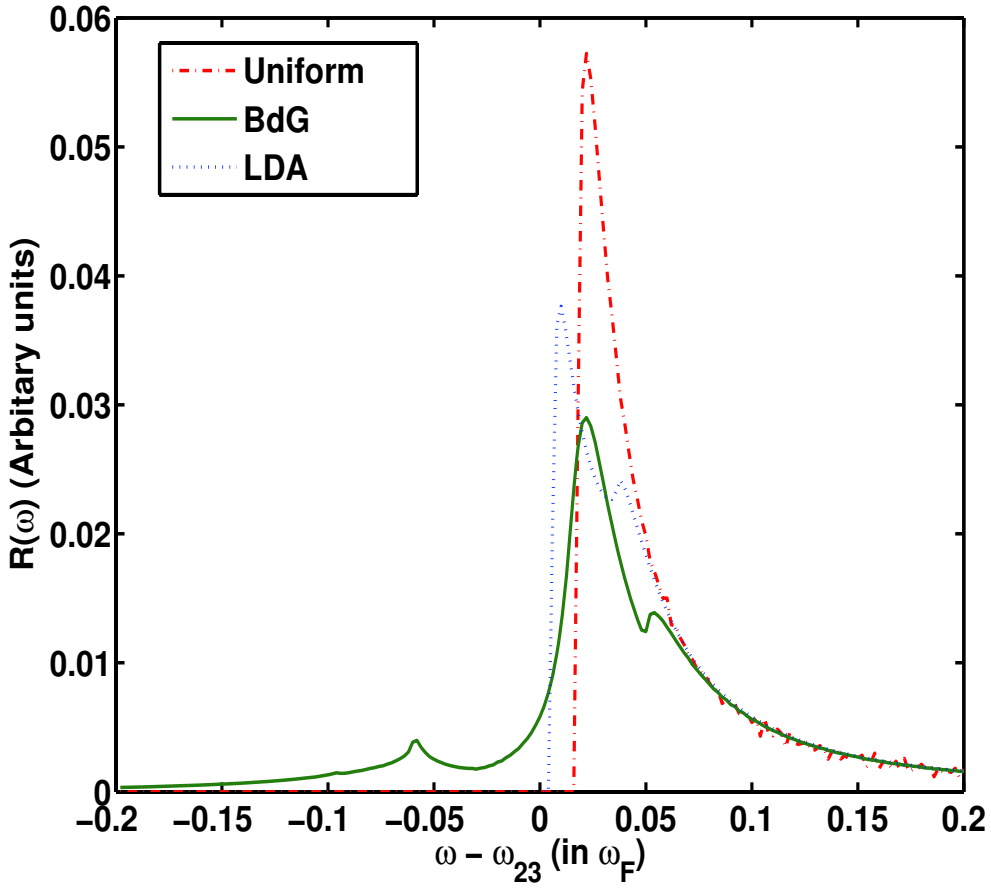

Figure 5.4: The RF spectra are plotted for a homogenous system and the spatially modulated system. The RF signals for the modulated system are calculated both by LDA method and by BdG method. We have used the numerical values as Figure(5.2) for various parameters.

couples only to $u_{k\pm k_0}$, $v_{k\pm k_0}$ $u_{k\pm 2k_0}$, $v_{k\pm 2k_0}$, ... , $u_{k\pm nk_0}$ and $v_{k\pm nk_0}$, where n can be any integer. One can then decompose the Hilbert space into small subspaces for each k in the range of $(-k_0, k_0]$. This significantly simplifies the size of the problem. The RF signal calculated directly from equation (5.31) is plotted with the LDA signal in figure (5.4).

We note that the LDA calculation gives a clear threshold. This threshold behavior is artificial resulting from the assumption that qusiparticle excitation have well defined momenta. In the full BdG calculation, the qusiparticle wavefunction contains momenta differing by integer numbers of k_0. For $\hbar\omega < 0$, one already see non-negligible amount of weights in the RF spectrum. For $\hbar\omega > 0$, the LDA and BdG calculation predicts similar two peak structures. These two peaks correspond to the first and the second gap in the quasiparticle excitation spectrum. The position and strength of these two peaks are, however, different for LDA and BdG.

5.7 Summary

In conclusion, we studied a Fermi gas with spatially modulated interaction in a mean field theory at zero temperature. We also discussed its experimental realization and detection. Such a state has a periodic modulation of the order parameter similar to that of the FFLO states. Even though we considered a spatially varying interaction along one direction only, our analysis can be generalized easily to a system where the interaction is modulated in three directions. In the case that the second gaps along three directions overlaps, the system can have true additional excitation gaps. This should produce more pronounce signals in the RF spectrum. We hope this study will motivate experimental studies of the optical Feshbach resonances in Fermi gases.

CHAPTER VI

Summary and Future Study

6.1 Summary of the Thesis

In this thesis, we have presented a study of several many body effects in the atomic systems. Atomic systems have advantages over traditional systems in that they generally provide a clean environment in which parameters can be controlled using various techniques. With the rapid progress in cold atom physics, the theories presented in this thesis may find application in some interesting systems.

Chapters 2 and 3 were devoted to the study of single atom processes in a many-body environment. The environment-induced modifications of the both the decay rate and atomic recoil are among the basic processes investigated. A good understanding of those effects in a many body environment is necessary for future applications of cold atoms in quantum computation and precision measurement.

Macroscopically, the corrections to the decay rate are calculated using either real cavity or virtual cavity models. In a microscopic picture, a single atom decays by exchanging virtual photons with the environment. Inside a dielectric, the virtual photon is modified because of its scattering with the environment atoms. By including such corrections, we found the modification of the source atom decay rate. In our microscopic model, the atoms are modeled as randomly distributed fixed particles.

In first order perturbation theory, a correction of $\frac{7}{6}N\alpha\gamma$ to the vacuum decay rate was found. This result agrees with both the real cavity model and the virtual cavity model to first order in the dielectric density. To distinguish these two models, it is necessary to carry out this calculation to the second order in density. In second order, we found the correction is $\frac{71}{72}N^2\alpha^2\gamma$, which is different from both the real and virtual cavity model. In order to recover the result for the virtual cavity model, we have to include contributions from the situation where two medium atoms occupy the same space point.

In spontaneous decay, the source atom undergoes recoil when emitting a photon. When the atoms are cooled below a temperature corresponding to the recoil energy, this photon recoil phenomenon can be resolved. In the case where the source atom is inside an atomic gas, the source atom recoil is modified by its many particle environment. Experimentally, it was found that the source atom recoils according to $n\hbar k_0$. We provide a microscopic explanation of this phenomenon. The reason for the modification of the recoil momentum is that the photon radiated by the spontaneous decay of the source atom is scattered by the medium atoms. The interference of different scattering amplitudes effectively shifts the central frequency of the photon. Because of this shift, the momentum carried by the photon is modified according to $n\hbar k_0$, which results in a modification to the source atom recoil.

In Chapters 4 and 5, we studied two many body system that can be realized in ultra-cold atomic gas systems. This research focuses on the many body behavior, instead of single particle processes.

An impurity inside a many body system has always been an important topic in condensed matter systems. In a cold atom gas, the system is very clean and is generally free of any impurities. To generate effective impurities inside a cold atom

gas, one can add impurity atoms, ions or apply external fields to this system. We studied the many body coherence of a Tonks-Girardeau gas in the presence of a local potential. It was found that a local potential decreases the value of the largest eigenvalue of the single particle density matrix. The repulsive local potential always decreases the "condensate" density near the impurity while an attractive potential may increase or decrease the "condensate" density depending on the strength the potential. To observe this phenomenon, one can observe the momentum distribution of the gas with respect to different strengths of the local potential. This can be done by switching off the confining trap of the atomic gas and observing the time of flight image.

In Chapter 5, we discussed a cold atomic fermionic system with a spatially modulated interaction. The spatial modulation is achieved via an optical Feshbach resonance. In cases where the interaction strength is periodically modulated, we find that, in the ground state, the Cooper pair acquires non-zero momenta. In addition, the system's single particle excitation spectrum along a particular direction has multiple gap structures. The magnitude of the gap is related to non-zero center of mass pairing amplitudes. To observe the non-zero momentum pairing is straightforward. One does a fast sweep of external fields to project the Cooper pairs to bound molecules. The momentum distribution of the molecules give a direct measurement of the Cooper pair momenta. The single particle excitation, on the other hand, can be measured by the rf spectrum.

6.2 Future Directions

In the calculation of the spontaneous decay and photon recoil, we have used a microscopic model where the dielectric atoms are fixed and randomly distributed

point-like particles. We considered only the internal degrees of freedom and neglected their external motions. As we have seen in the calculation of the decay rate, however, the result depends critically on the atom-atom correlation in configuration space. This is a consequence of the fact that when two atoms are close to each other, the interaction energy between then can be quite large to invalidate the perturbative calculation. These kinds of divergences are usually circumvented by certain types of regularization procedures such as a high momentum cut off. Such procedures are not necessary if the atomic motion and the details of the interaction potentials are included in the theory. A full many body theory of the atoms and the photon fields is able to take into account both the atom and the field degrees of freedom and gives unambiguous pictures for photon propagation in a dielectric. Such systems may be fairly complicated and numerical computation, such as Monte Carlo simulation, may be necessary to find solutions.

In the study of the ultra-cold atomic gases, one usually utilizes a different modeling approach. In typical atomic gas theories, the atomic external degrees of freedom are treated quantum mechanically, while the photon fields are treated classically. There the external fields are considered only as a control knobs. A great amount of physics related to the properties of the photon fields may be lost in such a picture. In addition, even considering the external fields only as knobs, not all the properties of the fields have been used fully. For example, in a typical time of flight image measurement, only the field intensity is measured. This actually corresponds only to a very small part of the information that can be extracted from the photon fields.

In a many body theory where the photon fields and the atomic gases of such systems are treated on an equal footing, it is possible to ask the following question. Given an interaction of fields and atoms, how are correlations of electromagnetic

fields related to correlations of cold atom many body states, and vice versa?

By answering this question, we may find new ways of engineering interesting cold atom many body states by varying correlations of photon fields. It is equally possible to generate interesting photon states with particular cold atom states. On the other hand, one may be able to develop novel ways of detecting many body correlations by measuring correlations of the electromagnetic fields. In such a perspective, many techniques developed in traditional quantum optics, such as pump probe spectroscopy, photon echoes, four wave mixing, etc., can be applied to cold atom gases.

Such a theory can be useful in elucidating the deep connections between atom and photon correlations. As an example of one such application, let us consider a method for detecting cold atom many-body states.

The atom-atom correlations can be measured by measuring the electromagnetic field correlations. The detection of the cold atom many body states is optimal when the field correlations are significantly modified by the presence of the atoms and the atom-atom correlations are kept intact under the atom-field coupling. A weak quantum field would be of particular interest in this case. This limit is the opposite of the limit where the correlations of the electromagnetic fields are used to engineer the correlations of the atom gases. The simplest form of photon correlations used in measurements is intensities, as used in the time of flight image technique. Phase-contrast imaging techniques, where the phase difference between two optical fields is measured, have also been used. Beyond these techniques, there are some high-resolution photon spectroscopy measurements of a hydrogen condensate in a cascade setup. This measurement used the single particle correlation of the electromagnetic field, a method that is limited by the laser line width. If a pump probe scheme is used and both the pump and the probe beam are derived from the same laser

source, one may overcome the constraint on the laser width. Such measurements are generally not invasive and can be done with atoms inside a trap. In such spectroscopy measurements, only single-photon time correlations at the same position are measured. In quantum optics, spatial as well as higher order correlations can be measured. This can lead to the determination of higher order atomic correlations, which would provide a systematic method of probing all the information contained in many body atomic states.

BIBLIOGRAPHY

BIBLIOGRAPHY

[1] P. S. Jessen and I. H. Deutsch, Advances in Atomic, Molecular and Optical Physics 37, (1996)

[2] Anderson, M. H., J. R. Ensher, M. R. Matthews, C. E. Wieman, and E. A. Cornell, 1995, Science **269**,198

[3] Davis, K. B., M. -o. Mewes, M. R. Andrews, N. J. van Druten, D. S. Durfee, D. M. Kurn, and W. Ketterle, Phys. Rev. Lett. 75, 3969 (1995);

[4] M. Greiner, O. Mandel, T. Esslinger, T.W. Hansch, and I. Bloch , Nature 415, 39-44 (2002)

[5] Joseph Kinast, Andrey Turlapov, John E. Thomas, Qijin Chen, Jelena Stajic, and Kathryn Levin, Science 307, 1296 (2005)

[6] G. B. Partridge, K. E. Strecker, R. I. Kamar, M. W. Jack, and R. G. Hulet, Phys. Rev. Lett. 95, 020404 (2005)

[7] M. W. Zwierlein, C. H. Schunck, C. A. Stan, S. M. F. Raupach, and W. Ketterle, Phys. Rev. Lett. 94, 180401 (2005)

[8] Hao Fu and P. R. Berman, Phys. Rev. A 72, 022104 (2005)

[9] Hao Fu and P. R. Berman, quant-ph/0605242 (2006)

[10] Hao Fu and Alberto G. Rojo, Phys. Rev. A 74, 013620 (2006)

[11] Hao Fu and Alberto G. Rojo, cond-mat/0610844 (2007)

[12] S. Scheel, L. Knoll, D.-G. Welsch, and S.M. Barnett, Phys. Rev. A **60**, 1590 (1999), and references therein

[13] M. P. Haugan and F. V. Kowalski, Phys. Rev. A 25, 2102 (1982)

[14] C. Cohen-Tannoudji, J. Dupont-Roc, and G. Grynberg, *Atom-Photon Interactions* (Wiley, 1998) pp. 165-253

[15] F. J. P. Schuurmans, D. T. N. de Lang, G. H. Wegdam, R. Sprik, and A. Lagendijk, Phys. Rev. Lett. **80**, 5077 (1998)

[16] G. M. Kumar, D. N. Rao and G. S. Agarwal, Phys. Rev. Lett. **91**, 203903 (2003)

[17] G. L. J. A. Rikken and Y. A. R. R. Kessener, Phys. Rev. Lett. **74**, 880 (1995)

[18] R. S. Meltzer, S. P. Feofilov, B. Tissue, and H. B. Yuan, Phys. Rev. B **60**, 14012 (1999)

[19] R. V. Jones and J. C. S. Richards, Proc. R. Soc. London A 221, 480 (1954)

[20] R. V. Jones and J. C. S. Richards, Proc. R. Soc. London. A 360, 347 (1978)

[21] J. Kinast, S. L. Hemmer, M. E. Gehm, A. Turlapov, and J. E. Thomas, Phys. Rev. Lett. 92, 150402 (2004)

[22] M. Bartenstein, A. Altmeyer, S. Riedl, S. Jochim, C. Chin, J. Hecker Denschlag, and R. Grimm, Phys. Rev. Lett. 92, 203201 (2004)

[23] M. Greiner, C. A. Regal and D. S. Jin, Phys. Rev. Lett. 94, 070403 (2005)

[24] C. A. Regal, M. Greiner, and D. S. Jin. Phys. Rev. Lett. 92, 040403(2004)

[25] M. W. Zwierlein, C. A. Stan, C. H. Schunck, S. M. F. Raupach, A. J. Kerman, and W. Ketterle, Phys. Rev. Lett. 92, 120403 (2004)

[26] M. Zwierlein *et al.*, Nature 435, 1047 (2005)

[27] M. Girardeau, J. Math. Phys., 1, 516-523 (1960)

[28] Paredes, B. , Widera, A. , Murg, V., Mandl, O., Folling, S., Cirac, I. , Shlyapnikov, G. V., Hansch W. T., and Bloch, I., Nature, 429, 277, (2004)

[29] T. Kinoshita, T. R. Wenger and D. S. Weiss, Sicence, 305, 1125 (2004)

[30] S. Inouye et al. Nature, 392, 151, (1998)

[31] R. A. Duine and H. T. C. Stoof, Phys. Rep. 396, 115 (2004) and references therein.

[32] M. Griener, C. A. Regale and D. S. Jin, Nature, 426, 537 (2003)

[33] M. Zwierlein, Phys. Rev. Lett. 91, 250401 (2003)

[34] Peter Fulde and Richard A. Ferrell, Phys. Rev. 135, A550 (1964)

[35] A. Aslamazov and A. I. Larkin Sov. Phys. JETP 20, 762 (1965)

[36] V. Weisskopf and E. Wigner, Z. Phys. **63**, 54, (1930).

[37] D. Toptygin, J. Fluorensc. **13**, 201 (2003).

[38] A. Luks and V. Perinova, *Progress in Opitcs*, edited by E. Wolf (Elsevier, Amsterdam, 2002), vol. 43, pp. 295-431.

[39] J. Knoester and S. Mukamel, Phys. Rev. A **40**, 7065

[40] A. Thranhardt, C. Ell, G. Khitrova, and H. M. Gibbs, Phys, Rev. B **65**, 035327 (2002), and references therein.

[41] Pedro de Vries and Ad Lagendijk, Phys. Rev. Let. **81**, 1381 (1998) and reference therein

[42] M. Fleischhauer Phys. Rev. A **60**, 2534 (1999) and reference therein

[43] M. E. Crenshaw and C. M. Bowden, Phys. Rew. Lett. **85**, 1851 (2000)

[44] P. R. Berman and P. W. Milonni Phys. Rew. Lett. **92**, 053601 (2004)

[45] E. A. Power *Introductory Quantum Electrodynamics* (Elsevier, New York, 1965) Chapter 8

[46] M. Danos and L. C. Maximon J. of Math. Phys. **6**, 766 (1965)

[47] J. H. Stamper, Phys. Rev. J. Chem Phys. **43**, 759 (1965)

[48] M. G. Edwards, J. Phys. B **2**, 719 (1969)

[49] E. Speller, B. Staudenmayer, and V. Kempter, Z. Phys. A **291**, 311 (1979)

[50] P. W. Milloni and R. W. Boyd Laser Physics, Vol 15, No. 10, (2005), pp. 1432-1438

[51] G. K. Campbell etc. Phys. Rev. Lett. 94, 170403 (2005)

[52] R. Loudon, J. Mod. Opt. 48, 821 (2002)

[53] R. Loudon L. Allen and D. F. Nelson, Phys. Rev. E 55 1071 (1997)

[54] D. F. Nelson Phys. Rev. A 44, 3985 (1991)

[55] P. R. Berman and B. dubetsky Phys. Rev. A, 55 4060 (1997)

[56] P. R. Berman Phys. Rev. A 72, 025804 (2005)

[57] M. O. Scully and M. S. Zubairy, Quantum Optics, (Cambridge 1997) pp. 206-210

[58] J. J. Hopfield, Phys. Rev. 112, 1555–1567 (1958)

[59] P. W. Anderson, Phys. Rev. 109, 1492 (1958)

[60] T. Ando and Fukuyama, *Anderson Localization,* Springer Proceedings in Physics 28 (Springer, Berlin, 1988)

[61] A. Auerbach, *Interacting Eletrons and Quantum Magnetism* (Spinger, New York, 1994)

[62] E. H. Lieb, and W. Liniger, Phys. Rev. 130, 1605 (1963)

[63] A. Lenard, 1964, J of Math Phys, 5, 930

[64] Elliott H. Lieb, Robert Seiringer, and Jakob Yngvason, Phys. Rev. B. 66, 134529 (2002)

[65] M. Rigol and A. Muramatsu, Phys, Rev. A. 72, 013604 (2005)

[66] R. Cote, V. Kharchenko, and M. D. Lukin, Phys. Rev. Lett. 89, 093001 (2002)

[67] P. Horak, J.-Y. Courtois, and G. Grynberg, Phys. Rev. A 58, 3953 (1998)

[68] Roberto B. Diener, Georgios A. Georgakis, Jianxin Zhong, Mark Raizen, and Qian Niu, Phys. Rev. A 64, 033416 (2001)

[69] U. Gavish and Y. Castin, Phys. Rev. Lett. 95, 020401 (2005)

[70] J. E. Lye, L. Fallani, M. Modugno, D. S. Wiersma, C. Fort, and M. Inguscio, Phys. Rev. Lett. 95, 070401 (2005);

[71] David Clement, Andres F. Varon, Mathilde Hugbart, Jocelyn Retter, Philippe Bouyer, Laurent Sanchez-Palencia, Dimitri M. Gangardt, Georgy V. Shlyapnikov, Alain Aspect, cond-mat/0506638;

[72] T. Schulte, S. Drenkelforth, J. Kruse, W. Ertmer, J. Arlt, K. Sacha, J. Zakrzewski, M. Lewenstein, cond-mat/0507453

[73] F. D. M. Haldane, Phys. Rev. Lett. 47, 1840 (1981)

[74] D. Jaksch, C. Bruder, J. I. Cirac, C. W. Gardiner, and P. Zoller, Phys. Rev. Lett. 81, 3108 (1998)

[75] Oliver Penrose and Lars Onsager, Phys. Rev. 104, 576 (1956)

[76] E. N. Economou, *Green's Functions in Quantum Physics, 1983,* Page 99

[77] T. Kinoshita, T. R. Wenger and D. S. Weiss, Nature 440, 900 – 903 (2006)

[78] C. Chin, M. Bartenstein, A. Altmeyer, S. Riedl, S. Jochim, J. Hecker Denschlag, and R. Grimm, Science 305, 1128 (2004)

[79] Eddy Timmermans, Paolo Tommasini, Mahir Hussein and Arthur Kerman, Phys. Rep. 315, 199 (1999)

[80] S. J. J. M. F. Kokkelmans, J. N. Milstein, M. L. Chiofalo, R. Walser, and M. J. Holland, Phys. Rev. A, 65, 053617 (2002)

[81] Qijin Chen, Jelena Stajic, Shina Tan and K. Levin. Phys. Rep. 412, 1 (2005)

[82] Qijin Chen and K. Levin , Phys. Rev. Lett. 95, 260406 (2005)

[83] K. Dieckmann, C. A. Stan, S. Gupta, Z. Hadzibabic, C. H. Schunck, and W. Ketterle, Phys. Rev. Lett, 89, 203201 (2002)

[84] C. A. Regal and D. S. Jin, Phys. Rev. Lett, 90, 230404 (2003)

[85] T. Bourdel, J. Cubizolles, L. Khaykovich, K. M. F. Magalhaes, S. J. J. M. F. Kokkelmans, G. V. Shlyapnikov, and C. Salomon, Phys. Rev. Lett, 91, 020402

[86] Kevin E. Strecker, Guthrie B. Partridge, and Randall G. Hulet. Phys. Rev. Lett, 91, 080406

[87] M. Bartenstein, A. Altmeyer, S. Riedl, R. Geursen, S. Jochim, C. Chin, J. Hecker Denschlag, R. Grimm, A. Simoni, E. Tiesinga, C. J. Williams, and P. S. Julienne Phys. Rev. Lett, 94, 103201 (2005)

[88] P. O. Fedichev, Yu. Kagan, G. V. Shlyapnikov, and J. T. M. Walraven, Phys. Rev. Lett. 77, 2913 (1996)

[89] John L. Bohn and P. S. Julienne, Phys. Rev. A, 56, 1486 (1997)

[90] John L. Bohn and P. S. Julienne, Phys. Rev. A, 60, 414 (1999)

[91] F. K. Fatemi, K. M. Jones, and P. D. Lett, Phys. Rev. Lett. 85 4462

[92] H. T. C. Stoof, M. Bijlsma, and M. Houbiers, 101, 443, Journal of Research of the National Institute of Standard and Technology

[93] M. Theis, G. Thalhammer, K. Winkler, M. Hellwig, G. Ruff, R. Grimm, and J. Hecker Denschlag, Phys. Rev. Lett. 93, 123001 (2004)

[94] T. Zelevinsky, M. M. Boyd, A. D. Ludlow, T. Ido, J. Ye, R. Ciurylo, P. Naidon, and P. S. Julienne, Phys. Rev. Lett. 96, 203201 (2006)

[95] A. J. Leggett, Rev. of Mod. Phys. 73, 2001

[96] Daniel E. Sheehy and Leo Radzihovsky, cond-mat/0607803 and reference therein

[97] M. Greiner, C. A. Regal, J. T. Stewart, and D. S. Jin, Phys. Rev. Lett. 94, 110401 (2005)

[98] S. Folling, Nature 434, 481-484 (2005)

[99] P. Torma and P. Zoller, Phys. Rev. Lett. 85, 487 (2000)

[100] J. Kinnunen, M. Rodriguez, and P. Torma, Phys. Rev. Lett. 92, 230403 (2004)

[101] J. Kinnunen, M. Rodriguez, and P. Torma, Science 305, 1131 (2004)

[102] Roberto B. Diener and Tin-Lun Ho, cond-mat/0405174

[103] Y. Ohashi and A. Griffin, Phys. Rev. A 72, 013601 (2005)

[104] P. de Gennes, Superconductivity of metals and alloys, (W. A. Benjamin, Inc., New York, 1966)